UNCLASSIFIED

AD 407 961

DEFENSE DOCUMENTATION CENTER

FOR

SCIENTIFIC AND TECHNICAL INFORMATION

CAMERON STATION, ALEXANDRIA, VIRGINIA

UNCLASSIFIED

TECHNICAL REPORT

AIR FORCE OFFICE OF SCIENTIFIC RESEARCH

GRANT AF-AFOSR-62-378 and CONTRACT AF 49(638)-639

PROJECT NO. 9751

TASK NO. 37511

CONTRACTOR

UNIVERSITY OF OKLAHOMA RESEARCH INSTITUTE

A DIRECT METHOD FOR MEASURING LIFETIMES OF EXCITED ATOMIC STATES AND ITS APPLICATION TO HELIUM

BY

THOMAS M. HOLZBERLEIN

PROJECT DIRECTOR

RICHARD G. FOWLER
UNIVERSITY OF OKLAHOMA
NORMAN, OKLAHOMA

MAY 1963

TECHNICAL REPORT

AIR FORCE OFFICE OF SCIENTIFIC RESEARCH

GRANT AF-AFOSR-62-378 and CONTRACT AF 49(638)-639

PROJECT NO. 9751

TASK NO. 37511

CONTRACTOR

UNIVERSITY OF OKLAHOMA RESEARCH INSTITUTE

A DIRECT METHOD FOR MEASURING LIFETIMES OF EXCITED ATOMIC STATES AND ITS APPLICATION TO HELIUM

BY

THOMAS M. HOLZBERLEIN

PROJECT DIRECTOR

RICHARD G. FOWLER
UNIVERSITY OF OKLAHOMA
NORMAN, OKLAHOMA

MAY 1963

THE UNIVERSITY OF OKLAHOMA

GRADUATE COLLEGE

A DIRECT METHOD FOR MEASURING LIFETIMES OF EXCITED ATOMIC STATES AND ITS APPLICATION TO HELIUM

A THESIS

SUBMITTED TO THE GRADUATE FACULTY

in partial fulfillment of the requirements for the

degree of

DOCTOR OF PHILOSOPHY

BY

THOMAS MILTON HOLZBERLEIN

Norman, Oklahoma

1963

TABLE OF CONTENTS

TABLE OF CONTENTS (continued)

LIST OF ILLUSTRATIONS

LIST OF ILLUSTRATIONS (continued)

INTRODUCTION

Work Prior to 1955

At the time this research was started in 1955 there was a growing demand for experimental information on the relaxation times of excited atomic states. A literature search showed that no direct life time measurements had been made since World War II.

In fact only one article on atomic lifetime measurements had been published since 1936 and that paper was published a full decade before 1955.[1] Of these early lifetime measurements only two were on gases, hydrogen[2,3] and neon.[4] All other works were on metal vapors with Hg being given the most attention employing a single technique modified and improved from 1929 to 1932 the last paper of this group being by Garrett.[5] Other vapor studies were Na[6,7] and Cd[9,10]

---

[1]These findings have been confirmed through the National Bureau of Standards <u>Bibliography</u> on <u>Atomic</u> <u>Transition</u> <u>Probabilities</u> published in August of this year (1962).

[2]F. G. Slack, Phys Rev <u>23</u> 1-12 (1926).

[3]J. H. E. Griffiths, Proc Roy Soc London A <u>147</u>, 547-554(1934).

[4]J. H. E. Griffiths,Proc Roy Soc London A <u>143</u>, 588-604 (1934).

[5]Garrett, P. H. Phys Rev <u>40</u>, 779-790 (1932).

[6]Hupfeld, Z. Physik <u>54</u>, 484-497 (1929).

[7]F. Duschinsky, Z. Physik <u>78</u>, 586-602 (1932).

[8]D. Sinclair and H. W. Webb Phys Rev <u>50</u>, 440-445 (1936).

[9]H. D. Koenig and A. Ellett, Phys Rev <u>39</u>, 576-584 (1932).

[10]H. W. Webb and H. A. Messenger, Phys Rev <u>66</u>, 78-86 (1944).

Published Work Since 1955

It should be pointed out that a number of metal vapors have been added to the above list as late as 1962. A large number of the new metal vapors have been studied by W. Demtroder at the University of Bonn.[11]

The only new atomic gas studies published prior to the date of publication of the National Bureau of Standards bibliography[12] in 1962 has been on Helium.[13,14] Both groups, whose works were published after this work was well under way, employed advanced electronic coincidence techniques which yielded the actual relaxation curves of the states which have lifetimes longer than the sampling pulse used in their work.

The work of Bennett and Dalby employs the more sophisticated electronic timing techniques and a readout method which graphs the relaxation curve by means of a recorder. Their work on helium is very limited since it was only used as a calibration check on the system. The more comprehensive work on helium was done by Heron, et al., at the earlier date.

Returning to the conditions in 1955: Since electronic art had grown tremendously since 1944, it seemed wise to devise a scheme

---

[11]W. Demtroder, Z. Physik, 166. 42-45 (1962).

[12]Op. Cit. 1. Anyone doing new research in the field should use this bibliography since there are many other techniques for obtaining information on transition probabilities than life time measurements, and current work is too voluminous to give complete information here.

[13]S. Heron, R.W.P. McWhirter and E. H. Phoderick Proc Roy Soc London A 234, 565-582 (1956).

[14]R. G. Bennett and F. W. Dalby, Jochem, Phys 31, 434-441 (1959).

employing modern electronic techniques to obtain the actual relaxation time curve for a gas. All previous work on neutral gases had employed phase shift consideration between a modulated excitation source and the light being observed. Although extremely good time resolutions have been quoted, the technique could not show the true shape of the relaxation curves. In fact the exponential nature of the relaxation curve had to be assumed in order to extract relaxation time data from phase shift data. The early workers knew the relaxation curves would be nonexponential because of cascading but they had to assume this contribution would be small. This emphasized a need for a display of the true curve shape. An examination of Landolt-Bornstein tables[15] showed that many relaxation times determined by theory and by indirect experimental means fall into the 10^{-8} sec and longer time range. These atomic lives seemed accessible to electronic measurement through a display of the actual light decay on an oscilloscope using a pulsed photomultiplier as the light detector.[16] The conditions under which the photomultiplier output current truly represents the same time function as that of the density of atoms of a given excited state are made clear in Chapter I.

---

[15]Landolt-Bornstein, Zahlenwerte and Funktionen Teil 1 Atome-ionen, Vol. I, pp. 262-264.

[16]R. F. Post, Nucleonics, 10 No. 5, 46-50 (1952).

A DIRECT METHOD FOR MEASURING LIFETIMES OF EXCITED ATOMIC STATES AND ITS APPLICATION TO HELIUM

CHAPTER I

THEORY

Glossary of Terms and Symbols

It is well to establish a glossary of terms and symbols at the outset since there is a great deal of material to be presented using them. Most of the symbols will be self explanatory in the text and therefore will not need to be identified with each equation.

N_e	=	Electron density in electrons/cc
N_a	=	Atomic density in atoms/cc
$N_{i.j}$	=	Number of atoms in the i and j state/cc (here n=i and ℓ=j and multiplicity is not given)
$N_{i.j,k.l}$	=	Number of atoms in the ith level decaying to the kth level. Frequently the ℓ values will be dropped leaving $N_{i.k}$ where no confusion arises
N_I	=	Ion density ions/cc
V_e	=	Velocity of electron
V_I	=	Velocity of ions
$\overline{V}_a$	=	Mean velocity for atoms of the gas
C	=	Velocity of light
$\overline{X}_e$	=	Mean free path of electron
$\overline{X}_a$	=	Mean free path of atom in gas
e	=	Electronic charge

$\lambda_{i,j}$ = Wave length associated with a photon emitted in an i to j transition

$\sigma_{i.k}$ = The true impact cross section for the production of atoms in the i.k state. This is not to be confused with the apparent or total production cross section

$\sigma'_{i.k}$ = This is the apparent cross section as obtained from experimental observation and is made up of information on the production of states as the result of direct electron impact plus other production terms initiated by impact.

σ_I = Ionization cross section (all cross sections are assumed to be in square centimeters)

$A_{i.k,j.\ell}$ = Transition probability for spontaneous emission by change of state i.k to $j.\ell$.

$A_{i.k}$ = Total transition probability from the i.k state by spontaneous emission $A_{i.k} = \sum_{j,\ell} A_{i.k,j.\ell}$

$B_{i.k,j.\ell}$ = The probability of a photon induced transition between state i.k and state $j.\ell$.

$\tau_{i.k}$ = Natural life of an excited state

$$\tau_{i.k} \equiv 1/A_{i.k}$$

$\bar{t}_{i.k}$ = The relaxation time of the shortest lived exponential component of the light emitted by state i.k.

$I^*_{i.k,j.\ell}$ = Photon intensity of light source equal to the number of Photons of the i.k to $j.\ell$ transition per unit volume and time

$I_{i.k,j.\ell}$ = True monochromatic light intensity in ergs per unit volume and time $I = I^* hc/\lambda_{i.k,j.\ell}$

$\mathcal{J}^*$ = Photon flux in photons per unit area and time

$\mathcal{J}$ = Light flux in ergs per unit area and time

i_{ex} = Excitation current in amperes

ξ_i = Electron production rate for state i $\xi_i = N_e N_a V_e \sigma_{eI}$

$\rho_{i,j}$ = Monochromatic photon density for photons, having wavelengths arising from transitions from state i to state j.

Fundamental Concepts

It seems appropriate to present the theory behind the emission of light first since light is the observable quantity in excitation cross section and atomic life measurements on neutral atoms.

The light emitted from a single atom is assumed to arise from a purely spontaneous process. This emplies that no condition external to the atom will change the probability that an atom will emit radiation. Under the conditions of this experiment this assumption will be assumed to be rigorously satisfied.

This spontaneity assumption may be put in the form of a differential equation.

$$\left(\frac{dN_i}{dt}\right)_{\substack{spont\\emiss.}} = -A_i N_i \qquad 1)$$

This equation says in words that the rate of loss of the i state density by spontaneous emission is proportional to the density of the atoms in state i. A_i is the constant of proportionality known as the transition probability per unit time and hereafter it will be called simply the "transition probability". That there may be many other rate processes contributing to the rate of change of state density will be seen later. Should this process be the only loss process, as would be the case for atoms isolated from their neighbors, and from radiation and also if none of these atoms are excited to higher levels that can cascade into the state being measured, then

$$\frac{dN_i}{dt} = -A_i N_i \qquad 2)$$

hence $$N_i(t) = N_i(0)\, e^{-A_i t} \qquad 3)$$

The "Natural Life" of an atomic state is defined as the mean life of the state if the only process involved in changing the state density is spontaneous emission. Since the state density expression 3) was derived on these grounds one may use it and equation 2) in the derivation of the mean life expression.

Clearly the mean life τ is given by the following.

$$\tau_i = \int_0^{N_i(0)} t \, dN_i / N_i(0) \qquad 4)$$

or $$\tau_i = \int_0^{\infty} t \left(\frac{dN_i}{dt}\right) dt / N_i(0) \qquad 5)$$

and applying equation 2) and 3)

$$\tau_i = -A_i \int_0^{\infty} t \, e^{-A_i t} dt \qquad 6)$$

integrating by parts and applying L'Hopital's rule one has

$$\tau_i = 1/A_i \qquad 7)$$

The restrictions on the definition of "Natural Life" are so great that τ is rarely determined experimentally. It is therefore useful to define $\bar{t}$ which is the mean life of the shortest lived exponential component making up the radiation curve. It will be the same as τ except for cases when only cascading processes exist.

Should there be more than one lower state accessible through radiation then it is helpful to write separate equations analagous to equation 1) but applied to specific transitions.

$$dN_{i,1}/dt = -A_{i,1}\,N_i$$
$$dN_{i,j}/dt = -A_{i,j}\,N_i \qquad 8)$$
$$dN_{i,n}/dt = -A_{i,n}\,N_i$$

Here the transition probability $A_{i,j}$ is defined for each specific transition rather than for the entire state.

Since the rate of loss of state i is the rate of loss summed over all loss processes, equations 8) may be added to obtain the equivalent of equation 1).

$$\left(\frac{dN_i}{dt}\right)_{\substack{spont.\\ emiss.}} = \sum_j dN_{i,j}/dt = \left(\sum_j A_{i,j}\right) N_i \qquad 9)$$

Comparing equation 9) with equation 1) one sees that

$$A_i \equiv \sum_j A_{i,j} \qquad 10)$$

Here the total transition probability which determines the natural life of the ith state is the sum of the individual transition probabilities for individual transitions making up this loss. Light intensity data and radiation theory give values for the $A_{i,j}$'s, while the measured relaxation curves yield values for A_i's if the only state density rate process is spontaneous emission.

Now the photon source intensity[17] is defined

$$I^*_{i,j} \equiv dN_{i,j}/dt \qquad 11)$$

---

[17]The photon intensity is proportional to the signal read on a photon counter.

and returning to equation 1) it can be seen that

$$I^*_{i,j} = -A_{i,j} N_i \qquad 12)$$

If one wishes to compare photon intensities for two different lines.

$$\frac{I^*_{i,k}}{I^*_{j,\ell}} = \frac{A_{i,k} N_i}{A_{j,\ell} N_\ell} \qquad 13)$$

If both lines are produced by emmission from the same state the photon intensities are simply the ratio of the transition probabilities associated with each line.

$$\frac{I^*_{i,k}}{I^*_{i,\ell}} = \frac{A_{i,k}}{A_{i,\ell}} \qquad \text{(Common Upper State)} \qquad 14)$$

If true light source intensities are desired then the power per unit volume is important and each of the above equations can be adapted to the required form by simply multiplying each $I^*_{i,k}$ by the photon energy $hc/\lambda_{i,k}$. Thus 13) becomes

$$\frac{I_{i,k}}{I_{j,\ell}} = \frac{A_{i,k}}{A_{j,\ell}} \frac{N_i}{N_j} \frac{\lambda_{j,\ell}}{\lambda_{i,k}} \qquad 15)$$

and from 14) $\dfrac{I_{i,k}}{I_{i,\ell}} = \dfrac{A_{i,k}}{A_{i\ell}} \dfrac{\lambda_{i\ell}}{\lambda_{ik}}$ (Common Upper State) 16)

Time Relationship Between State Density and Observed Light

In order to investigate the relationship, between the light being observed externally and the state density giving rise to that light one may take the following line of thought.

$I^*_{i,j}$, the number of photons radiated per unit volume and

time, is equal to dN_{ij}/dt by definition; see equation 11). If one can assume that none of the photons are reabsorbed in the gas then the number of photons per second passing through a unit area at a distance r from the volume element and having an angle of inclination θ to the normal vector of the area as seen in Figure 1), will be given by equation 17).

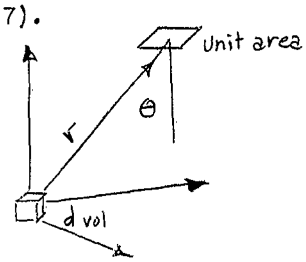

$$d\mathcal{J}^* = \frac{I^* \cos\theta \, d\,\mathrm{vol}}{4\pi r^2} \tag{17}$$

Figure 1

To find the photon flux intensity at the window one must integrate over the volume of entire source, and the equation becomes

$$\mathcal{J}^* = \int_{\mathrm{vol}} I^* \cos\theta / 4\pi r^2 \, d\,\mathrm{vol} \tag{18}$$

Now consider a nonresonant state which will have the same time dependance throughout the volume. One may write $N_i(v,t)$ in the following form where v is the volume.

$$N_i(v,t) = N_i(v,0)\, f(t) \tag{19}$$

In equation 3) $f(t) = e^{-A_i t}$ for example.

Since $I^*_{i,j} = A_{i,j} N_i(v,t) = A_{i,j} N_i(v,0) f(t)$ 20)

Substitution into 18) gives

$$\mathcal{J}^* = f(t)\, A_{i,j} \int_{\mathrm{vol}} \left(N_i(v,0) \cos\theta / 4\pi r^2 \right) d\,\mathrm{vol} \tag{21}$$

Since for a given experimental arrangement the integral is constant

$$\mathcal{J}^* = f(t)\, K. \tag{22}$$

Now it is a small step to go from photon intensity to photomultiplier anode current if one knows the area of window a, the window efficiency $\mathcal{E}_\omega$, the cathode efficiency $\mathcal{E}_c$ and the multiplication of the photomultiplier M. Without carrying out the minutia of details the anode current is

$$i_{anode} = \mathcal{I}^* a\, \mathcal{E}_c\, \mathcal{E}_\omega\, M e \qquad 23)$$

and combining with 18) and lumping all constants

$$i_{anode} = K' f(t) \quad \text{where } K' = A_{i,j}\left(\int_{Vol} \frac{N_i(v,0)}{4\pi r^2} d_{vol}\right) a\, \mathcal{E}_c\, \mathcal{E}_\omega\, M e \qquad 24)$$

Thus for a common time dependence throughout the volume, no blockading of radiation, and if there are no false counts or saturation which affect the M of the photomultiplier then its anode current-vs-time curve is the same as the state density-vs-time curve within a multiplying constant K .

The K above is not important if only the time dependence is required. But in the feasibility study for the instrument design it had to be checked in detail in order to decide the volume and density of excited states that would be needed to produce a good output current curve. When the light level is too low, statistical noise obscures the true curve shape. The volume integral used in this study is given in Appendix I since it may be useful in future design considerations involving cylindrical symmetry.

Populating and Loss Processes Related to State Density

Now that the theory of state density measurement by means of light observation has been presented one needs to consider the factors governing the time dependence of the state densities.

Clearly the state density is going to be equal to the initial number of particles plus the time integral of gain processes and minus the time integral of loss processes. Given as follows:

$$N_i(t) = N_i(0) + \sum_i \int_0^t (\text{gain rate process})_i \, dt \; - \sum_j \int_0^t (\text{loss rate process})_j \, dt \qquad 25)$$

State Production Processes

The only gain process internal to an atom is the cascading from upper states to the state in question and this will be given theoretical consideration later and may be a major contribution to the state density in some cases.

External gain processes are:

a) photon interaction

b) charged particle – electron
ion

c) neutral particle – internal energy conversion
kinetic energy conversion

d) walls of container – thermal energy

a) The photon interactions which can produce a given atomic state fall into two classes: Photoelevation of a lower state, and stimulated emission between an upper state and the one being considered. These two processes are given by the following expression:

$$\frac{dN_i}{dt} = \rho_{i,0} \, N_0 \, B_{0,i} \qquad 26)$$

for photoelevation and

$$\frac{dN_i}{dt} = \rho_{i,j} \sum N_j \, B_{j,i} \qquad 27)$$

for stimulated emission.

Since ground state atoms have a very high density, and because

resonance radiation is very intense, due to funneling of energy through resonance states to the ground state, photoelevation of ground state atoms to these resonance states is important. This reabsorption will be spoken of as blockading or radiation imprisonment. All other photoproduction processes will be neglected with the reservation that for metastable states some caution is warranted.

b) State production by impact of charged particles falls into two categories. The electron or light particle and the ion or heavy particle processes constitute these divisions.

$$\left(\frac{dN_i}{dt}\right)_{\substack{electron\\beam}} = \sigma_{e\,i}\, N_a N_e v_e \equiv \xi_i \qquad 28)$$

$$\left(\frac{dN_i}{dt}\right)_{ion} = \int_{velocity} N_a N_I V_I \sigma_I(V_I)\, dV_I \qquad 29)$$

In this experiment $\bar{v}_I$ is always much lower than $\bar{v}_e$ because of $m_e \ll m_I$ and because $\bar{v}_e$ is field produced while $\bar{v}_I$ found within the excitation zone is thermally produced. Thus without reservation one may neglect 29). Equation 28) gives the main production term in this experiment.

It should be pointed out quite carefully that in the separate treatment of rate processes in this study σ_{ei} is the true impact cross section and is not σ_{ei}' the gross cross section obtained in experiment where σ_{ei}' is defined by the following equation:

$$\sigma_{ei}' \equiv I^* / N_a N_e V_e \qquad 30)$$

In the experimental cross section determination, many of the i states are not produced directly but rather are the result of cascading from upper states created by electron impact. Since cascading is treated separately the true impact cross section concept must be used here.

c) Neutral particle production of excited states may come

about through collisions of the second kind where internal energies are transferred from one atom to the next with the excess energy being given off as kinetic energy of the two neutrals. This process would be dependent upon the density of states lying above the one being studied and upon the density of neutrals.

The interaction parameter is small if the conversion of internal energy must be given off in part to an entire atom rather than to a single electron as in the Penning effect. Along with this conjecture one finds that the collision frequency between excited states and neutrals is low compared with lives of states in this experimental work. Therefore this interaction must contribute little to the change observed in lifetime studies unless the natural lives exceed 10^{-7}sec. As a check, notice for H_e at 1100° K. and .13 mm Hg, $\overline{X}$ = .135cm, while $\overline{V}$ of $H_e = 2.4 \times 10^5$ cm/sec.[18] Thus, an estimated mean life contribution, if this process alone governed the losses, is

$$\bar{t} \approx \frac{.135\,\mathrm{cm}}{2.4 \times 10^5\,\mathrm{cm/sec}} \approx .54 \times 10^{-6}\,\mathrm{sec} \tag{31}$$

On the grounds of the low interaction probability the author considers this process to be negligible.

Neutral - neutral excitation by impact between ground state atoms is extremely improbable since the neutral thermal energy at 1100° K is of the order of 0.1ev while the lowest excitation potential is two hundred times larger.

d) The excitation of neutral ground state atoms by contact with walls in this experiment is completely ruled out by the same argument as given in the previous paragraph.

---

[18]See Appendix II for more data on Helium.

Reviewing then, one sees that cascading, radiation imprisonment, and electron impact are the only production processes of consequence for this work.

Loss Processes

The possible loss processes are divided into internal and external processes too, with the only internal process being spontaneous emission. The external processes are divided in a way similar to the gain processes just discussed.

a) photon	elevation to higher states enforced emission to lower states
b) electron	impact elevation impact loss (collision of second kind)
c) ion	impact elevation impact loss
d) neutral	Penning effect in raising or lowering a state
e) wall effect	

a) Photon losses. Here the photon losses are divided into the same categories as the production processes and are governed by the same form of equation. The one point of interest is that the state density appears linearly in the expression.

$$\frac{dN_i}{dt} = \sum_{k>i} \rho_{i,k} N_i B_{i,k} \qquad \text{for elevation} \qquad 32)$$

$$\frac{dN_i}{dt} = \sum_{j<i} \rho_{i,j} N_i B_{i,j} \qquad \text{for stimulated emission to lower states} \qquad 33)$$

The only states which are likely to have appreciable elevation losses are ground states, and metastable states on rare occasion. Since neither of these states is a source of light this loss process is never likely to be observed.

b) Electron losses may also be divided into energy-elevation or energy-loss processes. The first process is a stage process in which multiple excitation plays a role. The second process is a collision of the second kind where an electron takes away the excitation energy.

$$\frac{dN_i}{dt} = \underset{\text{(from swarm electrons)}}{\int N_i \sigma_e(v) N_e(v) V\,dV} + \underset{\text{(from beam electrons)}}{\sum \sigma_{i,j} N_e N_i V_e} \qquad \text{electron elevation} \quad 34)$$

$$\frac{dN_i}{dt} = K_i N_e N_i \quad (K_i = \text{reaction parameter}) \qquad \text{for second kind reaction rates} \quad 35)$$

Electron initiated loss processes do not require high energy electrons and therefore may be triggered by the electron cloud which is held by the ions in this experiment. The beam electrons will likely contribute only to the elevation component of these losses because of their high energy. The electron beam loss is given as the second term in the elevation expression.

There is no significant loss process that can be initiated by an ion, as seen by the author. Their velocities are too low to have any appreciable cross section. The neutral atom loss process due to collisions of the second kind are also deemed unimportant. The Penning effect resulting from a foreign gas and long lived excited states may become important however, but gas purity should control this.

This leaves one with only two types of loss processes to be considered. Spontaneous emission, already considered, and electron impact processes. The electron beam component of the loss process may be investigated for an order of magnitude feasibility study.

Since $\sigma_{e_{i,j}}$ the elevation cross-section is unknown it might be informative to consider it to be the same order of magnitude as the ionization cross section for ground state atoms. It may be considerably

larger but it seems unlikely to be more than an order of magnitude larger. With this in mind one finds the elevation rate (ionization rate) to be given by the following expression

$$\left(\frac{T_o P}{T P_o}\right) \mathcal{E}_I \frac{i_{ex}}{e} D \times 10^{-6} = \text{ion/usec} \qquad 36)$$

where $\mathcal{E}_I$ is the ionization efficiency in ions/cm electron and is found to be 1.25 ions/electron cm for these conditions.[19]

i_{ex} = impact current

D = electron path length (Diameter of system)

e = electronic charge

In this experiment $\left(\frac{T_o P}{T P_o}\right) \frac{1.25 \text{ ions}}{\text{elec. cm}} \frac{.8 \text{ coulomb/sec}}{1.6 \times 10^{-19} \frac{\text{coul}}{\text{elect}}} \frac{1.27 \text{ cm}}{10^6 \frac{\mu\text{sec}}{\text{sec}}} = \frac{\text{Ions}}{\mu\text{-sec}}$

Since there are 35.35 10^{15} atoms/cc at 1.0 mm of Hg and 273°K, the ratio of ions to neutral after one μ-Sec of excitation is

$$\frac{N_I}{N_a} = \frac{1.24 \cdot .8 \quad 1.27 \times 10^{-6}}{1.6 \times 10^{-19} \quad 35.3 \times 10^{15}} = 2.22 \times 10^{-4} \text{ ions/neutral} \qquad 37)$$

Here the correction for pressure and temperature cancel. Thus, even if the state elevation cross-section were greater than the ionization cross-section the stage processes are highly unlikely when compared to direct processes where the interaction is with the ground state atoms. The loss processes to the electron cloud in the plasma created in this excitation tube will be neglected except for high level states where it is assumed to strip the gas of high level states. This needs more investigation however.

---

[19] P. T. Smith, Phys. Rev 36, 1293–1299 (1930).

One important last comment is that every loss process (except for the possible interaction between two atoms of the same state) is linearly dependent upon the state density N_i. This fact will be important in the discussion of the differential equation governing the state density which will now be developed.

State Density Equation

Returning to equation 25) one may put it into differential form by taking the time derivative of all terms.

$$\frac{dN_i(t)}{dt} = \sum_i (\text{gain rate process})_i - \sum_j (\text{loss rate process})_j \qquad 38)$$

It will be remembered that the only gain processes deemed pertinent for most experimental work are the internal cascading term, the electron impact term and the radiation imprisonment term. These terms taken separately are as follows:

$$\left(\frac{dN_{i.k}}{dt}\right)_{cascade} = \sum_{j>i}^{\infty} A_{j.\ell,i.k}\, N_{j\ell} \qquad 39)$$

where $\ell = k \pm 1$ 40)

Here j and i subscripts apply to principal quantum numbers and k and ℓ apply to orbital quantum numbers. The stipulation that $\ell = k \pm 1$ is simply that $\Delta l = \pm 1$ angular momentum selection rule. Clearly $j > i$ implies the j state energy must be above the i state energy, otherwise cascading to the ith state would be impossible.

$$\left(\frac{dN_{i.k}}{dt}\right)_{electron\ impact} = \sigma_{i.k}\, N_a N_e V_e = \sigma_{i.k} N_a \frac{\dot{i}_{ex}}{Ae} \qquad 41)$$

Here A is the area through which current must pass and e is the electronic charge.

The resonance radiation term will not be treated in general at

this point but will be discussed in Appendix III. Under the conditions of full blockading every transition to the ground state results in the elevation of another neutral to that state by the capture of the photon. Thus under full blockading there is no net loss to the ground state. Therefore, the only alteration of the general nonblockaded analysis will be to treat the $A_{i.k,0.0}$ states as though they are zero for the system as whole even though these transition probabilities are the largest in the atom, when the atoms are considered individually.

$$A_{i.k,00} = 0 \qquad \text{(for full blockading)} \qquad 42)$$

The loss processes will be considered as made up of only two terms, the spontaneous emission term and the total of all other loss processes lumped into a single term. The spontaneous emission term as in equation 9) is:

$$\left(\frac{dN_{i.k}}{dt}\right)_{\substack{\text{spont.}\\ \text{emiss.}}} = \sum_{j<i} A_{i.k,j.l}\, N_{i.k} = A_{i.k} N_{i.k} \qquad 43)$$

Here again, $l = k\pm 1$ but $j < i$ means those states whose energy is below that of state i.

All other losses are considered small and are lumped together factoring out the $N_{i.k}$ dependence which was mentioned in previous discussion.

$$\underbrace{\sum}_{\text{all losses except spont. emission}} \left(\frac{dN_{i.k}}{dt}\right)_{loss} = N_{i.k}\,\mathcal{L}\,(\text{Pressure, Volume, Time, etc.}) \qquad 44)$$

Thus the final form for the state differential equation 38) becomes the following under full blockading.

$$\frac{dN_{i.k}}{dt} = \underbrace{\sum_{j>i}^{\infty} A_{j.l,i.k} N_{j.l}}_{\text{cascade gain}} + \underbrace{\sigma_{i.k} N_a N_e V_e}_{\text{electron impact gain}} - \underbrace{N_{i.k} \sum_{j=1}^{j<i} A_{i.k,j.l}}_{\text{spont. emiss. loss}} - \underbrace{N_{i.k}\,\mathcal{L}(P,V,T)}_{\text{lumped losses}} \qquad 45)$$

Now the last terms may be lumped together with the common factor $N_{j,\ell}$ and the electron impact terms may be written $\xi_{i,k}$ and $\sum A_{i,k,j,\ell} = A_{i,k}$ and transposing the loss terms one has

$$\frac{dN_{i,k}}{dt} + N_{i,k}\left[A_{i,k} + \mathcal{L}(P,V,T)\right] = \xi_{i,k} + \sum_{j>i}^{\infty} A_{j,\ell,i,k}\, N_{j,\ell} \qquad 46)$$

This equation is the form

$$\frac{dN}{dt} + N\, f(t) = g(t) \qquad 47)$$

and can be solved for N as a function of time explicitly provided f(t) is not too awkward. The solution is found in mathematics texts covering ordinary linear differential equations. It takes the following form:

$$N = \left(\frac{1}{P}\right)\int P\, g(t)\, dt + N(0)/P \qquad 48)$$

where $$P = e^{\int^{t} f(t)\,dt} \qquad 49)$$

Applying this solution to equation 46) results in the following expression:

$$N_{i,k}(t) = \frac{1}{e^{\int(A_{i,k}+\mathcal{L})dt}} \int e^{\int_0^t (A_{i,k}+\mathcal{L})dt} (\underbrace{\xi_{i,k}}_{\text{electron impact Production}} + \underbrace{\sum_{j>i}^{\infty} A_{j,\ell,i,k} N_{j,\ell}}_{\text{cascade}})dt + \frac{N_{i,k}(0)}{e^{\int(A_{i,k}+\mathcal{L})dt}} \qquad 50)$$

The thing which makes equation 50) awkward is that the $N_{j,\ell}$'s within the infinite sum arising from the cascading of upper levels are all governed by expressions similar to 50) itself. Thus the analytical solution of the equation looks hopelessly difficult unless one can eliminate most of the cascading terms.

One way would be to assume an excitation source which could only excite atoms up to an energy well below the ionization energy, a condition not feasible with the present experimental light source. Another method would be to select only those terms which appear to give an appreciable contribution while neglecting any cascading which

might make a contribution to those upper levels under steady state conditions.

The effect of the very long lived upper level on the state density of lower levels is governed by the fact that excitation only continues for a finite period of time and these upper levels never acquire their full steady state density. The fraction of their steady state density acquired during finite excitation times may be approximated by the following expression which will be derived later.

$$\frac{N_i(t_{ex})}{N_i(\infty)} \approx \left(1 - e^{-t_{ex}/\tau}\right) \tag{51}$$

Here t_{ex} is the excitation time and $N_i(\infty)$ is the steady state density of the i state atoms.

Special Case Solutions of State Equation

The Relaxation Curve Without Cascading

First it is informative to notice that Equation 50) simplifies considerably if one may neglect cascading and at the same time assume the electron beam which has excited the i state is suddenly cut off. After cutoff both production prosses are zero hence the integral in 50) becomes zero also and N_{ik} is given as follows:

$$N_{i.k}(t) = 0 + N_{i.k}(0)\, e^{-\int (A_{i.k} + \mathcal{L})\,dt} \tag{52}$$

If one assumes the lumped loss term $\mathcal{L}$ to be independent of time then one obtains a relaxation curve.

$$N_{i.k}(t) = N_{ik}(0)\, e^{-(A_{ik} + \mathcal{L})\,t} \tag{53}$$

Here it is clear that it will be impossible to extract the true natural life time from experimental data unless the laboratory parameters can be adjusted to see what effect they have on the relaxation curve.

By extrapolation one could possibly remove their dependence. Since the density of neutrals as well as almost every other term which might affect the losses increases with pressure one would expect the decay curve to fall away more rapidly at high pressure, hence a shorter life at high pressure would imply that losses other than photomission need to be considered.

Electron Excitation Without Cascading

In this case the original equation for $N_{i,k(t)}$ simplifies considerably. $N_{i,k(o)}$ will be considered zero.

$$N_{i,k}(t) = e^{-(A_{i,k}+\mathcal{L})t}\int_0^t \xi_{i,k}\, e^{(A_{i,k}+\mathcal{L})t}\,dt = \frac{\xi_{i,k}}{A_{i,k}+\mathcal{L}}\left(1 - e^{-(A_{i,k}+\mathcal{L})t}\right) \qquad 54)$$

Here it is clear that as one starts to bombard a ground state gas there is a build-up of states approaching a level $\xi_{i,k}/(A_{i,k}+\mathcal{L})$ after two or three relaxation times. Thus other things being equal the long lived states acquire larger densities with time.

To study the initial rate of build-up of a state one can expand the exponential and obtain the following term:

$$\lim_{t\to 0} \frac{\xi_{i,k}}{A_{i,k}+\mathcal{L}} = \left(1 - \left[1 - \frac{A_{i,k}+\mathcal{L}}{1!} + \frac{(A_{i,k}+\mathcal{L})^2}{2!} \cdots\right]\right) = \xi_{i,k} \qquad 55)$$

Equation 55) makes it clear that at t = o the rate of increase of a state is purely proportioned to its true impact parameter and independent of the decay rate of the state. The no-cascading assumption is valid here since at t=o there are no states to cascade into the state of interest. This gives a means of searching for the true $\sigma_{e\,i,k}$ values. The decay rate of the state, however, clearly determines the limiting state density, with fast transition states building up to a peak quickly, while slow ones build up as rapidly for equal cross sections but to much higher values.

Thus, an order of magnitude difference in the transition probability should give an order of magnitude difference in the state density acquired under steady state bombardment assuming the σ's are nearly equal and neglecting cascade contributions to state densities. The steady state photon intensity from each state should be proportional to the cross sections and independent of the transition probability under steady state conditions, provided cascading can be neglected.

In all the laboratory work on excitation cross sections known to the author the cascading terms are not taken into account so the result obtained is not the true impact cross section as defined in this work but the σ' cross section.

Derivation of Expression for Two Stage Cascading

If one takes the complete expression for N_i as found in equation 50) and then substitutes a similar expression into the cascading term and then again into the new cascading term one will have equation 57) shown on page 25 which is applicable to two stages of cascading. It is assumed that the terms in stage two are not fed by cascading as is seen by the zero in the parenthesis of the integrand of the (k) integral in equation 57).

In order to simplify equation 57) there are four useful identities which may be employed. They are as follows:

$$\frac{1}{e^{A_1 t}}\int_0^t e^{A_1 t}\,dt \equiv \frac{1}{A_1}\frac{1}{e^{A_1 t}}\left(e^{A_1 t}-1\right) \equiv \frac{1}{A_1}\left(1-e^{-A_1 t}\right) \qquad \text{56a)}$$

$$\frac{1}{e^{A_1 t}}\int_0^t e^{A_1 t}e^{-A_2 t}\,dt \equiv \frac{1}{A_1-A_2}\frac{1}{e^{A_1 t}}\left(e^{(A_1-A_2)t}-1\right) \equiv \frac{1}{A_1-A_2}\left(e^{-A_2 t}-e^{-A_1 t}\right) \qquad \text{56b)}$$

$$\frac{1}{e^{A_1 t}} \int_0^t e^{A_1 t}(1-e^{-A_2 t})dt \equiv \frac{1}{A_1}(1-e^{-A_1 t}) + \frac{1}{A_1-A_2}(e^{-A_1 t} - e^{-A_2 t}) \qquad \text{56c)}$$

notice sign change

$$\frac{1}{e^{A_1 t}} \int_0^t e^{A_1 t}(e^{-A_2 t} - e^{-A_3 t}) \equiv \frac{1}{A_1-A_2}(e^{-A_2 t} - e^{-A_1 t}) - \frac{1}{A_1-A_3}(e^{-A_3 t} - e^{-A_1 t}) \qquad \text{56d)}$$

c) and d) follow directly from a) and b) but they occur so frequently in the expansion of N that it is useful to write them out at this point.

It should also be pointed out that the operators $\sum$ and $\int$ are commutative with each other and that they are both distributive over sums of terms.

In order to save space $N_{i,k}(o) \equiv N_i'$ and of course $A_i \equiv A_{ij} \equiv \sum_{j<i} A_{i,k,j,l}$ where $j < i$ means all j's with less energy than i.

If other losses enter the problem then a loss term must be added to A_i as can be seen in equation 53) for example.

$$N_i = \frac{N_i'}{e^{A_i t}} + \frac{1}{e^{A_i t}} \int_{0\,(i)}^{t} e^{A_i t}\left(\xi_i + \sum_j A_{j,i}\left[\frac{N_j'}{e^{A_j t}} + \frac{1}{e^{A_j t}} \int_{0\,(j)}^{t} e^{A_j t}\left(\xi_j + \sum_k A_{kj}\left[\frac{N_k'}{e^{A_k t}} + \frac{1}{e^{A_k t}} \int_{0\,(k)}^{t} e^{A_k t}(\xi_k + 0)\,dt\right]\right)dt\right]\right)dt \qquad 57)$$

by distributive law of operators one can now expand the expression and by the associative law of sums collect all terms having N's and those which have ξ's.

$$N_i = \left\{\frac{N_i'}{e^{A_i t}} + \sum_j A_{ji} \frac{1}{e^{A_i t}} \int_0^t e^{A_i t} N_j' e^{-A_j t} dt + \sum_j A_{j,i} \sum_k A_{kj} \frac{1}{e^{A_i t}} \int e^{A_i t} \frac{1}{e^{A_j t}} \int e^{A_j t} N_k e^{-A_k t} dt\,dt\right\}$$

$$+ \left[\frac{1}{e^{A_i t}} \int_0^t e^{A_i t} \xi_i\, dt + \sum_j A_{ji} \frac{1}{e^{A_i t}} \int_0^t e^{A_i t} \frac{1}{e^{A_j t}} \int_0^t e^{A_j t} \xi_j\, dt\,dt + \sum_j A_{ji} \sum A_{kj} \frac{1}{e^{A_i t}} \int_0^t e^{A_i t} \frac{1}{e^{A_j t}} \int_0^t e^{A_j t} \frac{1}{e^{A_k t}} \int_0^t e^{A_k t} \xi_k\, dt\,dt\,dt\right] \qquad 58)$$

The upper expression generates the function which governs the decay of states if there is no electron impact while the remainder of the expression gives the build-up of states if there are no excited states at t = o. Both will be needed if neither of these conditions hold however. The advantage of this form for the expression is that one may keep all of the terms from each stage of cascading lumped together and if it is desirable to only consider a single stage of cascade the last double sum term may be dropped all together. It also gives a method of recognizing the form for an n stage cascade formula.

Since $N = G(N_i', N_j', N_k') + F(\xi_i, \xi_j, \xi_k)$ one may carry out the expansion using identities 56 a) b) c) d) to assist.

$$G(N_i N_j N_k) = \frac{N_i'}{e^{A_i t}} + \underbrace{\sum_j A_{ji} \frac{1}{e^{A_i t}} \int_0^t e^{A_i t} N_j' e^{-A_j t} dt}_{\downarrow} + \underbrace{\sum A_{ji} \sum A_{kj} \frac{1}{e^{A_i t}} \int_0^t e^{A_i t} \frac{1}{e^{A_j t}} \int e^{A_j t} N_k' e^{-A_k t} \, dt\, dt}_{\sum A_{ji} \sum A_{kj} \frac{1}{e^{A_i t}} \int_0^t e^{A_i t} N_k' \left(\frac{e^{-A_k t} - e^{-A_j t}}{A_j - A_k} \right) dt} \qquad 59)$$

$$G(N_i N_j N_k) = \underset{\text{Spontaneous Emission}}{N_i' e^{-A_i t}} + \underset{\text{stage one cascade}}{\sum_j A_{ij} N_j' \left(\frac{e^{-A_j t} - e^{-A_i t}}{A_i - A_j} \right)} + \underset{\text{stage two cascade}}{\sum_j A_{ji} \sum_k A_{kj} \frac{N_k'}{A_j - A_k} \left(\frac{e^{-A_k t} - e^{-A_i t}}{A_i - A_k} - \frac{e^{-A_j t} - e^{-A_i t}}{A_i - A_j} \right)} \qquad 60)$$

The expansion of $f(\xi_i \xi_j \xi_k)$ will be found on the next page.

$$f(\xi_i,\xi_j,\xi_k)=\frac{1}{e^{A_it}}\int e^{A_it}\xi_i\,dt+\left\{\sum A_{ji}\frac{1}{e^{A_it}}\int e^{A_it}\frac{1}{e^{A_jt}}\int e^{A_jt}dt\,dt\right\}+\left[\sum A_{ji}\sum A_{kj}\frac{1}{e^{A_it}}\int e^{A_it}\!/e^{A_jt}\int e^{A_jt}\!/e^{A_kt}\int e^{A_kt}\xi_k\,dt\,dt\,dt\right] \quad 61)$$

USING (56a) (56a) (56a)

$$f(\xi_i,\xi_j,\xi_k)=\underline{\frac{\xi_i}{A_i}\left(1-e^{-A_it}\right)}+\left\{\sum A_{ji}\frac{1}{e^{A_it}}\int e^{A_it}\frac{\xi_j}{A_j}\left(1-e^{-A_jt}\right)dt\right\}+\left[\sum A_{ji}\sum A_{kj}\frac{1}{e^{A_it}}\int e^{A_it}\!/e^{A_jt}\int e^{A_jt}\frac{\xi_k}{A_k}\left(1-e^{-A_kt}\right)dt\,dt\right]$$

(56c) (56c)

$$+\underline{\left\{\sum_j\frac{A_{ji}}{A_j}\xi_j\left(\frac{1-e^{-A_it}}{A_i}+\frac{e^{-A_it}-e^{-A_jt}}{A_i-A_j}\right)\right\}}+\left[\sum A_{ji}\sum A_{kj}\frac{1}{e^{A_it}}\int e^{A_it}\frac{\xi_k}{A_k}\left(\frac{1-e^{-A_jt}}{A_j}+\frac{e^{-A_jt}-e^{-A_kt}}{A_j-A_k}\right)\right]$$

(56c) (56d)

$$+\underline{\sum A_{ji}\sum A_{kj}\frac{\xi_k}{A_k}\left[\frac{1}{A_j}\left(\frac{1-e^{-A_it}}{A_i}+\frac{e^{-A_it}-e^{-A_jt}}{A_i-A_j}\right)+\frac{1}{A_j-A_k}\left(\frac{e^{-A_jt}-e^{-A_it}}{A_i-A_j}-\frac{e^{-A_kt}-e^{-A_it}}{A_i-A_k}\right)\right]}$$

$$f(\xi_i,\xi_j,\xi_k)=\frac{\xi_i}{A_i}\left(1-e^{-A_it}\right)+\sum\frac{A_{ji}}{A_j}\xi_j\left(\frac{1-e^{-A_it}}{A_i}+\frac{e^{-A_it}-e^{-A_jt}}{A_i-A_j}\right)+$$

$$\sum A_{ji}A_{kj}\frac{\xi_k}{A_k}\left[\frac{1}{A_j}\left(\frac{1-e^{-A_it}}{A_i}+\frac{e^{-A_it}-e^{-A_jt}}{A_i-A_j}\right)+\frac{1}{A_j-A_k}\left(\frac{e^{-A_jt}-e^{-A_it}}{A_i-A_j}-\frac{e^{-A_kt}-e^{-A_it}}{A_i-A_k}\right)\right] \quad 62)$$

$f(\xi_i,\xi_j,\xi_k)$ is the sum of the heavily underscored terms.

A review of equation 60) and 62) shows that the first terms are just the terms one would expect without cascading. Namely

$$N_i(t) = N_i(0)\, e^{-A_i t} + \frac{\rho_i}{A_i}\left(1 - e^{A_i t}\right) \tag{63}$$

as was found in equation 53) and 54).

Simple One Stage Cascade With Single Cascade Level

Next, one might consider a very special cascade case in which one term so dominates the cascading that all other terms may be dropped. One must retain the first cascade term in equation 60) and 62) and obtain the following form after dropping the summation sign.

$$N_i(t) = N_i' e^{-A_i t} + \frac{\rho_i}{A_i}\left(1 - e^{-A_i t}\right) + A_{ji} N_j' \left(\frac{e^{-A_j t} - e^{-A_i t}}{A_i - A_j}\right) + A_{ji} \frac{\rho_j}{A_j}\left[\frac{1 - e^{-A_i t}}{A_i} + \frac{e^{-A_i t} - e^{-A_j t}}{A_i - A_j}\right] \tag{64}$$

In the experimental arrangement employed both N_i and N_j are zero before the excitation step is applied. After the step is applied the state densities build up according to the terms involving ρ_i in equation 64). Since the step function is quite long compared to the mean lives of the states being observed one has

$$t_{cutoff} \gg \frac{1}{A_i} \text{ and } \frac{1}{A_j}. \tag{65}$$

Applying this condition to 64) one finds the final state density at the time of cutoff to be

$$N_i = \frac{\rho_i}{A_i} + \frac{\rho_j}{A_i A_j}\left(A_{j,i}\right) \tag{66}$$

Assuming N_j to have no cascade component one has

$$N_j = \rho_j / A_j \tag{67}$$

These values may now be used as the N' values for the cut off condition.

After cut off only the terms containing N' are nonzero in equation 64) and one has by substitution of 66) and 67) into 64) the following expression.

$$N_i = \left(\frac{\xi_i}{A_i} + \frac{\xi_j}{A_i A_j} A_{ji} \right) e^{-A_i t} + A_{ji} \frac{\xi_j}{A_j} \left(\frac{e^{-A_j t} - e^{-A_i t}}{A_i - A_j} \right) \qquad 68)$$

$$N_i = \frac{\xi_i}{A_i} e^{-A_i t} + \frac{A_{ji} \xi_j}{A_j} \left(\frac{e^{-A_i t}}{A_i} + \frac{e^{-A_j t} - e^{-A_i t}}{A_i - A_j} \right)$$

After finding the common denominator for the expression in the parenthises one has

$$N_i = \frac{\xi_i}{A_i} e^{-A_i t} + \frac{A_{ji} \xi_j}{A_i A_j (A_i - A_j)} \left(A_i e^{-A_j} - A_j e^{-A_i t} \right)$$

$$N_i = \left(\frac{\xi_i}{A_i} - \frac{A_{ji} \xi_j}{A_i (A_i - A_j)} \right) e^{-A_i t} + \left(\frac{A_{ji} \xi_j}{A_j (A_i - A_j)} \right) e^{-A_j t}$$

Now remembering that $I^* = N_i A_i$

one has

$$I^* = \left(\xi_i - \frac{A_{ji} \xi_j}{A_i - A_j} \right) e^{-A_i t} + \left(\frac{A_i}{A_j} \frac{A_{ji} \xi_j}{A_i - A_j} \right) e^{-A_j t} \qquad 69)$$

In this expression $\xi_i = \sigma_{ei} N_e N_a V_e$,

$\xi_j = \sigma_{ej} N_e N_o V_e$ and $A_i = \sum_j A_{ij}$.

It should be pointed out that the final expression for the differential equation governing state densities was derived on the basis of no wall effects. This was a valid assumption for very fast decay components. Under circumstances where this does not hold true the wall effects show up in the equation as a diffusion term of the form $D\nabla^2 N$; where D is the diffusion coeffecient. Under these circumstances one has the general expression from the <u>Handbuch der Physik</u>[20] in the following form.

$$\frac{\partial N_j}{\partial t} = D_j \nabla^2 N_j + B_{oj}\, \rho_{oj}\, N_a - A_j N_j + \sum A_{kj} N_k + P \qquad 70)$$

Here P is the lumped production term which might find its cause in something other than electron impact under other experimental conditions than those employed in this laboratory.

<u>Transition Probabilities in Helium</u>

Since helium is the gas being studied in this experiment it will be informative to consider the trends in transition probabilities as one goes to higher N values in helium. The discussion will center on the data on helium found in Landolt-Bornstein Tables.[21]

The transition probabilities are not given directly but must be extracted from the oscillator strength and the wave length data

---

[20] R. G. Fowler, "Radiation From Low Pressure Discharges" <u>Handbuch der Physik</u> (ed.) Flugge, XXII, (1956).

[21] <u>Op. Cit</u>.

using the formula given in the National Bureau of Standards Monograph.[22] It is as follows

$$A_{i,j} = f_{j,i} \frac{g_j}{g_i} 6.65 \times 10^{15} / \lambda^2_{ij} \qquad 71)$$

here the g's are the statistical weights which are $2(l+1)$ for singlets and $3(2l+1)$ for triplets where l is the angular momentum quantum number.

The $A_{i,j}$'s tend to diminish as i increases. This is best seen by taking the formula for $f(2,n)$ given for the transition from h^3p state to the 2^3S.

$$f_{2,n} = 1.695 \times 10^{30} \lambda^2 / c^2 n^3 \qquad 72)$$

Substituting 72) into 71) one has

$A_{n.1,20} = K/n^3$. Here it becomes quite clear that the $A_{i,j}$'s fall off very rapidly as n increases. The total transition probability $A_i = \sum_j A_{i,j}$ also falls off rapidly with increasing n. Although there are essentially 2 n states lower than the nth state which must be added in order to find A_i, the $\frac{1}{n^3}$ dependence of the A_{ij}'s dominates this greater number of contributing terms and A_i falls off at least as fast as $\frac{1}{n^2}$. Since $\tau_i = \frac{1}{A_i}$ the state lifetime therefore increases at least as fast as n^2 for large n and more than likely will have more nearly an n^3 dependence since transition to the lower levels tend to dominate the rest of the 2n accessible states in spontaneous emission loss rates. This fact alone implies that the cascading

---

[22] Op. Cit.

contribution will be small from upper n values when the excitation source is of a short time duration.

It seems appropriate to discuss trends in excitation at this point, since this too will govern the cascading contribution at lower levels. The rigid selection rules which hold for photon interaction are somewhat relaxed for electron interaction. Thus the $\Delta l = \pm 1$ selection rule expresses a trend but not a fixed law in electron excitation. From this one would expect the P states to be populated more densely than S or D states by impact. The application of Bohr's correspondence principle implies that the state density distribution will fan out over large l values as the energy levels approach the continuum, however.

With this background it will be possible to proceed to the actual experiment and its interpretation.

CHAPTER II

EXPERIMENTAL APPARATUS

Design Considerations

During the early literature search the author became aware of the need for direct determination of the true relaxation curves. At the same time it became obvious that a completely new type of research apparatus would be needed in order to accomplish this.

The experimental apparatus envisioned by the author employed the most direct method possible. It would require an excitation source which could be cut off very quickly compared with the relaxation time of the atomic state being observed, a means of detecting the state density, and some means of recording the density-time information.

To obtain some idea of the requirements on the apparatus a search through Landolt-Bornstein[23] showed that theory predicted many atomic states with 10^{-8} sec and longer natural lifetimes. Helium had several states in this category which were also in the visible range of photomultipliers. This along with the knowledge of excitation cross sections and other pertinent information on helium led to the

[23] *Op. Cit.* 15. 261-264 for Helium.

selection of it as the gas to be used in the feasibility study. It was also to be the first gas studied but the design of the apparatus was to be left as flexible as possible for the study of as many gases as would be compatible with the excitation tube.

The 10^{-8} sec lifetimes to be observed dictated an approximate time resolution of 10^{-9} seconds. Since the shorter lifetimes can be obtained by line profile studies it was felt that this resolution time would make the long lived states electronically accessible while the short lived states would be accessible to optical means with the hope of enough overlap in accessibility to make a consistency check between the two methods.

The work of R. F. Post[24] on pulsed photomultipliers indicated that the 931A operated at around 4000 volts for 2μ-sec could produce a large enough anode charge burst from a single cathode electron to be displayed and photographed on an oscilloscope. The burst half width was approximately 0.5×10^{-9} sec. This one article indicated that both photomultiplier and oscilloscope time resolution used in experimental work at that time would just fall within the specified 10^{-9} sec time resolution requirement.

With this in mind an excitation source with a 10^{-9} sec cutoff time was needed. Only two modes of efficient excitation with this cutoff time appeared to be electron bombardment and photoexcitation employing Kerr shutters for cutoff. Since photoexcitation is only applicable to resonance radiation the use of electron impact excitation could lend more flexibility to a system employing this mode of

---

[24] _Op. Cit._ 16.

excitation. Unfortunately the flight time of 100 ev. electrons through one centimeter of gas is of the order of 3 n-sec (nanosecond or 10^{-9} sec) and the light intensity required to give good statistics on the oscilloscope display would not allow the use of much smaller dimensions. Thus, if one employs the ultimate in modern electronic techniques the electron flight time dictates the limit in time resolution that may be attained. With the decision to use electron impact excitation a source had to be designed. Feasibility studies showed that there was a reasonable chance of obtaining usable data if around 5 amperes of current could be produced in the excitation zone.

Early Development

Once the general scheme for instrumentation was settled the work concentrated on the oscilloscope design. This decision was governed by a need for a fast oscilloscope and for the development of other fast electronic circuits. By the time an inflexible but fast oscilloscope was developed and a complicated photographic technique for recording traces was devised a much more flexible and more sensitive instrument was available on the market with essentially the same rise-time characteristic. It is the Tektronix 519 employing a 10 v/cm and .3 n-sec rise-time traveling wave cathode ray tube. It was purchased and used in taking some of the data on alignment. This was not the only change in plans which evolved over the years as will be seen.

The combined requirements of 5 amperes and fast cutoff grid action in the excitation tube seemed to require a coaxial construction with a large external cathode. The cathode was to emit electrons inward into an excitation zone to be observed from the end of the

cylinder. The size of the cathode capable of producing the high emission current seemed to need around 500 watts heater power to make up for radiation losses and thermal conduction at water cooled supports. A great deal of time was spent building the elements of a prototype excitation tube having only a few volts on the heater to avoid arc-over to other tube elements. The entire design had to be abandoned when the special order kovar glass was depleted before a workable tube could be built. At that time Dr. P. F. Little, visiting professor from Oxford University, suggested that the external cathode allowed the use of an induction heater. This eliminated many glass to metal seals and simplified the tube design immeasurably. A 1.0 kilowatt Ther-Monic induction Heater was purchased and after some adaptation was found to work quite satisfactorily as a cathode heater.

Another consideration was the excitation tube step function bias signal generator. The excitation source needed to be cut off in approximately 10^{-9} seconds if it was not to affect the time resolution of the system. It was decided that a coaxial line feeding the cylindrical grid system of the excitation tube would be needed in order to be certain of the signal rise-time inside the glass envelope. The geometry of the excitation zone and high current cathode set the characteristic impedance of the grid structure at 19 ohms. Since reflections were to be kept at a minimum the external bias source generator had to have an impedance of nearly the same value. This low impedance, 10^{-9} sec rise-time, and 100-v bias signal requirement seemed to allow but one choice of bias signal switch,[25] the coaxial relay employing metal to metal

[25] I. D. Lewis and F. H. Wells, Millimicrosecond Pulse Techniques, p. 102, (McGraw-Hill, 1954).

contacts with its inherent jitter and slow operation.[26]

A vacuum enclosed coaxial mechanical relay was finally built which, with appropriate electronic timing circuits, could be synchronized to hit within a 2μ-sec time interval about 50% of the time. This time interval was dictated by the 2μ-sec on-time of the pulsed photomultiplier which was to observe the decay of light. The coaxial relay did not give consistent rise-time signals on each closure, so a thyratron bias circuit was devised having a $5\ \mu$-sec rise-time for the purpose of equipment alignment. Since this loss in time resolution was less than the true cut off time of the plasma filled excitation tube it did not affect the time resolution of the present design and this new slower rising but consistently operating bias step generator was therefore used for the cutoff switch in the final system. The use of this circuit also reduced the number of timing circuit elements considerably, a point greatly appreciated in any research work.

The details of the equipment designed for this system will now be given. The electronic circuitry will be discussed in a separate chapter, however.

---

[26]The Tektronix 519 has a gate generator capable of .5 n-sec rise-time employing an avalanche transistor. This possibility seems worthy of careful consideration for future development. Unfortunately to the author's knowledge only low voltage pulses of the order of 20V have been produced with this technique while about 4 times that amount is required in our present equipment. Series operation might well be possible with avalanche transistors but the finding of transistors which will give .5 n-sec avalanches is extremely unpredictable at this time. Further search into this was put off for future study.

The Excitation Tube

Principles of Construction

Since the excitation tube constitutes the heart of the experimental apparatus and is wholly original with this experiment it might prove useful to discuss the design, construction, and theory of operation in more detail than was felt necessary with other elements of the instrumentation.

As was pointed out in the previous chapter, the demand for enough light flux to produce a relatively smooth relaxation curve instead of statistical noise, has forced this study into the use of a high current and optimum optical geometry. The geometry is made clear in Figure 2. The design and construction of the excitation tube are now given in some detail.

The cathode electrode was machined from manganese free electrolytic nickel bar stock, and was out-gassed for several days at bright red heat with continuous pumping. There was an apparent diffusion of gas molecules entrained in the metal which eventually were exhausted to a sufficient extent to produce no objectionable contamination of the gas under study. After outgassing, the nickel metal was cooled; then the envelope was opened so the cathode could be fitted with shutters, painted, and mounted in the excitation tube. The cathode did not absorb gasses into its structure to any great extent at room temperature and quickly outgassed when assembled into the final tube again.

In order to avoid appreciable darkening of the window at the end of the excitation chamber during the activation process it was

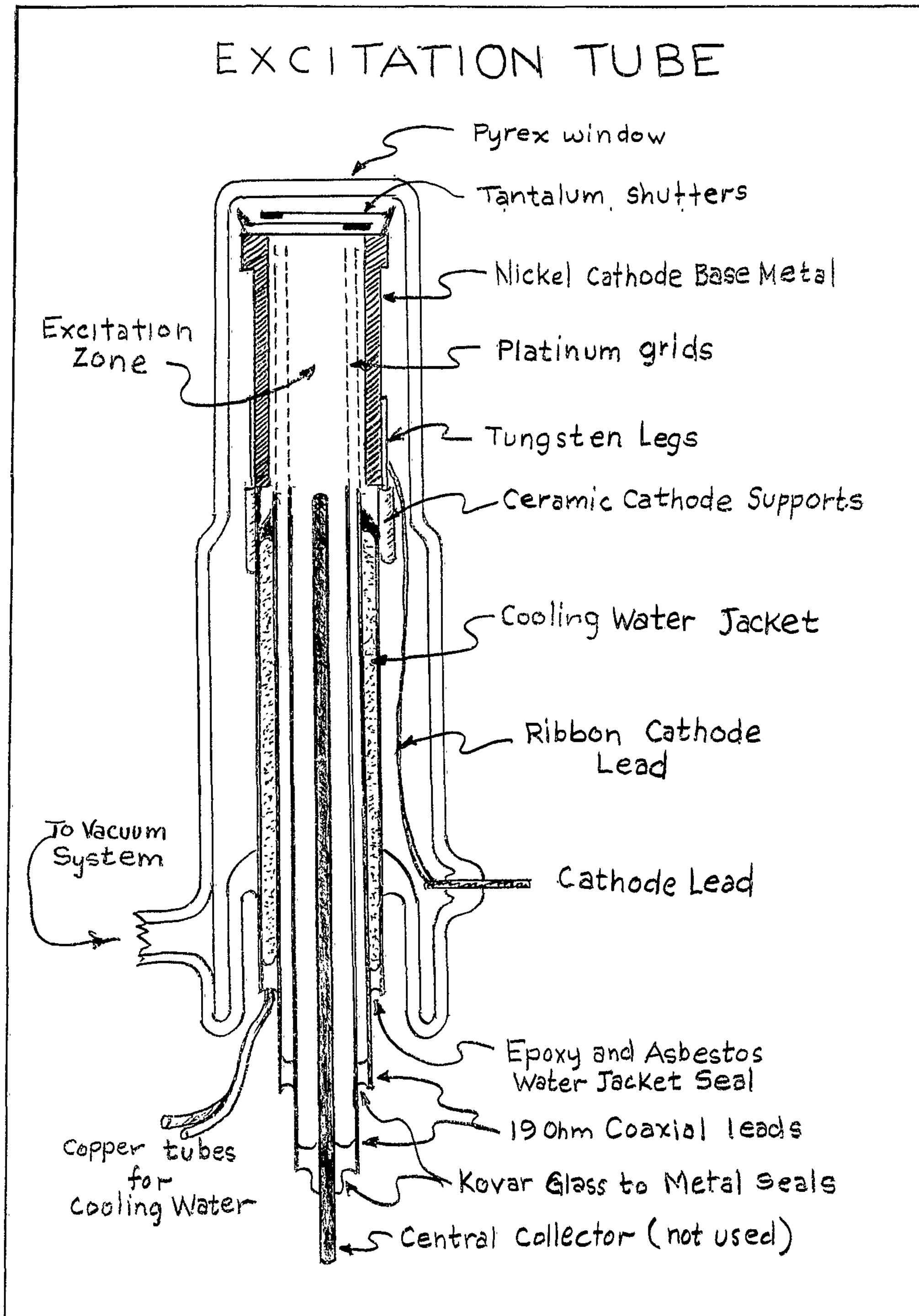
EXCITATION TUBE
Pyrex window
Tantalum shutters
Nickel Cathode Base Metal
Excitation Zone
Platinum grids
Tungsten Legs
Ceramic Cathode Supports
Cooling Water Jacket
Ribbon Cathode Lead
To Vacuum System
Cathode Lead
Epoxy and Asbestos Water Jacket Seal
19 Ohm Coaxial leads
Copper tubes for Cooling Water
Kovar Glass to Metal Seals
Central Collector (not used)

Figure 2

found necessary to employ tantalum shutters. The use of tungsten, molybdenum and stainless steel were tried. The brittleness if tungsten made it very hard to handle after being heated. Molybdenum tended to darken the window as badly as the cathode vapors (but with a different color). Stainless steel also darkened the window but has the additional property of melting down over the grid structure making it difficult to maintain an open circuit between grids and other elements, a condition found detrimental to proper operation (in the extreme).

Although tantalum became slightly brittle when heated it did not shatter as tungsten did and it showed no appreciable evaporation when heated. In order to open these shutters after cathode activation was completed nickel magnetic pulls were spot welded to the underside of the shutters. Thus they could be manipulated with an external magnet. A tantalum iris diaphragm was also spot welded to the top of the cathode to reduce the deposition of nickel vapor from the cathode onto the window. This iris also served to collimate the light from the excitation zone.

In order to prepare the cathode for the barium compound it was etched in nitric acid, carefully washed in distilled water and dried with clean acetone. After drying the inner surface was painted with one thin coat of barium compound. Before application this paint had been tumbled until thoroughly mixed. The paint survived long periods of contact with air prior to activation, but normally the cathode was not painted until other elements of the tube were prepared.

The first grids were made of nickel mesh but after the first tube was opened the grids crumbled as though the gases given off in

cathode activation had reacted with them converting them to nonmetalic compounds. The next grids were made of platinum mesh .004 inch diameter wire with 52 wires to the linear inch. They were formed over aluminum mandrels and spot welded to the coaxially mounted kovar metal tubes. Special care was taken to preserve the diameters of the coaxial surfaces carrying the grid signal into the tube.

Although kovar and kovar-sealing-glass were used in construction of the coaxial system it was impossible to inspect some of the interior glass seals. When they were found to leak a coating of epoxy or glyptal produced the desired vacuum. Later very slow leaks developed due to cracking of these materials. The application of a silicone grease coating produced a self healing seal over these microscopic cracks.

Before the final model of the induction heated excitation tube was built it was found that water cooling would be necessary to avoid costly repairs in the cracked glass. Thus the final design incorporated a kovar water jacket surrounding the outer conductor of the coaxial grid leads. The water tubes were cemented in place with epoxy and asbestos. The asbestos provided the body to prevent the epoxy from running into the water jacket (the tube was inverted during the construction operation).

Since the rise-time on the excitation source was not critical a simple external cathode lead was employed.

In the final assembly of the excitation tube ceramic tubes were used as grid spacers. A wire was run through the cermic tubes and spot welded at each end in order to mount them. Since the grid to grid spacing was not so close, only end spacers were required.

The massive cathode had to be mounted rigidly to the water

jacket but electrically insulted from it. To accomplish this, ceramic tubes were salvaged from television picture tube electron guns. These ceramic tubes were already fitted with tight fitting metal sleeves which could be spot welded to the water jacket. Then tungsten inserts were etched in sodium nitrite until they fit into the ceramic sleeves. After insertion into the ceramic sockets these tungsten rods were spot welded to the nickel cathode employing metal straps cut from the television tube elements. A band of kovar glass with metal tabs in it was used to anchor the cathode securely in this slip-fit mounting. To accomplish this, nickel wires were spot welded to the cathode and to these tabs.

The glass envelope which had been sealed, checked for leaks, and cracked open to allow the completion of the tube interior was now ready to reseal. A special precaution was needed in resealing the completed tube. It was the use of water cooling during the final seal. The author resealed the original envelope three times successfully but nine months later when the cathode was ruined by a vacuum system breakdown the tube was completely demolished because the cooling water was not used during the resealing process.

The activation process was not always carried out according to a fixed schedule, but it normally consisted of a slow baking out for several hours followed by cathode pulsing during a brief period of intense heating at full power from the induction heater. When the activation temperature was reached the cathode emitted full value very quickly with about 4 amperes initial emission. After approximately a day of continuous pulsing the current stabilized at approximately 2 amperes total cathode emission. Over the months of operation, occasionally the liquid air trap would warm up and the cathode would

be poisoned. In each case an extended period of reactivation of two or more hours of pulsing at high temperatures restored the cathode to approximately 90% of its previous emission current. When the vacuum system was opened to the air, however, the cathode could not be restored even after pulsing all night at elevated temperatures.

Theory of Operation of the Excitation Tube

Before discussing the operation of the excitation tube it might prove useful to tabulate basic geometrical and electrical properties of the tube along with some physical properties of helium under the operating conditions. These values will hold to slide rule accuracy within the limits of the assumptions used in deriving them while the assumptions might be in error by 5% or 10% in some cases. For example the cathode temperature cannot be measured accurately since any glass viewing window facing the cathode has been darkened by metal vapors from the cathode. Another example is the use of mere geometrical opacity of the grid structure to compute the fraction of electrons which succeed in entering the excitation zone. These figures would be accurate so long as the cathode to grid fall space is much larger than the grid wire spacing. At high current, however, the virtual cathode might be moved to a position quite near the grid invalidating this criterion altogether. The figures are intended only to convey an impression as to how the tube functions without being accurate enough for detailed computation.

Geometrical Constants

L = length of cathode = 5 cm

D_c = diameter of cathode = 2 cm

A_c = area of cathode = 31.4 cm^2

D_1 = diameter of grid 1 = 1.76 cm

D_2 = diameter of grid 2 = 1.27 cm

A_2 ≅ area of grid 2 = 20 cm^2

Percent geometrical opening in grids mesh 67%
based on .004" wires at 1/52" spacing.

Percent geometrical opening for both grids 45%

Electric and Atomic Parameters

I_c = cathode current = 2 amperes

I_2 = inward component of current at grid 2 = I_c 45% = .9 amperes

I_{ex} = total impact current = 2(.9) = 1.8 amperes

this is because all electrons entering must also leave the central zone hence they have a possibility of impact on both radially inward and radially outward paths.

N_o = atom density at 1torr 273°K = 35.6 x 10^5 atom/cc

V_e = electron velocity for 100_{ev} electrons = 4.19 x 10^8cm/sec

T = flight time for electron D_2/V_e = 3.04 n-sec 100 volt electron
4.3 n-sec 50 volt ele ctron
6.08 n-sec 25 volt electron

V_I = ion velocity at 100_{ev} = $4.19(1/4(1836)^{\frac{1}{2}}$ = 5 x 10^6 cm/sec

V_o = mean thermal velocity 1100°K = 2.4x10^5 cm/sec

$\mathcal{E}$ = Ionization efficiency at 100v . for helium and 1 Torr = 1.245/electron-cm

$\frac{dIon}{dt}$ = ions produced per second at 100v and 1 Torr =

$$\frac{\mathcal{E}\, I_2 D_2}{e} = .88 \times 10^{19}$$

F = fraction of atoms ionized in one microsecond = $\frac{1}{4000}$

in this experimental arrangement $F = \frac{dI/dt \times 10^{-6}}{N_o}$

The probability of a single atom being ionized in 1 sec = $\frac{1}{4000}$ = F

Basic Data on the Gas at Operating Temperatures and Pressures is given below.

$T = 1100°K.$

P	1mmHg	.13mmHg	.092mmHg	.057mmHg	.04mmHg
λ_{oo} mean free path for H_e atoms in its own gas	.855mm	6.5mm	9.3mm	15.mm	22.5cm mm
N_a	35.33×10^{15}	1.14×10^{15}	$.81\times10^{15}$	$.502\times10^{15}$	$.334\times10^{15}$

The method of operation of the excitation tube is as follows. The cathode is driven negatively with respect to the grounded space charge grid. The cathode drive-pulse is a square wave 5 μ-sec in duration and 100 volts in amplitude. This pulse drives approximately two amperes of cathode current into the grid system. Of this two amperes only 45% actually get through the grid structure into the excitation zone.

The inner grid runs nearly 20 volts negative with respect to the space charge grid because of the IR drop created by the electrons it intercepts from the excitation beam. After the cathode has been turned on for several tenths of a microsecond the plasma necessary for the operation of the tube is built up in the central zone and the electrons can then penetrate the excitation region and a constant excitation rate follows. A model of the build up of this plasma condition is as follows. When the cathode is driven negatively, approximately .9 amperes of current enter the excitation region. But due to space charge effects these electrons are at first turned back into the grid system before they penetrate the empty space even one millimeter. The argument is carried out in Appendix IV. During the time these electrons make this small penetration they produce some ionization. These ions partially cancel the space charge of the beam electrons allowing the next electrons to penetrate more deeply. These in turn produce ions which allow still further electron penetration into the central zone. This may be thought of as a wave front of ionization progressing forward at a rate depending upon how rapidly ions can be created. The electrons creating the front run up from behind the front creating ions ahead of it before their motion is reversed by their own space charge. Thus the propagation of the front does not require motion of the ions themselves but only their

ability to allow electron penetration more deeply into this central zone.

At the low pressure end of the operating range the ions are created so infrequently because of the low neutral particle density that ion diffusion enhanced by the electron field ahead of the front may aid in the slow propagation of this wave through the view space under these conditions.

Once the entire central zone has enough ions within it to neutralize the space charge effects of the beam electrons a static potential is built up within the plasma. This static positive potential is just great enough to trap the slow speed electrons produced by the continuing ion creation processes within the plasma.

The excitation tube light output is essentially proportional to pressure in the operating pressure range of the apparatus. At the low pressure end of the range the light entensity falls off much more rapidly than linearly with pressure.

There is both experimental as well as theoretical evidence that this loss of light intensity is due to the inability of the current to build up enough ion concentration in the 1.5μ-sec excitation time to allow full penetration of the beam current into the central zone. The experimental evidence is that the light output-vs-time curve seen by the photomultiplier is increasing with time at the low pressure end of the operating range. This indicates that the steady state conditions have not been met at the time the photomultiplier is turned on. This light intensity-vs-time graph is flat in the upper pressure range.

The theoretical considerations involve the calculation of the number of ions created within the time interval of excitation. Because of the lack of knowledge of the actual build up pattern for the ion

cloud only order of magnitude calculations can be made. When they are carried out, however, they show that at the low pressure end the number of ions created is essentially the same as the number of electrons they must neutralize, justifying the assumption that the low pressure end of the operating range should require a longer excitation time in order to reach full light intensity.

To summarize, the steady state picture of the excitation zone is as follows: There are still far more neutral ground state atoms than any other species at the end of a microsecond. (See page 44 for this calculation.) Along with these neutral atoms is a radial distribution of 100ev beam electrons, a cloud of ions which is increasing in density, and a cloud of low energy electrons whose density accurately follows the ion density. Within this central plasma zone there can be no extended electric field since the electron cloud can quickly adjust to neutralize any field producing charge. There must be a radial field very near the grid which prevents the escape of slow electrons, however. This radial field is supplied by an ion sheath at the edge of the plasma which establishes ambipolar diffusion conditions for the escape of charged particles from the central zone. Since thermal velocities (2.4×10^5 cm/sec) will not allow much displacement of the ions in 1.5μ-sec, diffusion is neglected in this discussion. If longer excitation times are used at low pressures the thermal diffusion of ions from the central zone will be an important factor.

Theory of Electron Beam Cut Off

The existance of the ions which are required for the neutralization of beam electrons in the central zone complicates the cut off mechanism somewhat. In order to visualize the way in which this is accomplished one must consider the conditions outside the bias grid just prior to cut off.

Remembering that the cathode to space-charge grid has a high field strength the ions are swept out almost as fast as they are created in this high field zone. This means that a vacuum like picture will suffice in this cathode to space-charge grid region. Between the space-charge grid and the cut off grid is a zone which is about 2.5mm thick which is essentially field free. Therefore within this zone the ionization rate is essentially the same as it is within the field free excitation zone. When the bias signal is applied to the inner grid these ions must be swept out before the grid can gain full control. In the operating pressure range of around .03 to .06mm of Hg this ion cloud does not seem to affect the cut off time for the excitation source.

At higher pressures however there is a slight delay before the triplet excitation is cut off. This is not so obvious with the singlet excitation however. This is believed to be due to incomplete cut off caused by ions near the cut off grid. The different effect on singlet and triplet states under identical experimental conditions is believed to be due to the difference in the excitation function for these two different states. A study by Corrigan and von Engel[27] shows the triplet

---

[27]S. J. B. Corrigan and A. von Engel, Proc. Phys. Soc. 72, 786-790 (1958).

excitation cross section as having a peak very near its onset potential while singlet excitation rises rather slowly near the onset potential and peaks at a much higher excitation energy. With this in mind one can imagine that at high pressure the presence of ions near the grid mesh does not allow the potential to drop to complete cut off but rather allows electrons to pass with much lower kinetic energy than before. This then drops the singlet excitation to a small fraction of its former value while it actually enhances the triplet excitation. This then accounts for an actual rise in light output on the high pressure triplet curves while an immediate fall is observed for the singlet excitation under the same experimental conditions. A careful study of the delay between the bias signal shown on the bottom of each photograph with the onset of the light signal decay bears this out. See figures 15, 16, and 17 on pages 82 to 84.

To reassure the reader that a change in experimental conditions was not the cause of the difference between the delay observed on triplet and the singlet curves it is well to point out that the data taken during a constant pressure sequence was taken according to increasing or decreasing wave length of the light being studied. This resulted in taking the data for both singlet lines between the data taken on the 5876Å triplet line and the other triplet lines being studied. There is obvious consistency between the apparent delay in cut off shown in the 5876Å data and the delay observed on the other triplet data curves at high pressure. Appendix VI on experimental procedure provides the reader with information on the sequences used in taking data and observations made concerning the operation of the equipment at that time.

The Photomultiplier

The photomultiplier was a selected 931A which was chosen for its qualities of stability and high current output. A more sensitive tube was broken during the design of a vacuum cooling unit.

The output signal of the present tube increased rapidly with power supply pulse potential above 2000 volts. The highest stable operation seemed to be at 3500 volts although there was almost no tendency to arc over even at 4500 volts. The entire photomultiplier tube was fitted with a foil shield connected to the cathode lead as was suggested by R. F. Post.[28] This unit was inserted into a copper sleeve. (See figure 13 page 78 for geometrical details). The sleeve had been silver soldered to the end of a liquid air tube which ran into the vacuum chamber. This provided liquid air cooling in the hope of reducing the apparent tail on the light signal. The tail was believed to be the result of false counts created by vapors in the 931A dynode region. There was no apparent change in the signal before and after the liquid air was applied as was shown by an overlay of oscilloscope traces on a single film. Since the vacuum chamber had been properly positioned over the excitation tube and had all of the electrical connections made within it, it was used as a mounting socket without cooling for the taking of subsequent data.

It should be pointed out that other photomultiplier tubes have far better cathode efficiencies than the 931A. To the author's knowledge these tubes have never been used in pulse operation. Without

---

[28] Op. Cit.

high potentials, however, the time resolution is quite limited. See Appendix V for a derivation of the resolving time equation as a function of burst width.

Optical System

The optical system consisted of a short focal length lens mounted at the window of the excitation tube with an optical filter above it and the photomultiplier set above that. The photomultiplier was adjusted for maximum signal from the light course.

The optical filters were Baird-Atomic multi-layer filters for all lines studied except the 5016Å and 3889Å lines. Bausch and Lomb filters were used for them. No special study of the spectral purity of the light has been made. The light which reached the photomultiplier might have arrived from angles as great as 10° relative to the normal due to the convergence of the light beam. This clearly will broaden the apparent spectral width of the filter curve but no work has been carried out on this matter to date. In cases where bright lines are close to the ones being studied this matter needs more attention.

Vacuum System

The vacuum system consisted of a Cenco Megavac being fed by a dual stage mercury diffusion pump. A cold trap and stop cock isolated them from the rest of the high vacuum system. Behind this was a McLeod gauge and a dosing stopcock for letting in the helium. Between this section and the excitation tube there was another cold trap and stopcock which trapped mercury vapor from the McLeod gauge.

When the vacuum system was tight the McLeod gauge mercury would stick in the closed column and a drop of between 4 and 5

centimeters on the open column was needed to draw the closed column away from the end.

When the system was used for taking the final data the system pressure rose about 10^{-4} mm in 11 hours while being completely isolated. The cathode was hot during this period. This pressure rise was considered to be due to the continued outgassing of the new cathode. The amount of pressure rise extrapolated back to the 15 minute intervals required for each pressure run in the data showed the contamination of the gas to be less than 50 parts per million even at the lowest pressure. This was considered sufficient purity for this experiment. This purity figure might be in error somewhat however since during the 11 hour period there was no pulse current which might dislodge foreign atoms from the cathode or grids, while during the experiment the pulsing continued at one pulse per second with a total charge transfer of .0095 coulomb for the entire constant pressure data sequence.

CHAPTER III

THE ELECTRONIC CIRCUITRY

Special Demands

Since the excitation tube grid system must dissipate 200 watts during the excitation period it must be operated with a very low duty cycle. The pulsed operation which provides the low duty cycle also has the advantage of not allowing an internal arc discharge to reach destructive proportions when the gas pressure is too high. To provide the low duty cycle the cathode of the excitation tube is pulsed for 5μ-sec at a repetition rate of one pulse per second. The photomultiplier must be turned on for its 2μ-sec "on" period during the 5μ-sec excitation period. Then while the photomultiplier is "looking" at the gas the excitation must be cut off in order for it to "observe" the light decay. The time sequence is shown clearly in Figure 3.

One other timing requirement not indicated on the diagram stems from the use of an induction heater to heat the cathode. Since the power of the induction heater is so great that it cannot be effectively shielded from the electronics the whole timing sequence must be initiated during a period when the induction heater is off.

Fortunately the Ther-Monic Induction Heater used for heating

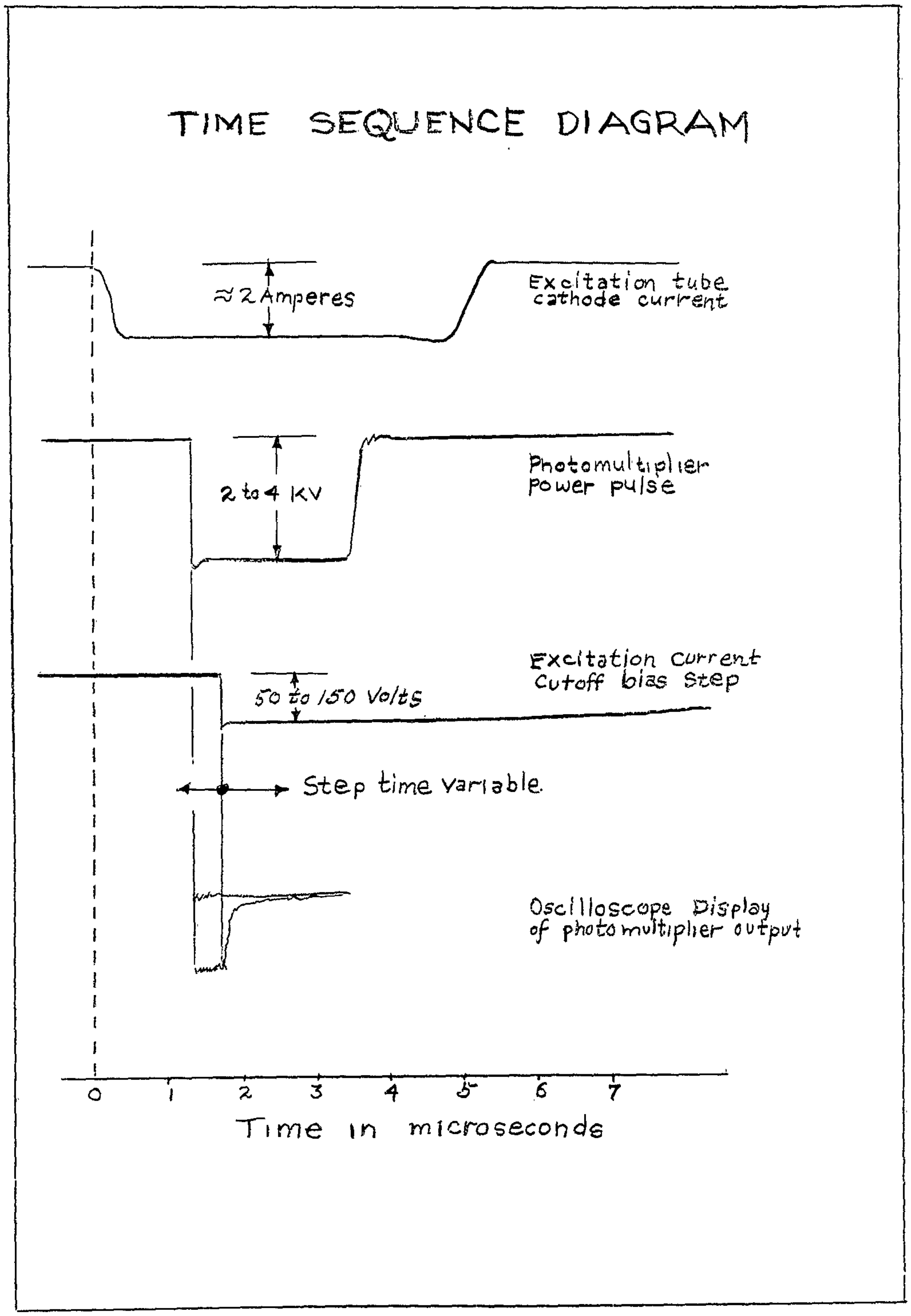
TIME SEQUENCE DIAGRAM
≈ 2 Amperes
Excitation tube cathode current
2 to 4 KV
Photomultiplier power pulse
Excitation current Cutoff bias step
50 to 150 Volts
Step time variable
Oscilloscope Display of photomultiplier output
0 1 2 3 4 5 6 7
Time in microseconds

Figure 3

the cathode is powered by a rectified but unfiltered power supply. This automatically provides a brief "off" period every 1/120th of a second when the 60 cycle power line voltage passed through zero. The instrumentation time is so short that the entire timing sequence can be interposed into this heater power "off" period using only a simple phase synchronization pulse applied to the initiating pulse generator grid. The block diagram, Figure 4 shows the relationship between the various electronic components. The arrows indicate the cause-to-effect relationship.

Description of Electronic Circuits

Phase Shifter

The phase shifter shown in Figure 5 is a simple series R-C circuit driven from each end by a push-pull sine wave. It is obvious that the junction between R and C will be in phase with the lower end of the push-pull circuit when R=0 and it would be in phase with the upper end when $R=\infty$. It is not so obvious however that the point will have a constant amplitude sine wave voltage relative to ground for all intermediate phase adjustments. To gain a clear understanding of its operation the reader is referred to one of the many electronics texts which discuss phase shifter theory.[29]

One difference in this phase shifter from those described in most texts is that a paraphase amplifier is used to provide the push-pull signal rather than the usual center-tapped transformer.

---

[29] M. R. Weed and W. L. Davis, Fundamentals of Electron Devices and Circuits (Prentice-Hall, 1959), p. 388.

BLOCK DIAGRAM
OF
ELECTRONICS AND OPTICS

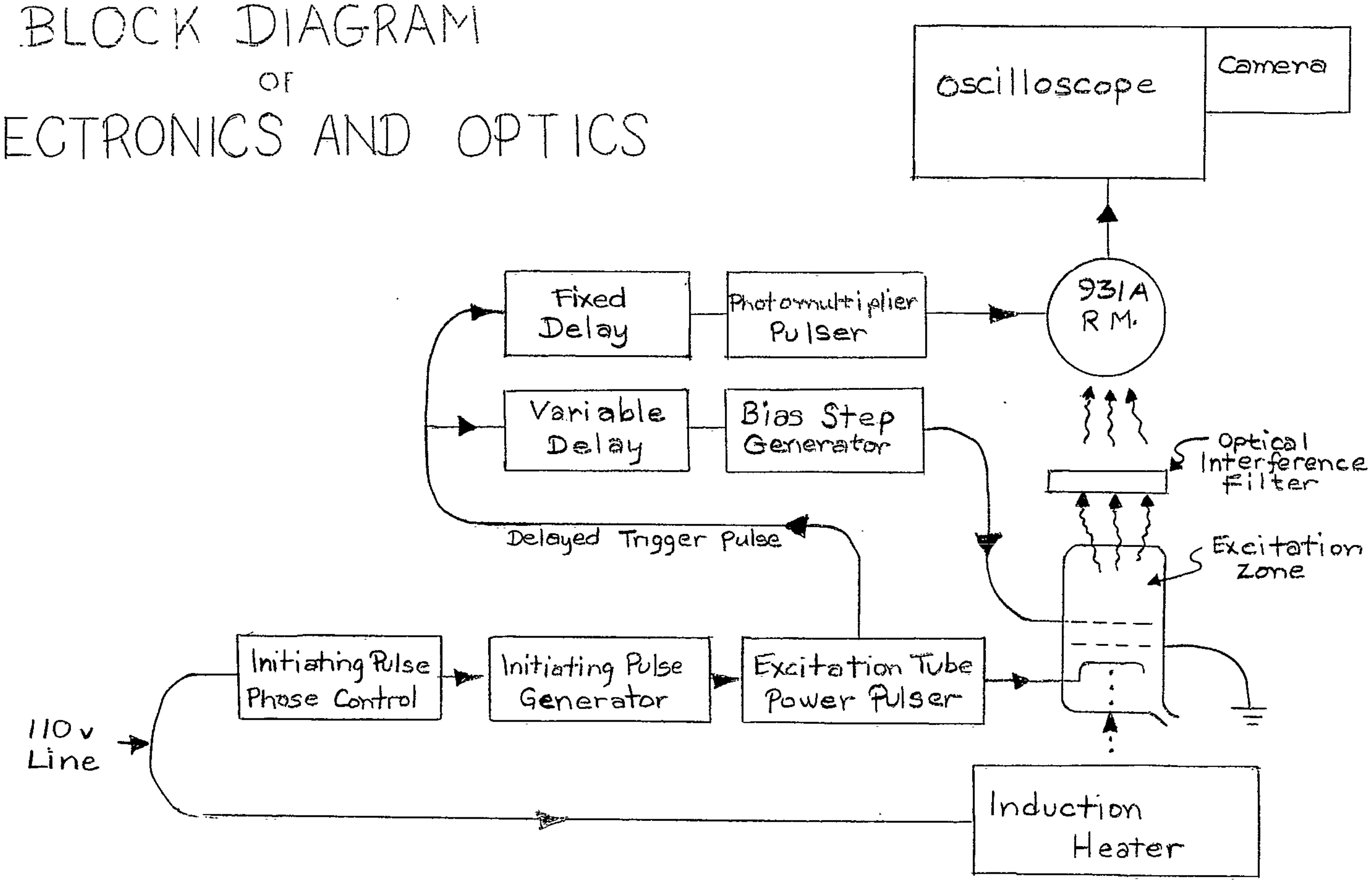

Figure 4

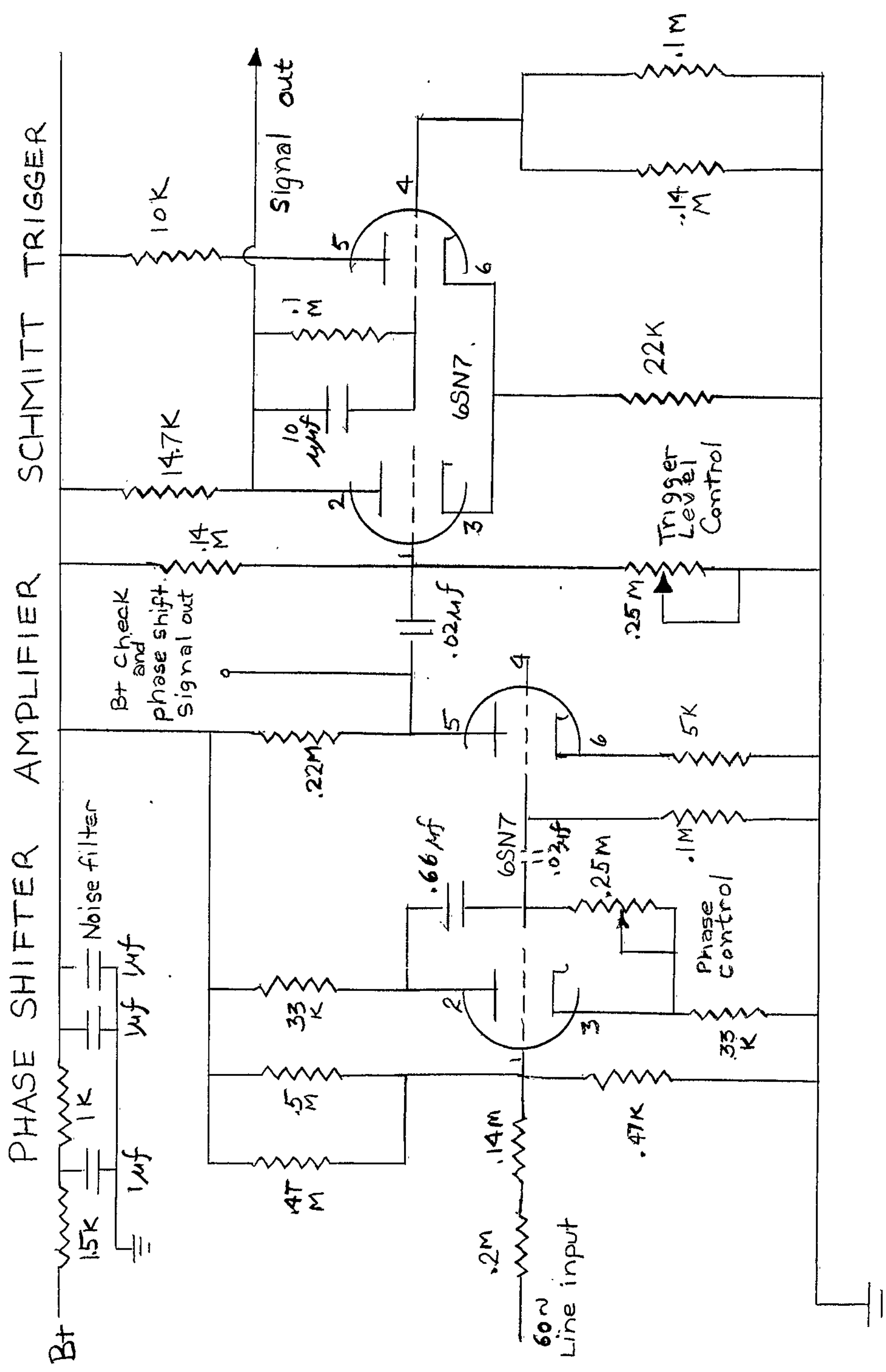
PHASE SHIFTER
AMPLIFIER
SCHMITT TRIGGER
B+
1.5K
1K
1µf
1µf
1µf
Noise filter
60~ Line input
.2M
.14M
.47M
.5M
33K
.66µf
6SN7
.02µf
.25M
Phase Control
.1M
33K
.47K
5K
.22M
B+ check and phase shift Signal out
.02µf
.14M
.25M
Trigger Level Control
14.7K
10µf
.1M
6SN7
22K
10K
Signal out
.14M
.1M
1
2
3
4
5
6

Figure 5

The paraphase amplifier incorporates the phase inversion property of the conventional amplifier and the noninversion property of the cathode follower in a single circuit. Since the anode and cathode loads of the 6SN7 triode are the same (33K in this instance) the plate current of the tube will develop the same signal amplitude across each resistor but with the phase inverted on the plate load output.

Buffer Amplifier

The use of a buffer amplifier reduces feed back between stages of a system and provides amplification when necessary.

The use of this element may be unnecessary in this sequence, but since the other half of the 6SN7 paraphase amplifier twin triode would have been idle it was felt that the decoupling that it could provide might add to the long term stability of the system.

Schmitt Trigger

The Schmitt trigger[30] circuit is a highly regenerative two tube circuit having two stable states. The regenerative feed back is provided by the cathode resistor and by coupling the first anode to the second grid. The signal level on the first grid determines which tube is in the conducting condition. If the grid on triode 1 is above the critical potential it conducts. The conduction of the first triode provides both cathode and grid signal to the second triode to keep it cut off.

---

[30] V. C. Rideout, Active Networks (Prentice-Hall, 1954), p. 426.

When the grid of triode 1 is lowered below the critical level the second triode begins to conduct and the regenerative feedback produces a sudden change of state with triode 1 being cutoff and triode 2 conducting. The first triode remains cut off until its grid is again raised above the critical level. The advantage of such a circuit is that it provides very sharply rising and falling wave fronts accurately timed ralative to some predetermined level on a slowly changing grid signal. The trigger level control sets the critical bias level at which the circuit regeneration sets in. It might be well to mention that this level can be adjusted in either direction far enough that the input signal cannot drive the grid into the critical condition and the circuit will fail to operate.

In Figure 6 the effect of the trigger level on the output wave-form is clearly shown. The most accurately phased spikes should occur when the sine wave intersects the stability axis with its greatest slope. This condition is shown on the left in the figure. The stability adjustment may be carried out by observing the wave form at the output of the amplifier which follows while adjusting the trigger level control until the negative pulses are equidistant between the positive spikes. The adjustment is not critical.

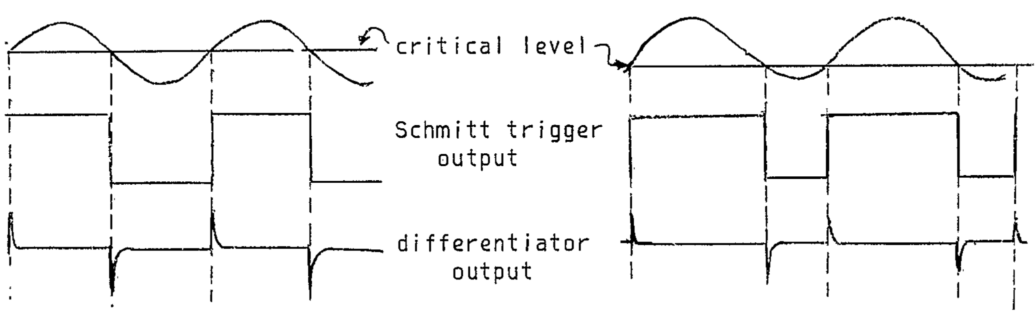

Figure 6

Differentiator

The differentiator and several more components will be found on Figure 7. The purpose of the differentiator is to take the square signal out of the Schmitt trigger circuit and shape it into short duration timing spikes as illustrated above. A simple RC circuit having a small RC time constant is all that is required.

When a step function voltage is applied across the circuit the capacitor will charge to essentially the full voltage almost immediately. After this no more current will flow through the RC circuit. The IR drop across the resistor (the output signal) is the result of this sudden charge surge to the capacitor. Thus, only sudden changes in the applied signal result in any appreciable signal output.

Selective Amplifier

Although a differentiator circuit effectively changes square waves into positive and negative trigger spikes, the signal amplitude is greatly reduced. In this work the negative signal spike is of no value, therefore, the amplifier stages which follow are deliberately biased into their nonlinear zones to reduce the unwanted signal and provide strong amplification of the desired spike.

The principle of this selective amplification is illustrated in Figure 8. It is well to note that the output voltage signal is the negative of the output current.

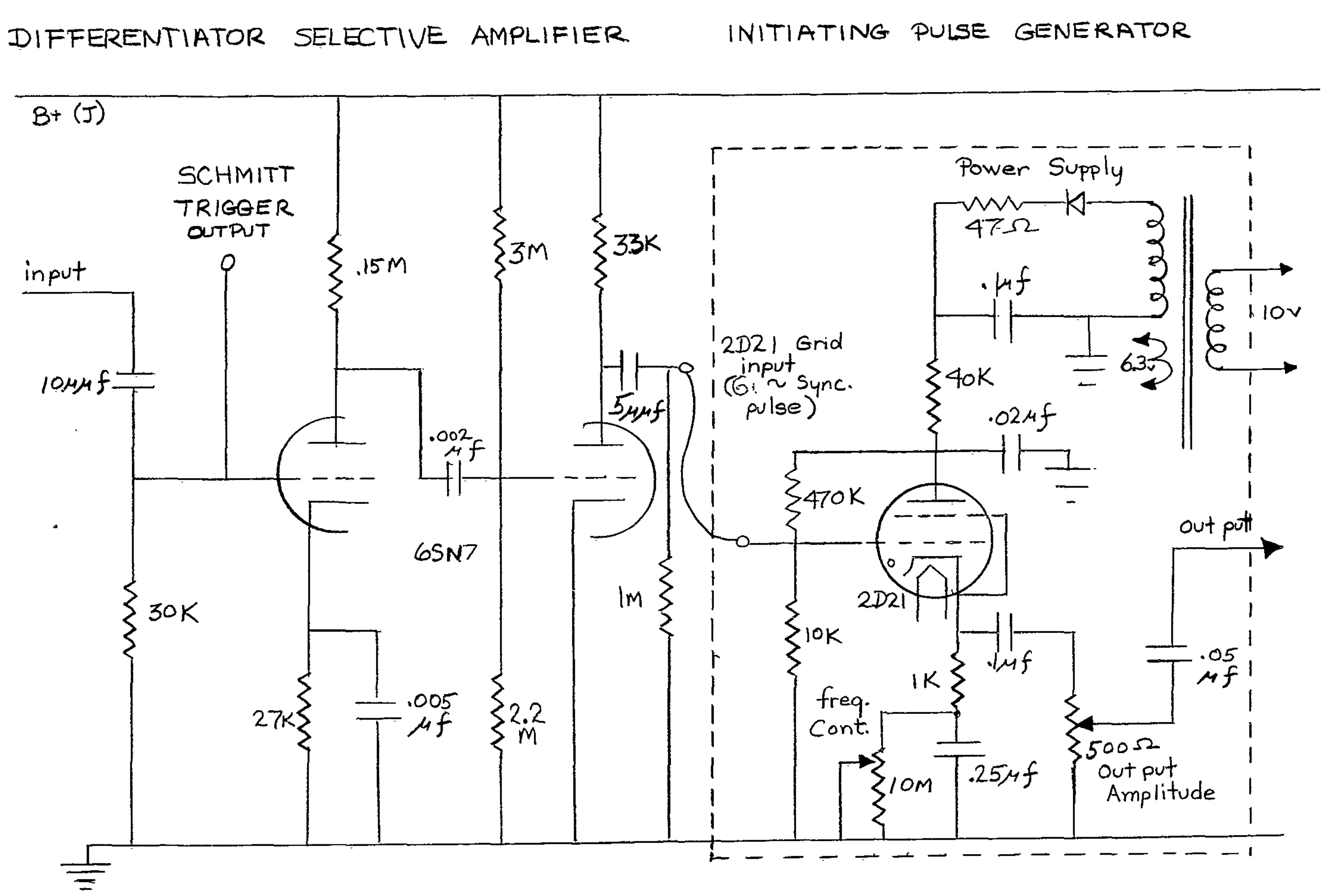
DIFFERENTIATOR
SELECTIVE AMPLIFIER
INITIATING PULSE GENERATOR
B+ (J)
SCHMITT TRIGGER OUTPUT
input
10μμf
30K
.15M
27K
.005 μf
.002 μf
6SN7
3M
2.2 M
33K
5μμf
1M
2D21 Grid input (G₁ ~ Sync. pulse)
Power Supply
47Ω
.1μf
6.3v
10v
40K
.02μf
470K
2D21
10K
.1μf
1K
freq. Cont.
10M
.25μf
out put
.05 μf
500Ω Out put Amplitude

Figure 7

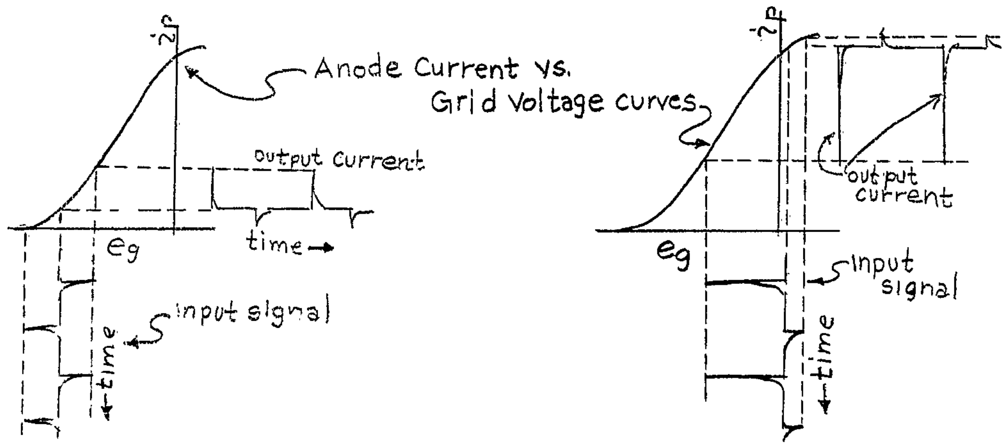

Stage 1

Stage 2

Figure 8

Stage 1 is biased very near cutoff by a large cathode resistor (27K) so the positive grid spike can give rise to a large anode current surge while the negative signal will drive the tube only further into cutoff.

The second stage is biased into saturation by 3 Megohm and 2.2 Megohm voltage divider connected to B+.. Remembering that the signal out of the first stage is a strong negative voltage spike and a weak positive pulse, this negative spike swings tube number 2 through its normal operating range while the positive pulse drives it further into the already saturated region. The output signal from the amplifier chain is a greatly amplified positive spike every 1/60th of a second with a much smaller negative pulse between these trigger spikes.

The entire circuit from the phase shifter to this point is represented in the block diagram by a single block designated the "initiating Pulse Phase Control".

Initiating Pulse Generator

The initiating pulse generator is a remote unit as indicated by the dashed outline on Figure 7. This unit has its own half wave power supply with an RC filter.

The operation of the pulse circuit is as follows. Assume that the 2D21 thyratron has just fired so the .02 μf plate capacitor is discharging and the cathode capacitor is being charged. When the cathode and anode potential draw close enough together the cathode current becomes too low to sustain the discharge within the tube and the grid regains control. At this time the tube is biased far into cutoff with cathode bias supplied by the charge on the .25 μf capacitor. The capacitor slowly discharges through the 10 Meg potentiometer decreasing the bias. The anode capacitor usually charges up to the B+ potential much more rapidly because of its smaller charge resistor. When the anode capacitor becomes charged the circuit, exclusive of the cathode, remains ready for another cycle. As the cathode bias potential slowly decreases a time finally arrives when one of the phase controlled trigger spikes, applied to the grid, overdrives the cathode bias and the tube fires again, repeating the sequence previously described. The frequency control simply adjusts the RC time constant of the cathode circuit thereby changing the rate of decrease of the cutoff bias. The repetition rate may be adjusted from around 60 pulses/sec to several seconds between pulses with each pulse accurately phased relative to the 60 cycle line as determined by the grid signal. Here again, a word of caution should be interjected. Lowering the cathode resistance too far produces a repetition rate which is too high to be properly synchronized by the grid signal and the operation becomes erratic.

At a slightly lower cathode resistance the current fails altogether because there is never enough cathode bias to hold the thyration cutoff. These faults could be eliminated by adding a series resistor in the cathode circuit which would establish a minimum resistance above the critical value. Since the circuit was always operated at the low repetition rate of 1 pulse per second and left at that adjustment, this modification never became necessary. The output signal is developed across the 1K cathode resistor and is differentiated by the .1 μf capacitor and the 500 ohm output potentiometer.

Differentiator and Pulse Amplifier

Both of these circuits were previously employed in a system which required the wave shaping and amplification that they provide. Although they are not believed to contribute to the effectiveness of the present circuit their use allowed the use of an input jack for the remotely controlled trigger without further modification of the system which may be needed in its former condition at a future date. These circuits will be found along with the next one to be discussed in Figure 9.

Excitation Tube Power Pulser

This circuit employs 2D21 thyratron and a lumped delay-line to produce a 5 μ-sec output pulse of a relatively square shape. Its operation is as follows:

In the off period the cathode bias is established by the 5 meg and 60K voltage divider while the anode potential is at the value established by B+. When a trigger spike arrives at the grid the

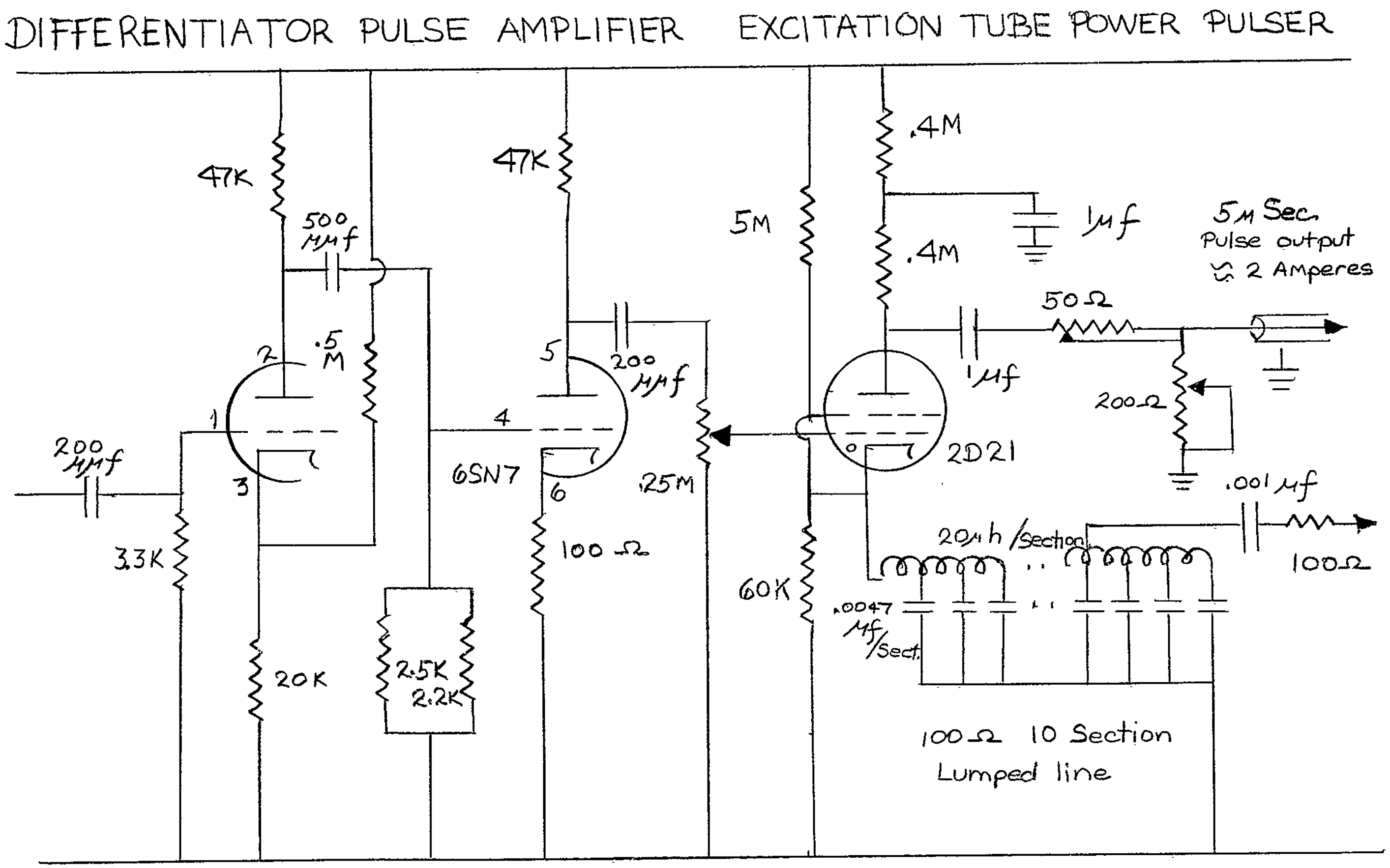
DIFFERENTIATOR PULSE AMPLIFIER
EXCITATION TUBE POWER PULSER
47K
500 μμf
.5 M
2
1
3
200 μμf
3.3K
20K
2.5K
2.2K
47K
5
4
6
200 μμf
6SN7
.25M
100 Ω
5M
60K
.4M
.4M
1μf
1μf
2D21
50 Ω
200 Ω
5μ Sec.
Pulse output
≈ 2 Amperes
.001 μf
100Ω
20μh /Section
.0047 μf/Sect.
100 Ω 10 Section
Lumped line

Figure 9

thyratron fires. This accomplishes the same result as connecting the charged anode capacitor and load resistance to the lumped delay-line at the cathode. Electrons flow from this delay-line at a constant rate until it becomes charged. This is the time required for the step function to propagate to the far end of the open line and be reflected back to the cathode. At this instant the current stops because the voltage across the line is now equal to the voltage supplied by the anode capacitor. The thyratron grid now regains control. The circuit returns to its former state as soon as the lumped line discharges through the bias bleeder and the anode becomes charged through the two .4 Meg resistors. The 1 μf capacitor between these .4 Meg resistors decouples the anode circuit from the B+, thereby reducing the possibility of triggering other circuits using this common B+ supply.

The load on the output must match the impedence of the dummy line in the cathode if the output square wave is to be properly formed. In order to provide an amplitude control and an impedence match the two potentiometers and the load provided by the excitation tube form a T-pad capable of enough adjustment to establish the proper wave shape when the excitation tube cathode is heated and in operation.

Another useful feature of this circuit is the fact that the lumpy line provides a chance to pick off a trigger signal with a fixed delay. This is employed to initiate the photomultiplier trigger circuit after the excitation tube has been "on" for a fixed period of time.

Photomultiplier Pulser Trigger

This is another 2D21 pulse generator employing a capacitor in the anode circuit and a cathode load which produces a positive output pulse. When the thryatron is triggered the anode capacitor charge is dumped through the cathode resistor resulting in a low impedance high voltage pulse of short duration on the cathode. This circuit is shown in figure 10.

When the anode capacitor becomes discharged the 5.6 Meg recharge resistor will not supply enough current to maintain the discharge and the grid circuit regains control. The Anode capacitor becomes recharged again in essentially the RC time established by 5.6 Meg.ohm and .05 μf or approximately one third of a second.

The cathode output signal is fed first into the APS/2 Radar modulator unit through a delay-line of roughly 1.0 μ-sec giving a fixed delay as well as establishing the output pulse width of that unit. The other branch of the output is fed into a delay-line which determines when the excitation tube bias step is initiated relative to the photomultiplier "on" period.

The bias step trigger pulse may be picked off the delay-line at intervals of a few tenths of a microsecond per section. To accomplish this an alligator clip is clamped to the capacitor lead at the delay interval desired.

The time sequence order will be broken at this point since the photomultiplier pulser will require some special discussion with regard to its power supply. The discussion will now proceed to the bias step generator which is found on the same figure as the previous circuit.

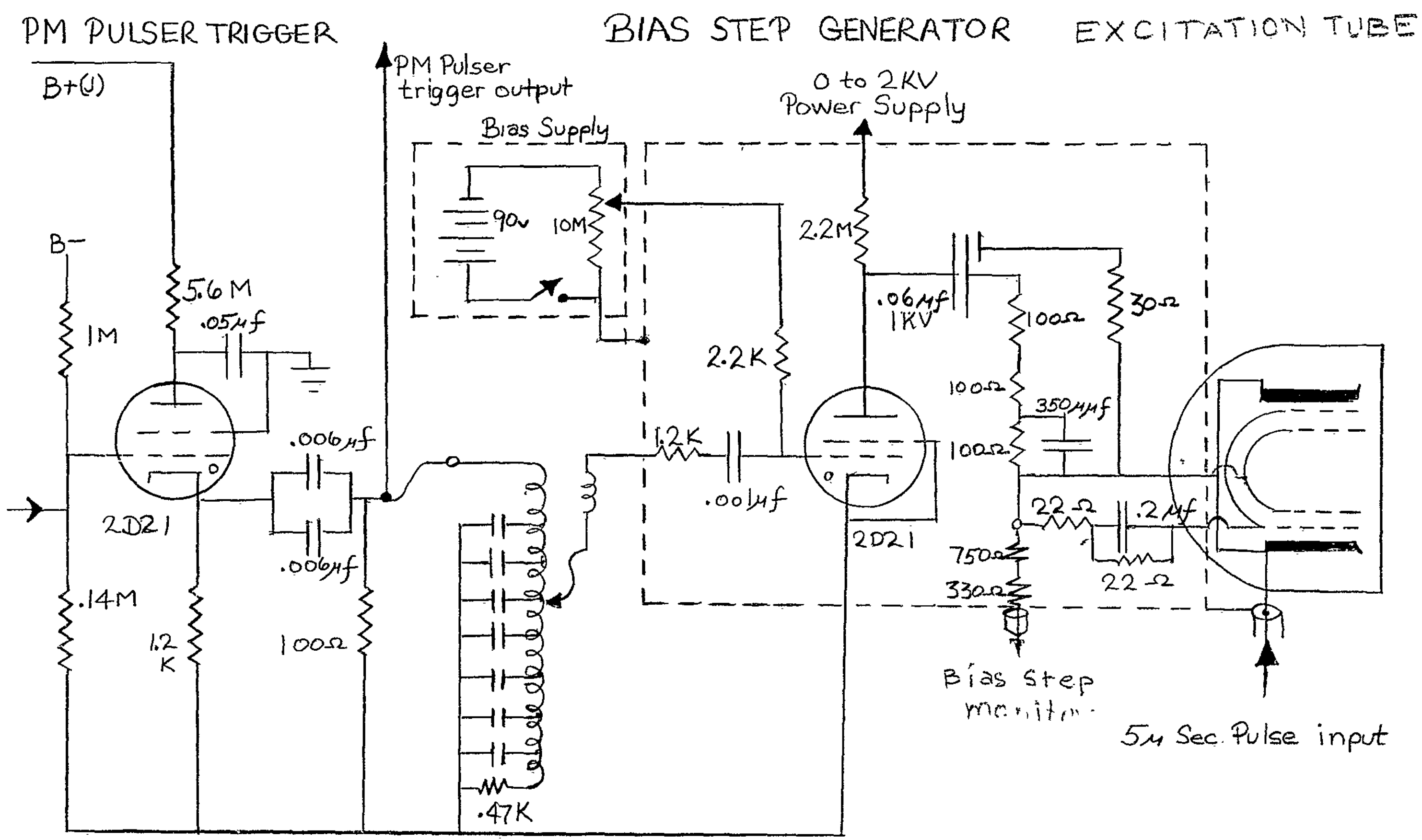
PM PULSER TRIGGER
BIAS STEP GENERATOR
EXCITATION TUBE
B+(J)
B−
5.6 M
.05µf
1M
2D21
.14M
1.2 K
PM Pulser trigger output
Bias Supply
90v
10M
.006µf
.006µf
100Ω
.47K
0 to 2KV Power Supply
2.2M
2.2K
1.2K
.001µf
2D21
.06µf 1KV
100Ω
100Ω
100Ω
350µµf
30Ω
22Ω
.2µf
22Ω
750Ω
330Ω
Bias Step monitor
5µ Sec. Pulse input

Figure 10

Bias Step Generator

The requirements on this circuit are stringent. It must have a low impedence (19 ohm), have a controlable output voltage around 100 volts, and have a rise-time of less than 10 n-sec and preferrably around 1 n-sec. A bit of checking showed that the only driver unit available in this laboratory which was capable of meeting the power control requirements seemed to be the much used 2D21 thyratron. All hard tubes in the laboratory which could handle 5 amperes were felt to be too large and inductive for such fast work.

An experimental check on the 2D21 tubes showed that at 1000 to 2000 volts the rise-time for the latter part of the breakdown was very fast, reaching from half signal to peak in around 2 n-sec with an estimated rise-time (10% to 90% signal) of around 5 n-sec.

The circuit used is shown in Figure 10 and is enclosed in a dashed line to indicate that it is remote from main timing unit.

While the 2D21 grid is in control the B+ voltage supplied by a variable laboratory supply is raised to around 1300v. The coupling capacitor made up of three parallel .02 μf 1kv disc-seramic capacitors becomes charged to the applied potential through 2.2 Meg resistor in the unit and a 5 Meg resistor at the power supply terminal.[31]

After the disc-ceramic capacitors become charged the circuit is ready to operate. A positive trigger overdrives the battery operated bias supply and the breakdown takes place. The full coupling capacitor

[31]This power supply resistor was used to protect any operator unfamiliar with the high voltage required by this small and innocent looking unit. It also saved the author from a discomforting thought of danger connected with the adjustment of this unit.

voltage then appears across the resistor string which drops the voltage from 1300v to approximately 100v on the grid of the excitation tube.

The capacitance of the electrode structure of the excitation tube loaded the circuit considerably and the sharp rise-time found on the work bench was not duplicated at the excitation tube. In order to compensate for this rounding of leading edge of the wave two aids were incorporated. First a 350$\mu\mu$ f capacitor was shunted across one resistor of the resistor string. This served to bypass the resistor during the early part of the signal filling in the badly rounded portion but failing to raise the leading edge of the step enough to give a really sharp front. In order to provide a sharper front a copper foil capacitive pick-up was slipped between two of the coupling capacitors and fed directly to the signal output. This produced an overshoot and ringing. The final solution incorporated a 30 ohm resistor in series with this capacitive pickup. By trial and error the area of the strip was altered until the desired amount of pickup was attained. The final signal had a very small overshoot on the leading edge. After the leading edge of the step was corrected and the research begun it was discovered that there were photomultiplier signal tails of long duration and it was necessary to hold the bias signal up for a much longer period than was possible with the resistor capacitor string. In order to compensate for this bias voltage fall a capacitor was put in series with the lower circuit element which would charge up at a rate to compensate for the fall rate on coupling capacitor. A perfect match[32] was not possible however because the d.c. impedence to

---

[32]To produce a perfect divider a series capacitor in the lower and of the voltage divider should be chosen such that the RC time constant of this lower section is equal to the RC time constant of the upper section.

ground must be kept low. This is because the excitation tube bias grid intercepts a large number of the cathode electrons during the conduction period and these electrons must find their way to ground without developing a large bias signal on the grid. By trial and error the 22 ohm .2 μf capacitor circuit provided a signal which rose slightly and fell again but which was flat to about 5% over the 3 μ-sec range. Since 3 μ-sec is longer than the photomultiplier activation period this was deemed more than sufficient for our present needs.

A word about construction of the unit might be given for the benefit of anyone who might wish to duplicate the circuit.

The use of tight fitting copper foil shielding was found to be necessary for the fast rise time. A careful study of the current paths in the circuit elements was also carried out to determine the geometrical location which would provide the least inductance. Once built the unit is almost impossible to repair without a complete rebuilding process. Only the 2D21 can be removed without unsoldering the outside shield and cutting apart the unit. The unit had to be rebuilt several times when the voltage divider resistors were broken down. When they break down, the step function does not have a clean leading edge but will fail to rise to full value on one trial and later will rise in multiple steps with a lack of any consistency. The use of larger 2 watt resistors and a longer resistor string had to be employed even at the expense of the added inductance it introduced but this has provided a dependable circuit. After the first failure of the voltage divider string the need for a signal monitoring lead was recognized. The coaxial monitor output terminal was built into this bias unit and was properly voltage divided and impedance matched to the requirements of the Tektronix 519 oscilloscope.

Another comment: The 2D21 tubes are rated at 600v maximum and some selection has to be made to find those which will properly stand off the 1500v or so required in this circuit. Those which failed in this circuit were not damaged, however, and function normally at voltages below the maximum listed in the tube manual. Only two out of six tubes tested were found to stand off the voltage to 2000v. The one presently in use has served well for the entire alignment and data taking period and shows no apparent aging in its operation.

APS/2 Radar Modulator Unit Modification

The photomultiplier driver circuit incorporates a modulator unit from an APS/2 radar unit. It has proved to be adequate for driving the photomultiplier with a minimum of modifications. It requires an 800 cycle generator to operate its power supply. See Figure 11. The only power supply modification was the use of a rheostat and a resistor in series with the primary of the high voltage supply transformer to provide for voltage adjustments from 2 to 5 kilo volts.

Two changes in the output driver unit were required when a low resistance photomultiplier voltage divider was employed. They were the need for a larger coupling capacitor (replacing a .05μf with a .4μf capacitor) and the use of another 715C power tetrode in parallel with the one already in use.

Minor conveniences such as power switches, metering probes, etc. have not been discussed.

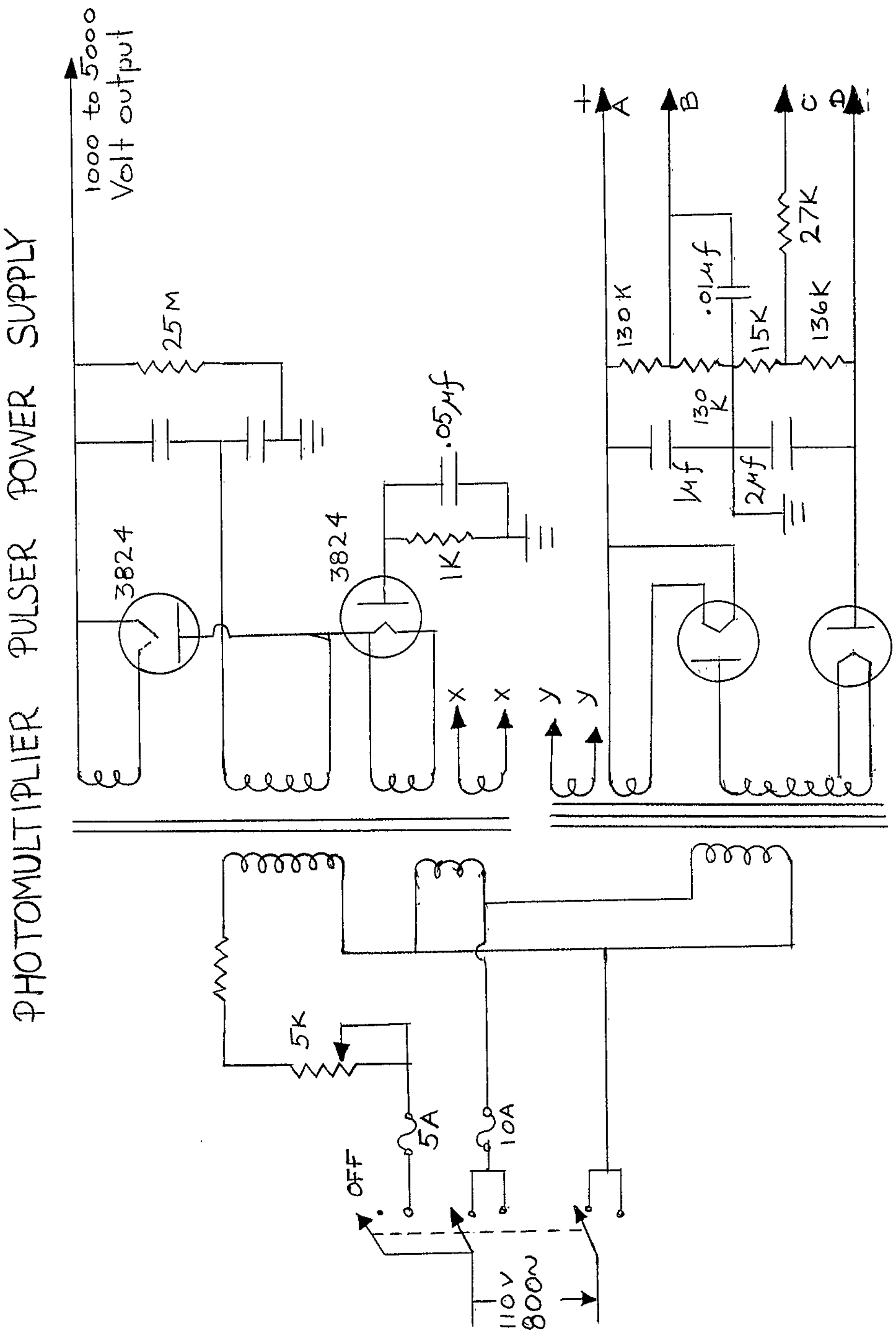
PHOTOMULTIPLIER PULSER POWER SUPPLY
1000 to 5000 Volt output
25M
3824
3824
.05μf
1K
x
x
y
y
+ A
B
C
D
130K
130 K
.01μf
15K
136K
27K
1μf
2μf
5K
5A
10A
OFF
110V 800~

Figure 11

The APS/2 Blocking Oscillator

This is a transformer-feed-back regenerative circuit which has an 829B tube normally in cutoff. See Figure 12 for a circuit diagram.

When the grid of this tube is driven positive with a trigger pulse sent through the dummy line at the bottom of the page the tube starts to conduct. As this happens the plate current sends a more positive signal to the grid driving the tube into saturation. The current continues at this high rate until a negative going grid signal triggers the cutoff condition. During the "on" period the grid section of the transformer was drawing electrons from the cathode by means of the positive grid. This resulted in sending a negative signal back into the 1 μ-sec dummy line. It is the reflection of the negative pulse which starts the reverse event. Thus the pulse width is determined by apparent length of the dummy line in the grid circuit.

The pulse width is 2 μ-sec long because the signal must make a double transit of the 1 μ-sec line. For further details see the Radar System Engineering text by Ridenour.[33]

Photomultiplier Pulser Driver

The photomultiplier pulser driver circuit is nothing but a high power parallel tetrode amplifier unit employing a capacitor coupling output. See Figure 12. The tube is normally cut off until the blocking oscillator signal hits the grid. It remains turned on until the blocking oscillator cuts it off again. Therefore it simply amplifies the blocking oscillator signal. In order to monitor the voltage wave-form a voltage divider is attached to the output.

---

[33]L. N. Rodenour, Radar Systems Engineering (M.I.T. Radiation Lab Series, McGraw-Hill: 1947), Vol. I, p. 371.

APS/2 BLOCKING OSCILLATOR PM PULSER DRIVER

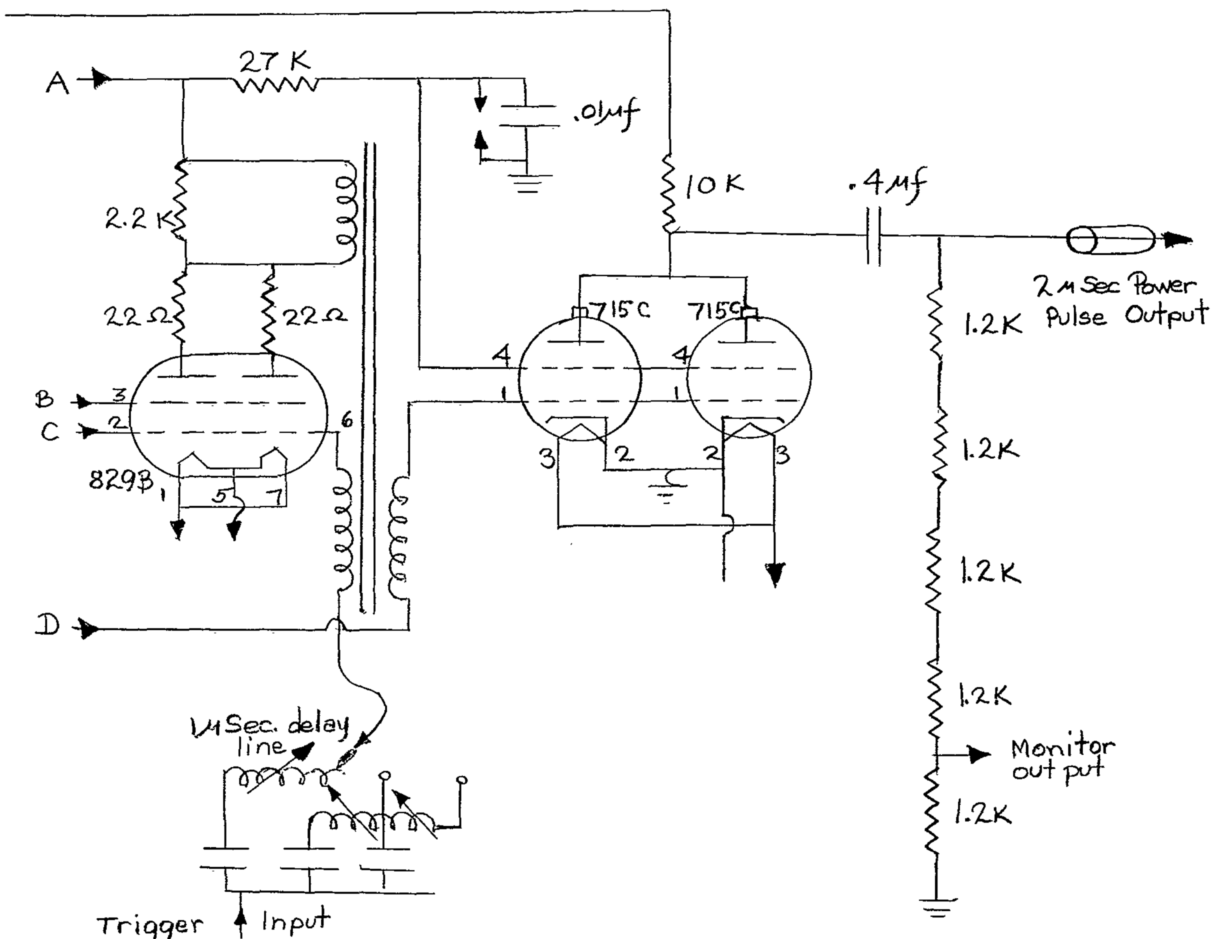

Figure 12

Photomultiplier Circuit

This circuit is a low impedance voltage divider incorporating escalating resistance values as one progresses from cathode to anode. This is similar to the circuit used by Signey Singer at Los Alamos.[34]

This escalation provides higher fields for sweeping out space-charge in the anode end of the dynode chain where saturation would occur. The photomultiplier itself was a 931A selected for the best stability and signal strength properties. No apparent saturation is observed in the output signals from this circuit even at rather high light levels.

Other elements in the system which were not discussed in detail are as follows:

a) Tektronix 519 and Tektronix 555 oscilloscopes which were used in conjunction with Tektronix Poloroid Camera for recording data.

b) Ther-Monic Induction Heater Model 50, 1 kw output. This was a commercial model only modified slightly for the convenience of operation in this application.

c) A war surplus 800 cycle motor generator required to drive the radar modulator.

d) A high voltage power supply available in the laboratory. The circuit is unknown to the author.

e) Dumont Model 29-1A power supply which was modified only slightly. A circuit diagram of this power supply is inserted without discussion. Figure 14.

---

[34]Sidney Singer "Measurements of Rise and Decay Time of Three Fast Scintillators including a Special Plastic." Report under Contract W-7405 - Eng. 36 at Los Alamos, New Mexico (1954).

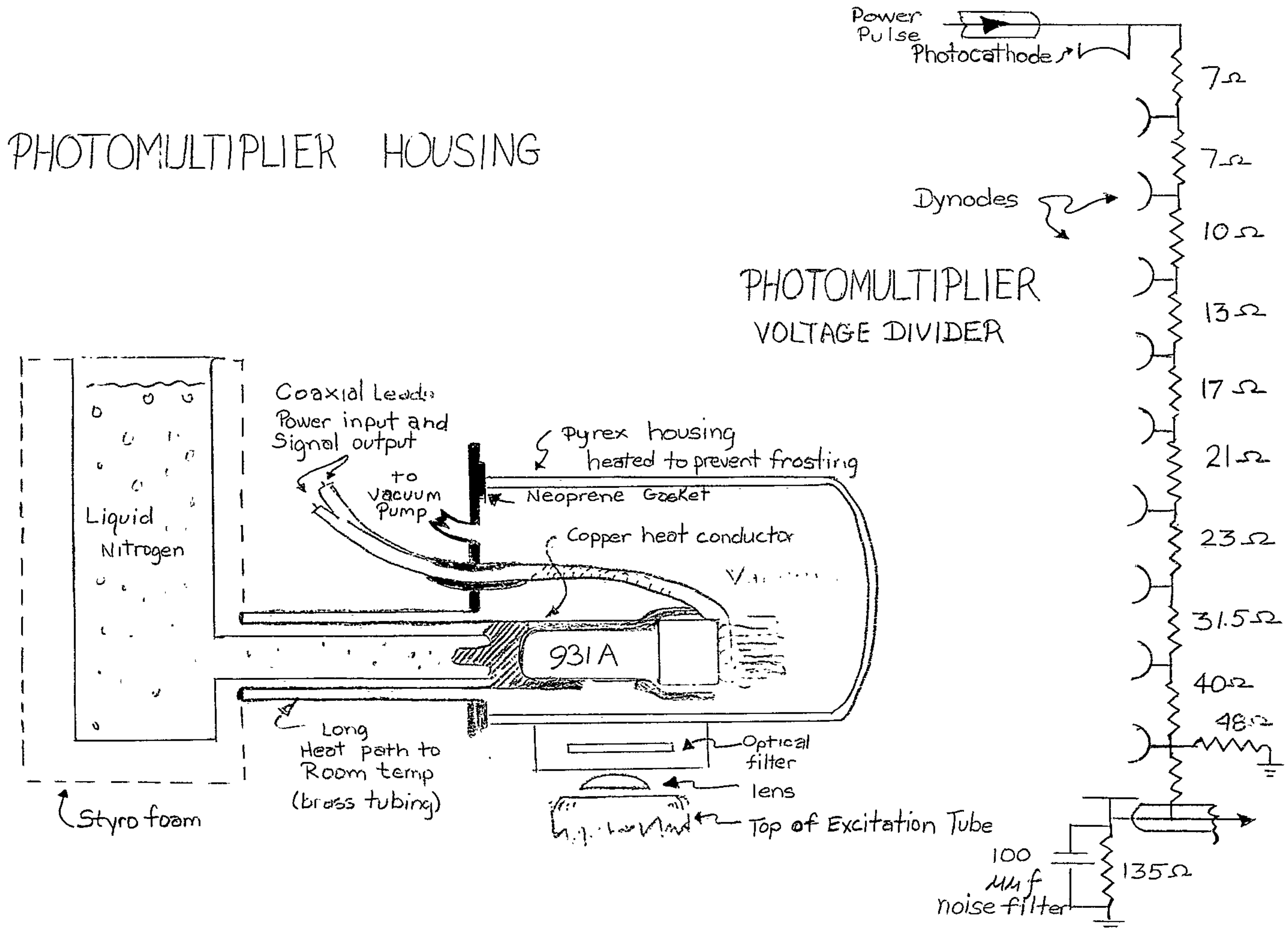
PHOTOMULTIPLIER HOUSING
Liquid Nitrogen
Styro foam
Coaxial Leads
Power input and Signal output
to Vacuum Pump
Pyrex housing heated to prevent frosting
Neoprene Gasket
Copper heat conductor
931A
Long Heat path to Room temp (brass tubing)
Optical filter
lens
Top of Excitation Tube
PHOTOMULTIPLIER VOLTAGE DIVIDER
Power Pulse
Photocathode
Dynodes
7Ω
7Ω
10Ω
13Ω
17Ω
21Ω
23Ω
31.5Ω
40Ω
48Ω
135Ω
100 μμf noise filter

Figure 13

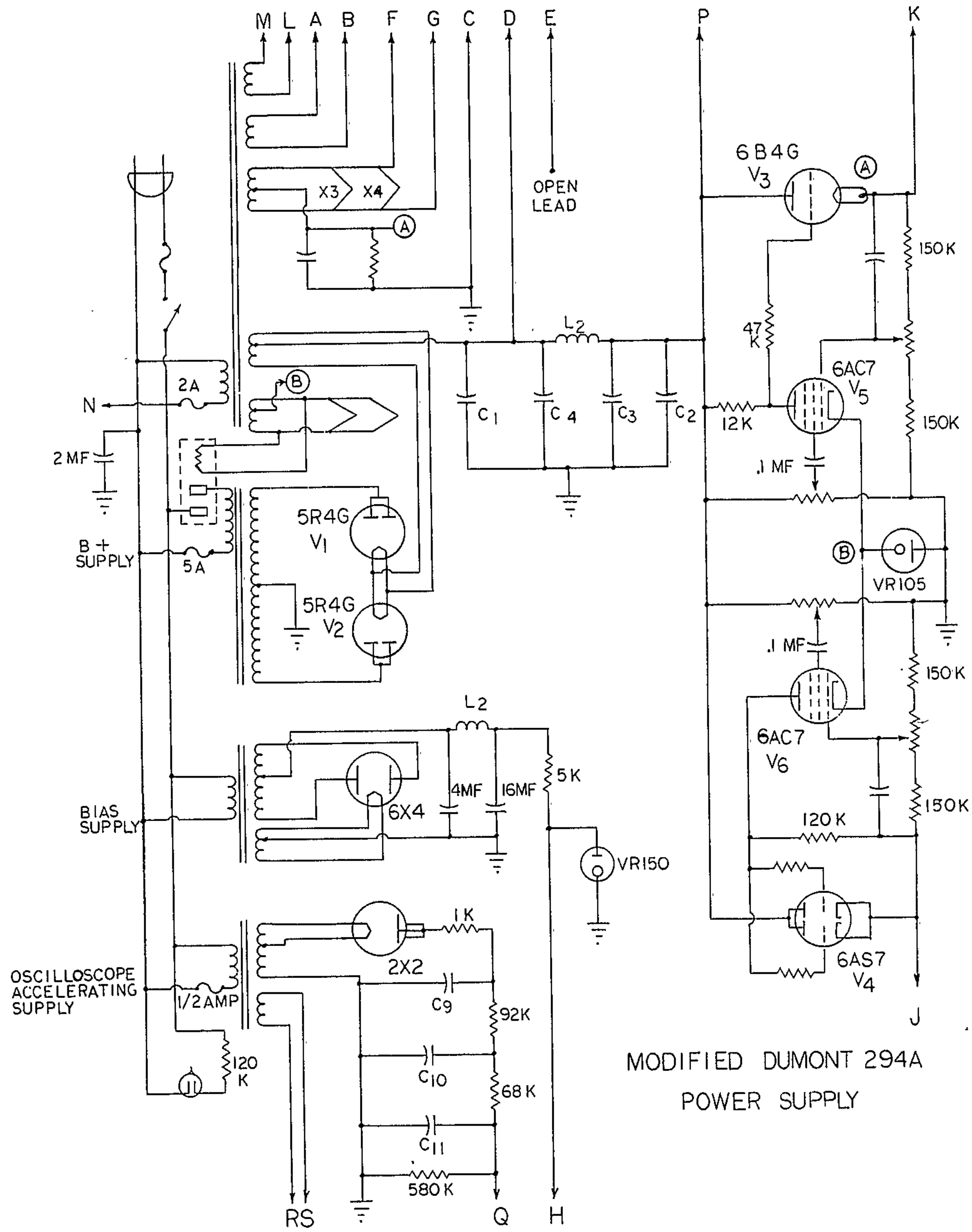
M L A B F G C D E P K
OPEN LEAD
6B4G
V_3
X3 X4
150K
47K
L_2
6AC7
V_5
N
2A
C_1 C_4 C_3 C_2
12K
150K
2 MF
.1 MF
5R4G
V_1
B+ SUPPLY
5A
VR105
5R4G
V_2
.1 MF
150K
L2
6AC7
V_6
5K
4MF
16MF
6X4
150K
BIAS SUPPLY
120 K
VR150
1K
2X2
6AS7
V_4
OSCILLOSCOPE ACCELERATING SUPPLY
1/2AMP
C9
92K
120 K
C10
68K
C11
580K
RS Q H J
MODIFIED DUMONT 294A POWER SUPPLY

Figure 14

The Electronic Circuitry As A Whole

The electronics functioned very well during a rather long period of adjustment, cathode activation, and the taking of data. When the new excitation tube was being activited the electronics were left on day and night for several days to age the cathode and dislodge impurities from the excitation tube elements. There was no apparent effect on the operation of the electronic circuits over this extended period of operation. This cathode aging process could have been completed much more quickly if a higher repetition rate on the pulse circuits could be attained. In future designs more careful attention should be given to the recovery time required by the pulse circuits. A pulse rate of 20 to 60 cycles per second would be helpful in the aging periods and very beneficial during the alignment procedure. The present alignment procedure is difficult because of memory lapse between successive traces at the 1 sec repetition rate. Thus minor adjustments which could be studied easily at a 20 to 60 cycle rate are quite difficult with the present timing circuits without the use of multiple exposure photographs to show the trends produced by these adjustments.

CHAPTER IV

DATA AND ANALYSIS

Peripheral Information from Data Curves

A discussion of the special precautions taken prior to the taking of data as well as the procedure for taking data is discussed in Appendix VI.

At this point a somewhat detailed discussion of the actual data curves will be given along with their interpretation. The actual data obtained from the system as a whole is in the form of photographs of the oscilloscope display of the photomultiplier output signal. The data for six different spectral lines taken for four different pressures is given in figures 15, 16, and 17. The reader is cautioned to observe the different time base used on the singlet curves from that used for all triplet curves.

The use of the Tektronix 555 dual beam oscilloscope made it possible to record the bias signal as well as the light decay curve. This extra bit of information allows a more detailed analysis than the decay curve alone could give.[35]

---

[35] It should be pointed out that the time resolution of the bias step signal preamplifier is not nearly so good as that of the light intensity curve preamplifier. This was clearly seen when the two traces were synchronized by applying the bias step to both circuits simultaneously. This difference is the result of using different types of plug-in preamplifier units in the oscilloscope. The actual rise time of the bias step function as monitored on the Tektronix 519 is truly very close to 5 n-sec.

5016A $3^1P \rightarrow 2^1S$

4922A $4^1D \rightarrow 2^1P$

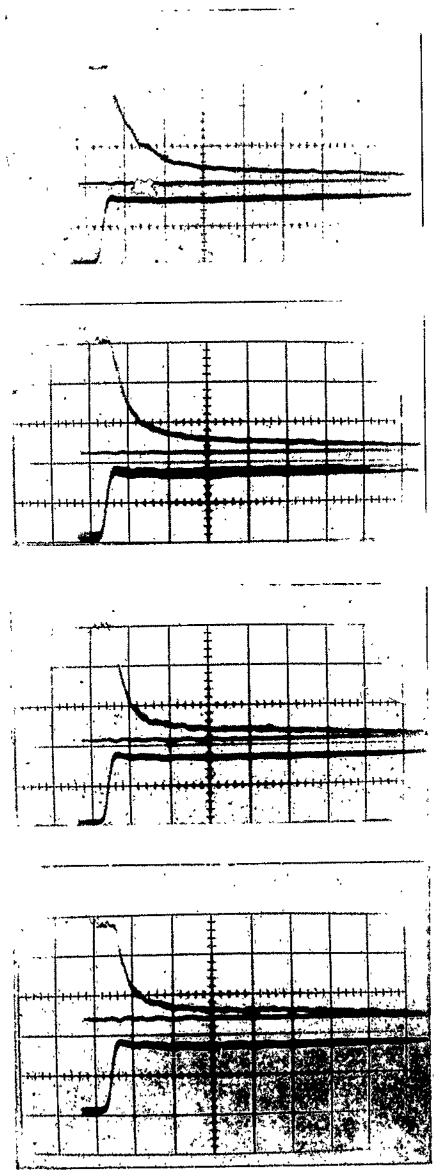

.13 mm Hg

.092 mm Hg

.057 mm Hg

.039 mm Hg

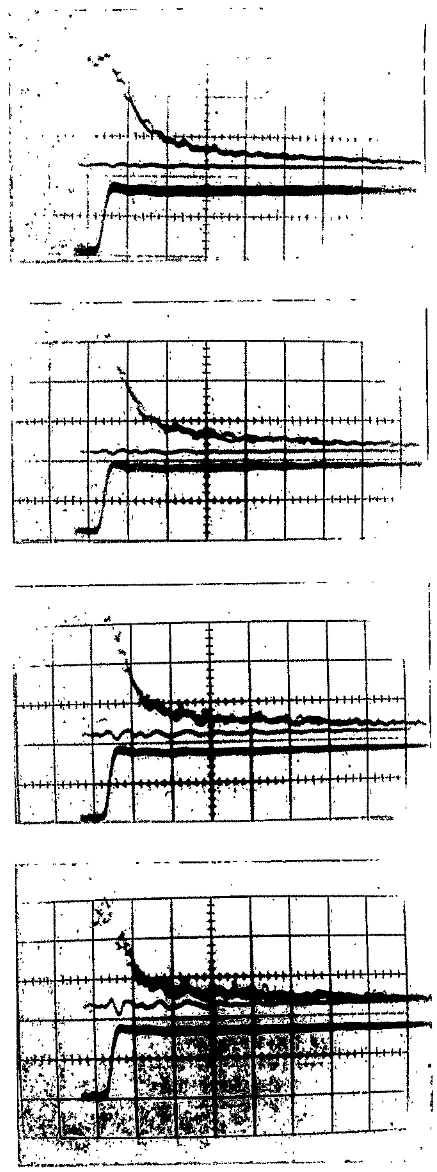

100 ns/division

100 ns/division

3889A $3^3P \rightarrow 2^3S$ 4713A $4^3S \rightarrow 2^3P$

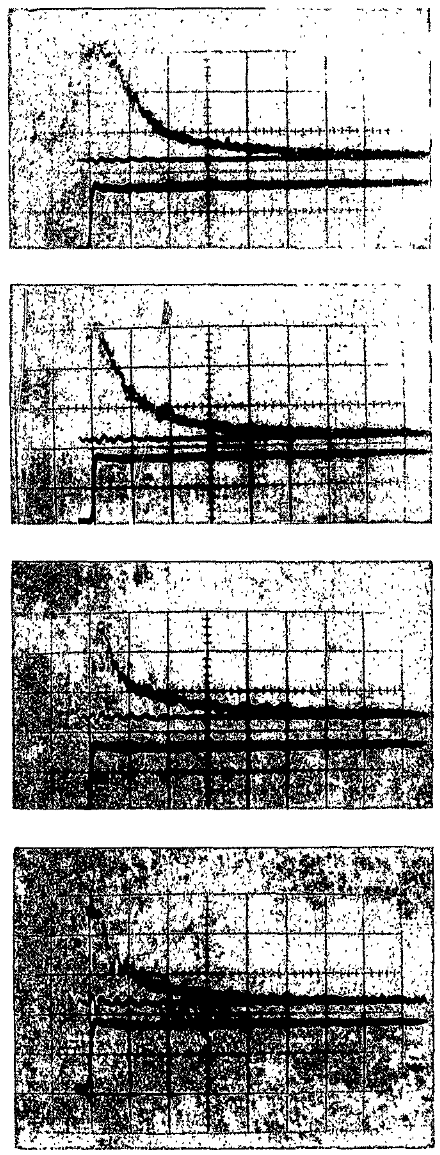

.13 mm Hg

.092 mm Hg

.057 mm Hg

.039 mm Hg

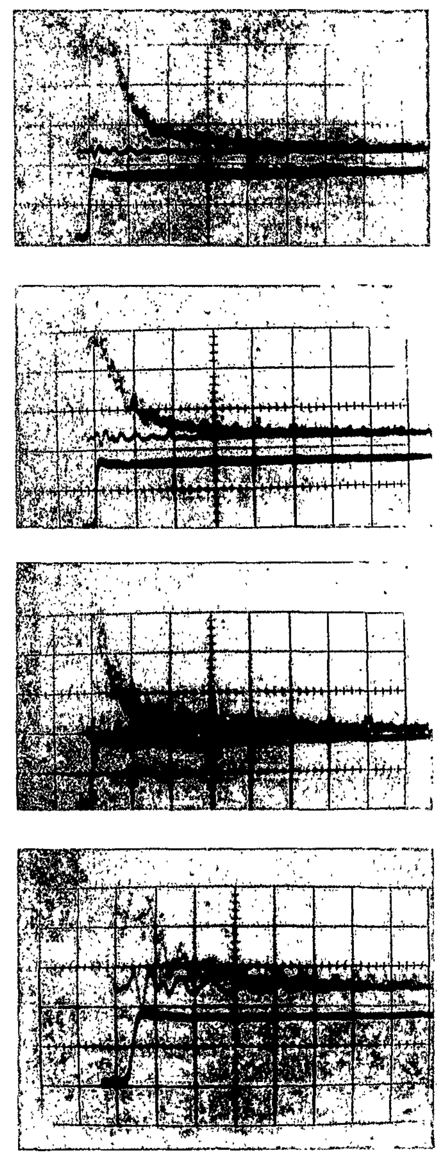

200 ns / division 200 ns / division

5876A $3^3D \rightarrow 2^3P$ 4471A $4^3D \rightarrow 2^3P$

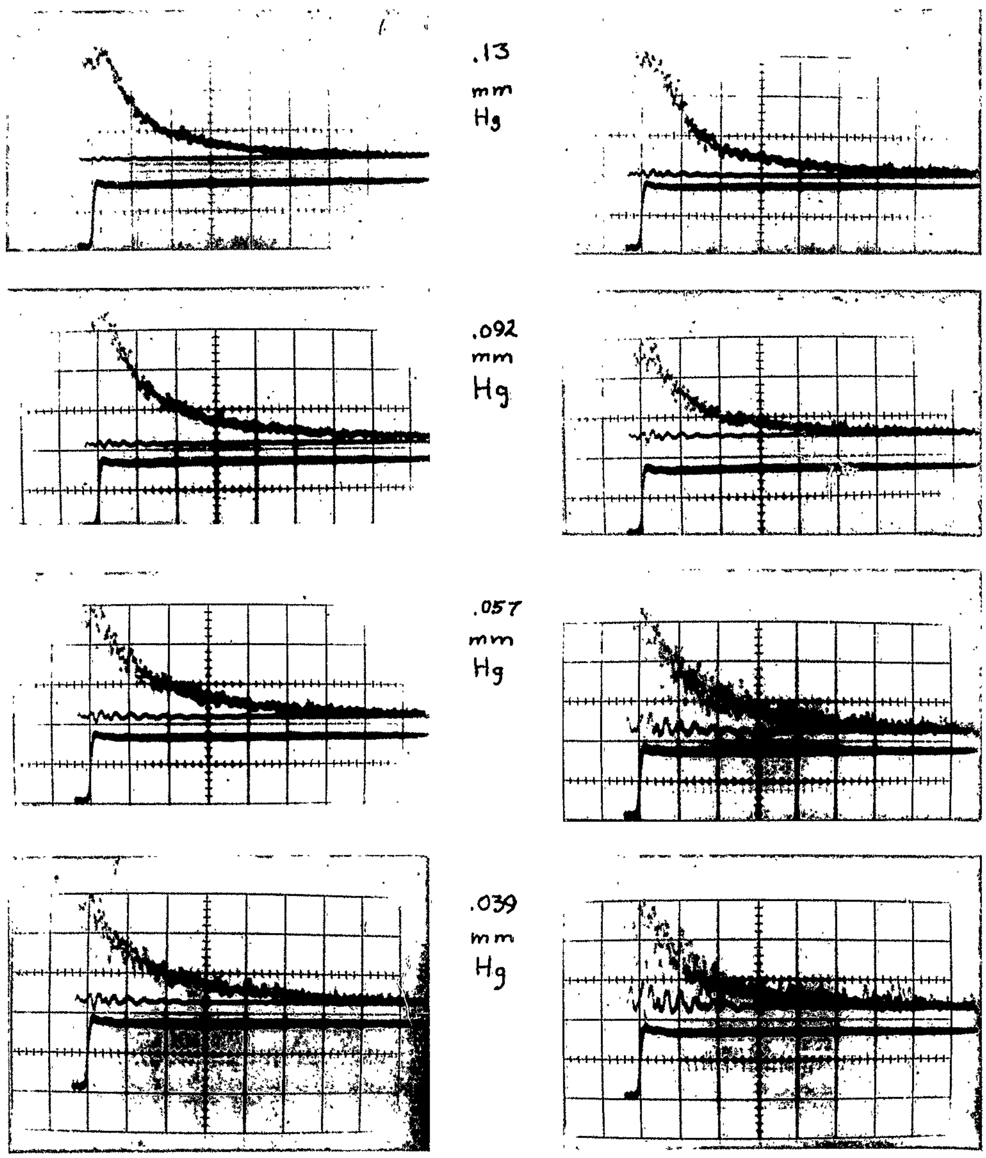

200 ns/division 200 ns/division

In order to aid in the separation of statistical fluctuations in the light signal from true deviations caused by other means each light decay curve is an overlay of from three to five traces. The zero light reference is obtained by taking a second exposure on the same photograph while an opaque card has been slid between the photomultiplier and the excitation tube. Thus each photograph is made up of three curves: a) the overlaid light curves, b) the zero light reference curve, and c) the bias step.

In carrying out the experiment both the upper and lower beams are driven by the same sweep circuit so there is no chance of maladjustment of the time synchronization between the two curves.

There are several observations which can be made with regard to the photographs before a discussion of the actual decay time data is presented.

The presence of statistical noise on the light curves with its apparent absence on the zero light trace clearly indicates that the electronic circuits have sufficient time resolution to follow any light decay shown. A photograph of the 5016Å curve at very fast sweep speeds showed that this is true for that curve as well although it is not obvious from the curves presented here.

The second observation is that the high pressure triplet curves do not decay immediately after the bias is applied at high pressure. This has been discussed in detail in the theory of the operation of the excitation tube on pages 49 and 50 of Chapter II.

Another observation is that there is a slowly decaying tail on each curve. This tail is apparently made up jointly of a slowly decaying light signal and a photomultiplier signal. That this is true

can be seen by the following two experiments that have been carried out. Holding the time sequence constant on the excitation pulse, the photomultiplier pulse and the bias step, a variation in the photomultiplier voltage produced an apparent change in the relaxation time on the tail. This clearly indicated that at least part of the tail signal is a property of the photomultiplier. The second experiment involved applying the bias signal to the excitation tube before the photomultiplier is turned on. When the photomultiplier was turned on a weak decaying signal was observed which could be eliminated completely by cutting out the light from the excitation tube with the opaque card. The rate of decay of this tail signal was much slower than the decay of the actual light curve when the bias step was initiated after the photomultiplier was turned on. Thus it becomes obvious that the tail is composed of a slowly decaying light signal and a photomultiplier signal. Unfortunately no meaningful data may be extracted from the tails of these photographs until more is known about the contribution due to photomultiplier after-pulses.

A final observation is that for the 5016Å line there is an obvious flattening of the tail curve at around 250 n-sec which persists to about 500 n-sec when the curve begins to fall again. In fact, at the lowest pressure this zone seems to provide a slight rise in the tail signal. This trend appears in the 4922Å curves too but statistical noise obscures it at low pressures. The triplet curves seem to lack any definite tendency in this direction. The reader should be cautioned that the singlet curves are obtained at different sweep speeds from the triplets therefore this must be taken into account when comparing data between these two sets of curves. Another point should

be emphasized as well. The pressures are McLeod gauge readings and must be corrected to around 1100°K to obtain particle densities in the excitation zone.

A final observation may be made. It is that the amount of pick-up signal shown on the zero light trace indicates the changes in the amplification of the oscilloscope so it can provide relative amplitude information if it is ever desirable for further analysis of these curves.

Lifetime Information From Data Curves

In order to obtain lifetime data from the photographs they were projected onto an 8 x 11 sheet of paper and a carefully sketched average curve was drawn through the center of the statistical noise. The same was done for the reference curve. Then while the curve was still being projected a straight edge was aligned with the graticle marks and 25 to 30 vertical lines were drawn between the two curves.

Amplitudes were measured at each of these 30 divisions and their data was plotted on semilogarithmic graph paper.

All of the curves were complex so by an iterative procedure the tail curve was approximated by a straight line which when subtracted from the strong light signal gave a good straight line graph of the differance. The mean life for this final curve was interpreted as the relaxation time for the state.

The procedure was applied to a synthetic curve made up of two straight lines plotted on semilogarithmic paper and transferred to another graph. In extracting the data from this curve the accuracy of the first component was within 10% of the original value while the data on the tail was somewhat less accurate. This method of analysis therefore

seemed to yield results compatible with the other inaccuracies provided by the statistical noise and hand tracing of the curves.

The data obtained in this manner are plotted in Figure 18. Since the data points were quite scattered they have been connected by straight lines in order to indicate which points apply to a given spectral line. On the same figure the average lives and their mean deviations are plotted. Data from the coincidence techniques studies of Heron, McWhirter, and Rhoderic,[36] and of Bennett and Dalby[37] are also given on this same graph. It should be pointed out that the obscissa of these average values on the graph implies nothing about the pressures used in finding them.

It can be seen that while there is general agreement between the 4713Å and the 3889Å data obtained in this laboratory with that of the other two groups, the mean values obtained in this laboratory tend to yield longer lives than are quoted from these other sources.

If best fit straight lines were drawn through the 4713Å and the 3889Å lines as an extrapolation to zero pressure there would be better agreement between the data from the various sources. The only justification for such a downward extrapolation is that the pressure dependant cutoff time might be reflected in the curvature of the light decay curve in such a way that the graphical analysis does not remove it. If this is true then the extrapolation is justified and the overall consistency in data from the various laboratories is good.

The 5876Å line which arises from the rapid decay of the 3^3D level shows an order of magnitude discrepancy however and deserves

---

[36] Op. Cit.

[37] Op. Cit.

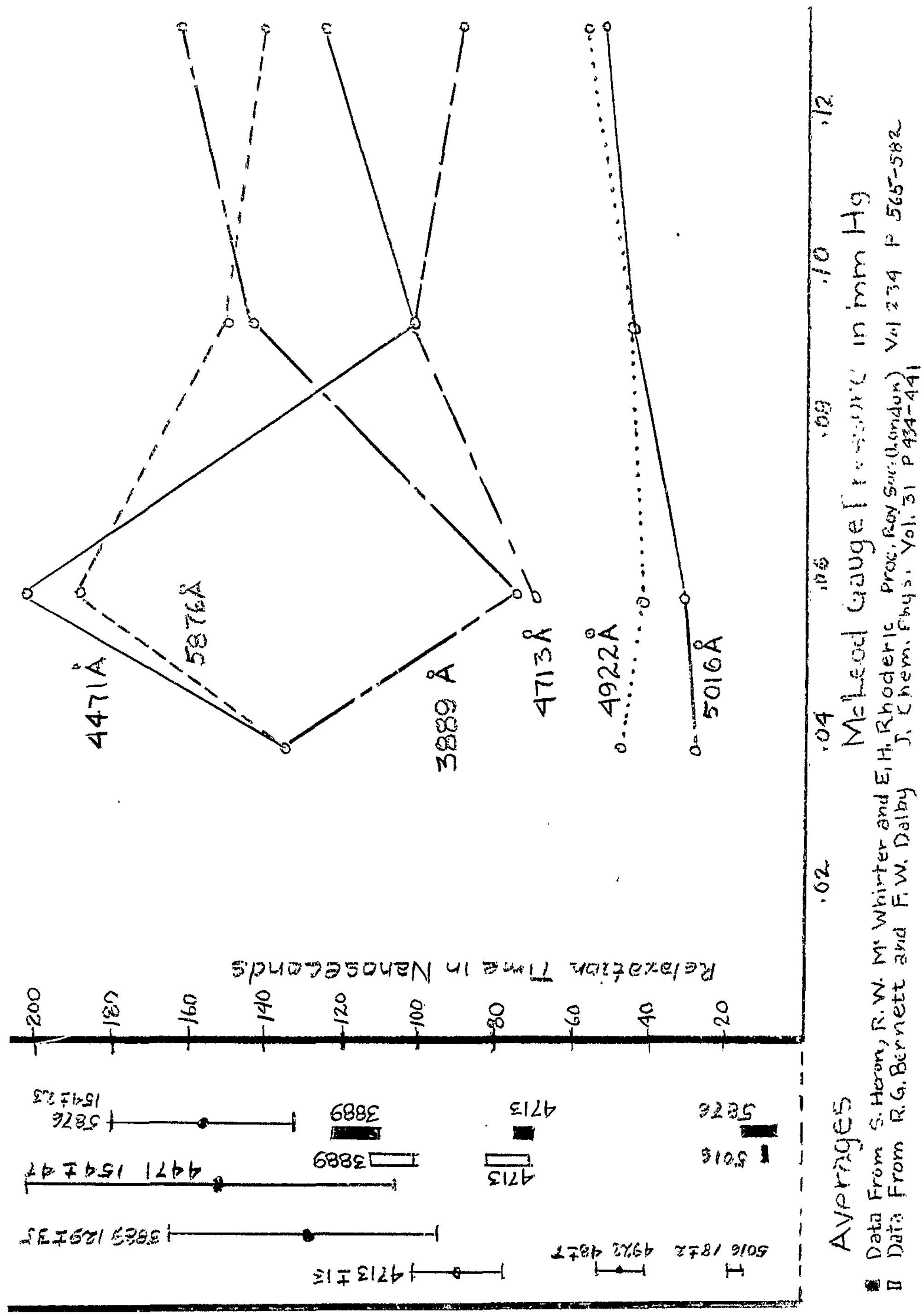
4471Å
5876Å
3889 Å
4713Å
4922Å
5016Å
.02
.04
.06
.08
.10
.12
McLeod Gauge Pressure in mm Hg
Relaxation Time in Nanoseconds
200
180
160
140
120
100
80
60
40
20
Averages
Data From S. Heron, R. W. McWhirter and E. H. Rhoderic Proc. Roy. Soc. (London) Vol 234 P 565-582
Data From R. G. Bernett and F. W. Dalby J. Chem. Phys. Vol. 31 P 934-941
4713 ± 13
3889 129 ± 37
4471 154 ± 47
5876 154 ± 23
3889
4713
5016
5876
5016 18 ± 2
4922 48 ± 7

Figure 18

careful study. A look at the position of the line in the helium spectrum as shown in Figure 19 clearly indicates that it stands alone. Therefore, the obvious first assumption of having picked either the wrong line or more than one line with the optical filter must be eliminated.

The work done in Glascow by Heron et. al. showed a distinct rapid component which they interpreted as the natural life of the 3^3D state which was followed by a very slow decay component which they attributed to flourescence of the walls. No such sharp leading edge is apparent on the photographs taken in this laboratory. If one interprets the 156 n-sec relaxation-time found in this laboratory as being due to cascading from higher levels then the absence of a sudden drop at the outset would seem to indicate that one of two properties peculiar to our excitation scheme is obscuring it. Either the 3^3D state is not being excited to any great extent by electron impact or the time resolution of the electron cutoff for the triplet states is so poor that the fast decay is obscured by continued excitation which decreases more slowly.[38] In this instance a combination of both effects might be justified. However the complete absence of the early rapid decay remains true even down to the lowest pressure where the cutoff time resolution is assumed to be good.

The presence of a strong cascading effect in this work which was not present in the work of Heron et. al. can be justified on two grounds. First the electron beam energy was adjusted for peak excitation of each line being studied in Glascow while the excitation energy in this laboratory was far greater than peak and thereby should not give

---

[38] See the theory of cutoff in Chapter II, page 49 for the reason triplet and singlet lines show different effects.

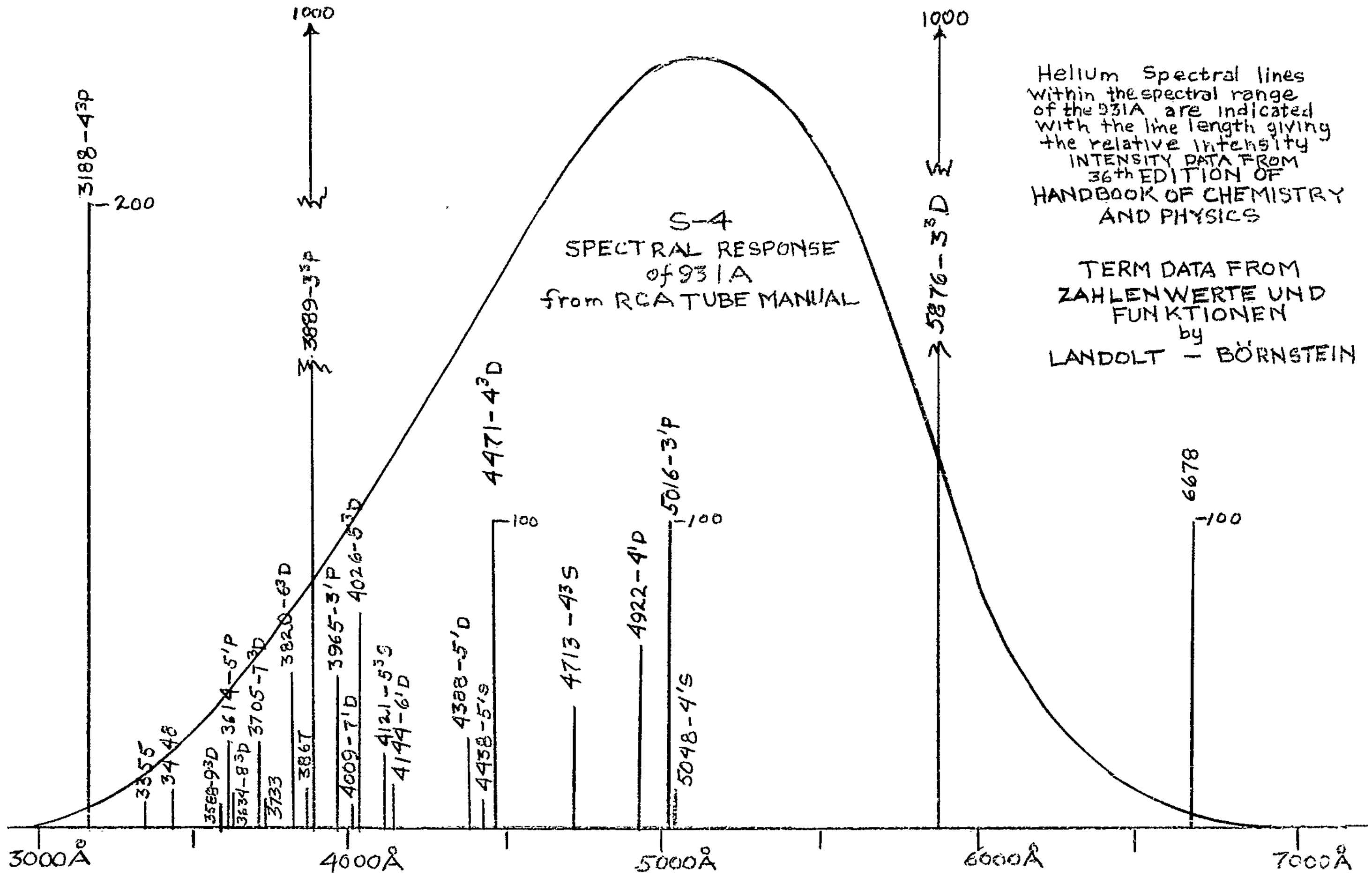
Helium Spectral lines within the spectral range of the 931A are indicated with the line length giving the relative intensity
INTENSITY DATA FROM 36th EDITION OF HANDBOOK OF CHEMISTRY AND PHYSICS
TERM DATA FROM ZAHLENWERTE UND FUNKTIONEN by LANDOLT – BÖRNSTEIN
S-4
SPECTRAL RESPONSE of 931A from RCA TUBE MANUAL
3188-4³P
200
1000
3889-3³P
5876-3³D
4471-4³D
100
4713-4³S
4922-4¹D
5016-3¹P
5048-4¹S
6678
3355
3448
3588-9³D
3614-5¹P
3634-8³P
3705-7³D
3733
3820-6³D
3867
3965-3¹P
4009-7¹D
4026-5³D
4121-5³S
4144-6¹D
4388-5¹D
4438-5¹S
3000Å
4000Å
5000Å
6000Å
7000Å

FIGURE 19

favorable preferential excitation. The second point is that the excitation source used in this laboratory was a step function or at least a very broad pulse of two orders of magnitude greater time duration than that used in the coincidence technique. As was pointed out in the theory section the build up to constant state densities requires continued excitation for several natural lives of the state being considered. In this instance the 20 n-sec excitation period employed by Heron et. al. was not long enough to build up any appreciable fraction of the steady-state density of the 156 n-sec component cascading into the 3^3D. Our 1500 n-sec excitation time more than provided enough time for steady-state densities to be reached for the 156 n-sec upper levels.

Once it became clear that cascading should provide the key to the apparent discrepancy between the apparent relaxation times of the 3^3D state the author converted the oscillator strengths given for helium in Landolt-Bornstein[39] to transition probabilities and from them determined the natural lives of the states. Both the limited range of the table and obvious tabulation errors of the $5^3S \rightarrow 2^3P$ and the $5^3P \rightarrow 3^3S$ oscillator strengths leave the picture quite incomplete. But the data that was obtained give some clues as to where the source might be. This information is shown in Figure 20 where the computed values are given on the energy level lines while the experimental relaxation times are given on the spectral transition lines studied to determine the lives of the upper level. It is clear from this diagram that both the 4471Å line and the 5876Å line experience the same type of cascading effects.

---

[39] _Op_. _Cit_.

HELIUM TRIPLET STATES

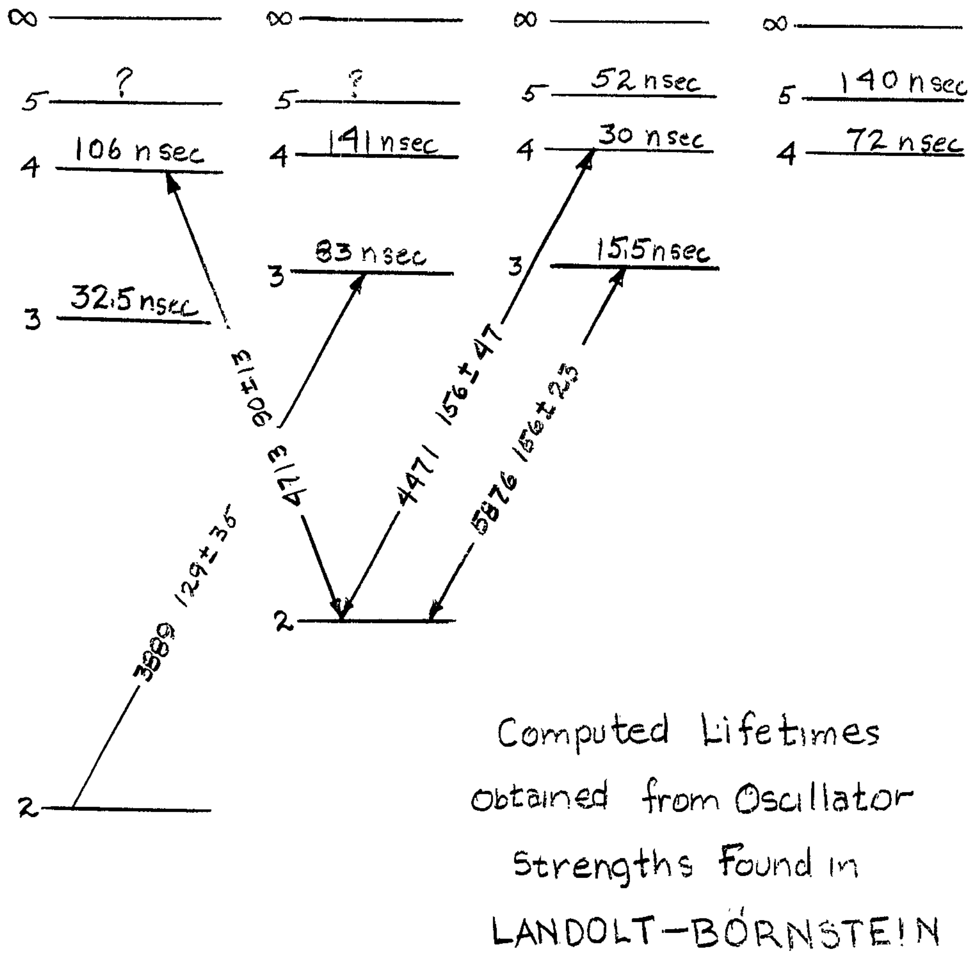

Figure 20

Even the trends are the same in the pressure-life-time graph but this might well be fortuitous error in the extraction of data from the photographs.

Clearly the trends toward longer natural lives as the n values increase seem to indicate that the bulk of the cascading components must come from local levels such as the 5^3F or the 4^3P. Not enough information is now known about excitation cross sections to make an accurate analysis of the upper P and F level densities but the data clearly points to a very small contribution from these large n levels. A much more careful study of the tails on the light curves might be carried out in order to determine something of the densities of these upper levels. There will need to be some changes in the present instrumentation before such a study can be carried out because of the apparent photomultiplier after-pulse contribution. The problem appears to be far from insurmountable however.

Thus in conclusion a very direct method has been devised for measuring atomic lives with a great deal of flexibility being built into the system. The results obtained clearly indicate the validity of the method while at the same time the steady state conditions show up as distinct from short pulse conditions in a way that indicates that cascading population of states may be a much more important effect than direct excitation for certain states and at certain electron energies.

BIBLIOGRAPHY

Articles

Bennett, R. G. and Dalby, F. W. "Experimental Determination of Oscillator Strength of The First Negative Bands of N_2^+," J. Chem. Phys. Vol. 31, p. 434-444, 1959.

Fowler, R. G. "Radiation from Low Pressure Discharges," Handbuch der Physik, Gasentladungen II, Volume 22, p. 209-253.

Heron, S., McWhirter, R.W.P. and Rhoderic E. H. "Measurements of Lifetimes of Excited States of Helium Atoms," Proceedings of the Royal Society of London, Vol. 234, p. 565-583.

Books

Bates, D. R. (ed.) Atomic and Molecular Processes. New York: Academic Press, 1962.

Condon, E. U. and Shortley, G. H. The Theory of Atomic Spectra. Cambridge: University Press, 1935.

Espe, W. and Knoll, M. Werkstoff Konde der Hochvakuumtechnik. Berlin: Verlag Julius Springer, 1936.

Herzberg, Gerhard. Atomic Spectra and Atomic Structure. New York: Dover Publications, 1944.

Hildebrand, F. B. Advanced Calculus for Engineers. New York: Prentice-Hall Inc., 1949.

Kimbark, Edward Wilson. Electrical Transmission of Power and Signals. New York: John Wiley and Sons, 1949.

Leighton, Robert B. Principles of Modern Physics. New York: McGraw-Hill Book Company, 1959.

Lewis, I.A.D. and Wells, F. H. Millimicrosecond Pulse Techniques. New York: McGraw-Hill Book Company, 1954.

Massey, H.S.W. and Burhop, E.H.S. Electronic and Ionic Impact Phenomena. Oxford: Clarendon Press, 1952.

Pirani, M. and Yarwood, J. Principles of Vacuum Engineering. New York: Reinhold Publishing Corporation, 1961.

Ridenour, Louis N. (ed.) Radar Systems Engineering. M. I. T. Radiation Laboratory Series, Vol. I, New York: McGraw-Hill Book Company., 1947.

Thompson, J. and Callick, E. B. Electron Physics and Technology. London: The English Universities Press Ltd., 1959.

von Engel, A. Ionized Gases. Oxford: Clarendon Press, 1955.

White, Harvey Elliott. Introduction to Atomic Spectra. New York: McGraw-Hill Book Company, Inc., 1934.

Public Documents

National Bureau of Standards, Monograph 50, Bibliography on Atomic Transition Probabilities. Washington, D. C., U. S. Government Printing Office, 1962.

The Bulletin of Engineering and Architecture No. 43, Millimicrosecond Pulse Technique. University of Kansas, 1959.

APPENDIX I

LIGHT INTENSITY FROM A CYLINDRICAL RADIATOR

In this experimental work it was desirable to find the total light intensity at some point external to a cylindrical radiating system which could radiate uniformly throughout its volume. It is assumed that none of the radiant energy is absorbed within the cylinder. Another consideration incorporated in this derivation involves the use of an iris which eliminates light external to a truncated cone at the end of the cylinder.

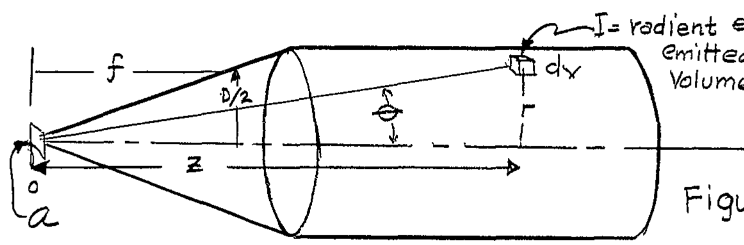

Figure 21

Ω solid angle subtended by a, $\Omega = \frac{a}{z^2+r^2}\cos\theta = \frac{a z}{(z^2+r^2)^{3/2}}$

$$d\mathcal{I} = \frac{\Omega}{4\pi} I \, dv$$

$$d\mathcal{I} = \frac{a I z}{4\pi (z^2+r^2)^{3/2}} dv$$

$$dv = 2\pi r dr dz$$

$$d\mathcal{I} = \frac{a I z r 2\pi}{4\pi (z^2+r^2)^{3/2}} = a\rho \frac{z r}{2(z^2+r^2)^{3/2}} dr dz$$

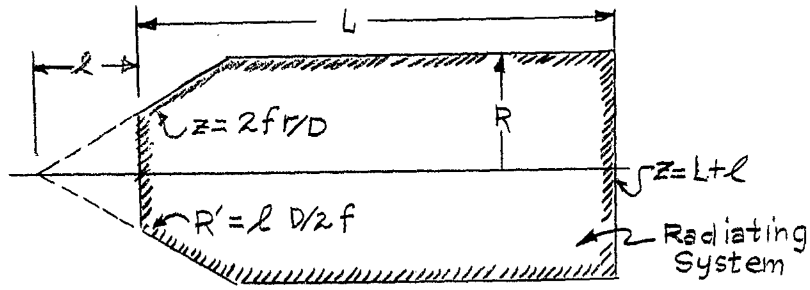

Figure 22

$$\mathcal{J} = \frac{a}{2} I \left[\int_0^R \int_{z=\frac{2f}{D}r}^{\ell+L} \frac{zr}{(z^2+r^2)^{3/2}}\, dr\, dz - \underbrace{\int_0^{R'} \int_{z=\frac{2f}{D}r}^{\ell} \frac{zr}{(z^2+r^2)^{3/2}}\, dr\, dz}_{\text{External cone}} \right]$$

$$\mathcal{J} = \frac{a}{2} I \left[\int_0^R \left[\frac{-r}{(z^2+r^2)^{1/2}} \right]_{\frac{2fr}{D}}^{\ell+L} dr - \int_0^{R'} \left[\frac{-r}{(z^2+r^2)^{1/2}} \right]_{\frac{2fr}{D}}^{\ell} dr \right]$$

$$\mathcal{J} = \frac{a}{2} I \int_0^R \frac{r}{\left[(\frac{2fr}{D})^2 + r^2\right]^{1/2}} dr - \int_0^R \frac{r}{\left[(\ell+L)^2 + r^2\right]^{1/2}} dr - \int_0^{R'} \frac{r}{\left[(\frac{2fr}{D})^2 + r^2\right]^{1/2}} dr + \int_0^{R'} \frac{r}{(\ell^2+r^2)^{1/2}} dr$$

$$\mathcal{J} = \frac{a}{2} I \left\{ \left[\frac{r}{\left[(\frac{2f}{D})^2 + 1\right]^{1/2}} \right]_0^R - \left[\frac{r}{\left[(\frac{2f}{D})^2 + 1\right]^{1/2}} \right]_0^{\ell \frac{D}{2f}} - \left[\left[(\ell+L)^2 + r^2\right]^{1/2} \right]_0^R + \left[(\ell^2 + r^2)^{1/2} \right]_0^{\ell \frac{D}{2f}} \right\}$$

$$\mathcal{J} = \frac{a}{2} I \left\{ \frac{R - \ell D/2f}{\left[(\frac{2f}{D})^2 + 1\right]^{1/2}} + \ell\left(\left[1 + (\tfrac{D}{2f})^2\right]^{1/2} - 1 \right) + (\ell+L) - \left[(\ell+L)^2 + R'^2\right]^{\frac{1}{2}} \right\}$$

These will cancel

$\ell + L \gg R \Rightarrow \left[(\ell+L)^2 + R^2\right]^{1/2}$ may be expanded to $\left[\ell + L + \frac{1}{2}\frac{R^2}{\ell+L} - \frac{1}{8}\frac{R^4}{(\ell+L)^3} \cdots\right]$

$$\mathcal{J} = \frac{a}{2} I \left\{ \left[\frac{R - \ell D/2f}{\left[(\frac{2f}{D})^2 + 1\right]^{1/2}} + \ell\left(\left[1 + (\tfrac{D}{2f})^2\right]^{1/2} - 1 \right) - \frac{1}{2}\frac{R^2}{\ell+L} \right\}$$

DATA ON ATOMIC HELIUM

	1 Torr	.13 Torr	.092 Torr	.057 Torr	.038 Torr
Number of particles/cc at 273°K	35.33×10^{15}	4.59×10^{15}	3.25×10^{15}	2.01×10^{15}	1.34×10^{15}
At 1100°K	8.8×10^{15}	1.14×10^{15}	$.81 \times 10^{15}$	$.502 \times 10^{15}$	$.334 \times 10^{15}$
Mean free path of He atom in He at 273°K	.176 mm	.135cm	.1915cm	.309cm	.463cm
At 1100°K	.855 mm	.658cm	.93cm	1.5cm	2.25cm
Ions/electron-cm 273° (at 110V)	1.256 (100V) 1.245 (100v) 1.22 (90v) 1.173 (80v)	.632 .162 – .153	.1155 .1145 – .083	.0715 .0709 – .0671	.0477 .0474 – .0448
1100°K Ions/electron cm	.311 (110v) .309 (100v) .303 (90v) .292 (80v)	.0404 .0402 .0393 .038	.0286 .0284 .0278 .02685	.0177 .0176 .01725 .0166	.0118 .1175 .0115 .0111

Velocity of atoms $\overline{V}$ 1100°K = 2.41×10^5 cm/sec ($\overline{v} = \sqrt{8KT/\pi m}$) (40)

The Sutherland equation for the ratio of mean free paths $\overline{x}_1/\overline{x}_2 = T_1(T_2+C)/T_2(T_1+C)$, C = 80 for Helium

Number of particles/cc obtained from Avogadro's Number and the Ideal Gas Laws.

Ionization efficiency obtained from P. T. Smith.[41]

[40] A. von Engel – Ionized Gases – The Clarendon Press (1955).

[41] P. T. Smith, Phys. Rev. 36 1293–1299 (1930).

APPENDIX III

SOME CONSIDERATIONS CONCERNING THE TREATMENT OF RADIATION IMPRISONMENT IN THE RELAXATION TIME EQUATION

Radiation imprisonment or blockading is the result of the recapture of photons within the radiating gas through photo excitation of other atoms of the same gas. Thus the light which might normally be expected to radiate in a straight line from within a gas actually only diffuses through random capture and reradiation provided there is a large enough density of atoms which can result in this capture phenomena.

In essentially all of the laboratory discharges the only atoms which acquire a large enough density to become important in imprisonment consideration are the ground state atoms. It is therefore the resonance radiation which suffers imprisonment.

If one assumes full blockading the rate of loss of states of an upper level is exactly matched by a regain of those states in neighboring atoms through the reabsorption of this radiation. Thus the $\frac{dN_{io}}{dt} = 0$ for the gas as a whole. Thus since $\frac{dN_{io}}{dt} = -A_{io}N_i$ in the usual sense, this implies that for the system as a whole $A_{io}=0$.

If a gas has been excited to all levels and suddenly the excitation is cut off the total number of excited atoms plus the number of resonance photons will always be the same under the condition of full blockading. What will happen of course will be that through

branching all resonance levels above the lowest resonance level will be depleted through branching to other states where by the emission of one or more photons they arrive back at a resonance state. Thus as time progresses non-resonance light continues to escape the gas while all of the excited atoms adjust to the final lowest resonance level. At this point the atoms continue to radiate individually but the gas as a whole does not lose energy. For each excited state lost there is a photon created and for each photon lost a new atom is excited.

Clearly there is no laboratory situation which could result in such a condition as stated above. If perfectly reflecting walls were possible or if the dimensions of the gas were very large indeed relative to the diffusion length for the photon then the conditions might be approximated. The diffusion of energy to the walls of the vessel will always deplete the gas of its energy however.

With this knowledge it is well to consider what alterations one might make in the loss rate equation which could account for the depletion.

The simplest and most direct solution follows if one can assume that the loss process is truly proportional to the particle density. If this is true then a coefficient $A^*_{i,o}$ may be found for this loss process such that $A_{i,o} > A^*_{i,o} > 0$. Using this system loss probability coefficient one would be able to find the apparent life of a state in which imprisonment and spontaneous emission are the only rate processes contributing to the state density function by the following simple expression.

$$\bar{t} = 1/\left(\sum_{j=1}^{j<i} A_{i,j} + A^*_{i,o}\right)$$ where it is

clear that $A^*_{i,o}$ plays the roll of the $A_{i,o}$ which would be used if imprisonment did not play a part.

The rate of loss of photons from a blockaded gas will depend on two obvious factors: a) the diffusion rate which in turn depends upon the ground state particle density, and b) the distance through which the energy must diffuse i.e. the dimensions of the container. It therefore becomes meaningless to state the apparent relaxation time blockading conditions without giving both pressure and vessel dimensions if a consistence check is to be made from theory.

For a more complete discussion of the diffusion of radiation the reader is referred to section 7, page 225-227 of the article by Professor R. G. Fowler entitled "Radiation from Low Pressure Discharges" in The Handbuch der Physik Vol. 22 (1956).

APPENDIX IV

SPACE CHARGE POTENTIAL WITHIN CYLINDER ARISING FROM CHARGES PROJECTED RADIALLY INWARD WITH A FINITE INITIAL VELOCITY

In order to investigate the problem one will assume the charge to be continuous and having a density ρ given by the following expression:

$$\rho = i / v a$$

Here i is the current, a is the area through which the charge passes while v is the velocity of the charge. Clearly for discrete charges one has

$$Ne = \rho = i / va$$

where the notation is the same as in the glossary found in Chapter I.

In order to solve the problem the end effects will be neglected and thereby the infinite cylinder equations will apply. It will be assumed that the current is directed radially inward and that there is a central electrode which will serve as a sink.

The equations are now presented in terms of the required expression followed by various expressions which are needed to solve for it.

$$V(r) = -\int_0^R E_r dr$$

where E_r = radial Electric field.

$$E(r) = \frac{q/\ell}{2\pi K_0 r}$$

This expression is the equation for the radial field due to charge per unit length q/ℓ enclosed in an infinite cylinder of radius r. It may be found in texts on Electricity and Magnitism.[42]

Clearly $\quad q/\ell = \frac{1}{L}\int_0^q dq$

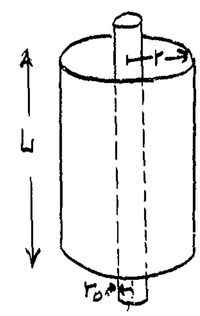

Figure 23

and $dq = \rho\, 2\pi r L dr$

Remembering that

$$\rho = i/va$$

where $a = 2\pi r L$ in this case

and $v = \sqrt{(E_0 - V(r))2\frac{e}{m}}$

where E_0 is the energy per unit charge entering at radius R the outer bound of the cylinder, one may write dq in the following way.

$$dq = \frac{i\,\cancel{2\pi r L}\,dr}{\cancel{A}\sqrt{(E_0 - V(r))2\frac{e}{m}}}$$

from which the q/ℓ expression may be found as follows

$$q/\ell = \frac{1}{L}\int_0^q dq = \frac{1}{L}\int_0^r \frac{i\,dr}{\sqrt{(E_0 - V(r))2\frac{e}{m}}}$$

Returning to the expression for E(r) one now has

$$Er = \frac{1}{2\pi L r K_0}\int_0^r \frac{i}{\sqrt{(E_0 - V(r))2\frac{e}{m}}}\,dr$$

---

[42]P. H. Harnwell, Principles of Electricity and Magnetism (McGraw-Hill, 1949), p. 20.

and from this expression V(r) follows in the following way.

$$V(r) = -\int_{r_0}^{r}\left[\frac{1}{L\,2\pi K_0 r}\int_{r_0}^{r}\frac{i}{\sqrt{(E_0 - V(r))2\frac{e}{m}}}\,dr\right]dr$$

taking the derivative of each side one has

$$\frac{dV(r)}{dr} = -\frac{1}{2\pi L K_0 r}\int_{r_0}^{r}\frac{i}{\sqrt{(E_0 - V(r))2\frac{e}{m}}}\,dr$$

transposing the r one has

$$r\frac{dv}{dr} = \frac{i}{2\pi L K_0\sqrt{2\frac{e}{m}}}\int_{r_0}^{r}\frac{dr}{\sqrt{E_0 - V(r)}}$$

and taking another r derivative one has the differential equation defining V(r).

$$r\frac{d^2V}{dr^2} + \frac{dv}{dr} = \frac{i}{2\pi L K_0\sqrt{2\frac{e}{m}}}\left(E - V(r)\right)^{-\frac{1}{2}}$$

For the differential equation above the boundary potentials are established by the potential on the central electrode and on the external boundary. If it should occur that the $E_0 - V_r = 0$ in the interval, as will be the case when the charge reaches a potential barrier established by its own space charge within the cylinder, then instabilities arise. Certainly, much of the charge will be turned back reversing its inward course. Its velosity is still established by $\sqrt{(E_0 - V(r))\,2\,\frac{e}{m}} = v$. The current to be employed in the charge density expression is $2i$ where i is assumed to be the current due to charges moving in one direction alone so long as cylindrical symmetry can be applied. If true symmetry should persist (a condition very unlikely because of the instabilities) then the boundary condition at the inner reach of the space charge will be $\frac{dV(r)}{dr} = 0$ since there will be no charge within that zone.

Should the charge density be very low the velocity of the injected charges might not be appreciably changed by space charge potential. Under these circumstances, one finds that the rather simple result follows immediately

$$q/\ell = \frac{1}{L}\int_0^r \frac{i\,dr}{v} = \frac{ir}{Lv} \qquad (\text{assume } r_0 = 0)$$

$$E_r = \frac{ir/Lv}{2\pi K_0 r} = \frac{i}{L}\,\frac{}{2\pi K_0 v}$$

$$V(r) = -\int_0^r E_r\,dr = -\frac{i\,r}{L 2\pi K_0 v}$$

It must be pointed out that this expression holds only if $V_r \ll E_0$, the kinetic energy of the incoming charge.

One could now use this approximate expression to see if the actual problem in this research will allow electrons to penetrate radially through the excitation zone. Assuming the electron energy is 100 volts and likewise assuming the total impact current of 2(.9) amperes is involved, since the electrons are not collected but rather must escape from the zone by the same path through which they entered one now has

$$V(r) = \frac{1.8 \text{ amperes } 1.27/2 \text{ cm}}{5\text{cm }(6.28)\ 8.85\times10^{-12}\frac{\text{coulmb}}{\text{Joule meter}}\sqrt{2(1.77)10^{11}\,[100]}} =$$

$$690\text{v}\ !!$$

Clearly 690v is not $\ll$ than 100. In fact the instability arises even closer to the grid than $\frac{100\text{v}}{690\text{v}}\ \frac{1.27}{2}$ cm = .92 mm since the potential

is no longer a linear function of r but a rapidly rising function due to the increased charge density which results from slowing the electrons. This computation clearly shows that the presence of a neutralizing space charge will be required in order to allow the large current available from the cathode to be effective in the central zone.

APPENDIX V

PHOTOMULTIPLIER FALL TIME THEORY

In order to understand the resolution time of a photomultiplier one needs to discover how rapidly the output signal will fall for an instantaneous cut off of the cathode current. There is an inherent delay time between the time the cathode is cut off and the time it takes for this information to reach the anode. This inherent dynode to dynode transit time will be disregarded since it only shifts the time axis for the entire output signal. The thing of interest in this work is the inherent time dispersion of the anode electron burst because of the varying path lengths and electron speeds at different points in the dynode structure.

The actual shape of the current bursts have been displayed on an oscilloscope and they have a form similar to that shown in figure 24.

Here $t = 0$ is the instant when the first anode signal is received from the cathode. As time advances the current builds up, crests and ultimately falls to zero again.

For high cathode currents the anode current is composed of an overlay of many of these single electron bursts.

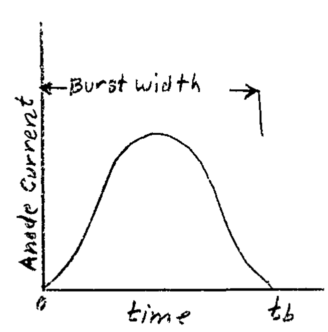

Figure 24

In order to derive an expression for the shape of the total anode current fall curve when a large cathode current is suddenly turned off one needs to look at the composition of the integrated anode current in terms of the overlay of these individual bursts.

A few simplifying assumptions will be made in order to attain a clear mental picture from which to work.

a) Assume that the bursts created at the anode by a single cathode electron are all of the same shape and size; these rigid limitations will be relaxed later.

b) Assume that the cathode current is so large that the anode current is essentially constant. This means that the excursions from the pure d c at the anode are extremely small compared to the signal strength. This assumption implies that the number of cathode electrons emitted within any small but finite time interval will be the same as the number emitted during any other time interval of the same duration.

c) The last assumption to be made is that the cathode current can be cut off instantly providing a true step function of cathode current.

To start the discussion one must observe the positions of burst a, b and c, which contribute to the d c signal as shown below

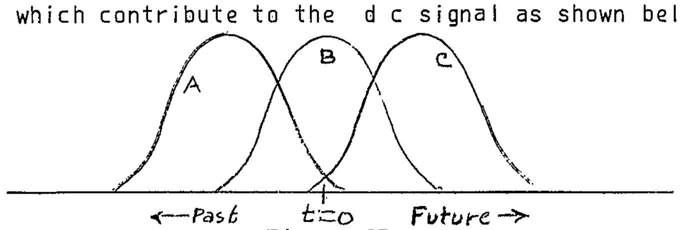

Figure 25

Assumption b) states that there will be just as many bursts near the A curve as there are near the B curve or the C curve. Burst A has nearly dissipated itself, B is near its peak and C is just beginning. Thus, even though the number of bursts of each phase is the same their contributions to the total current are quite different.

In order to produce a mathematical formulation one may identify the bursts by dividing the time axis into time intervals and classifying the bursts by the time interval in which they begin to appear at the anode; no other identification needs to be made.

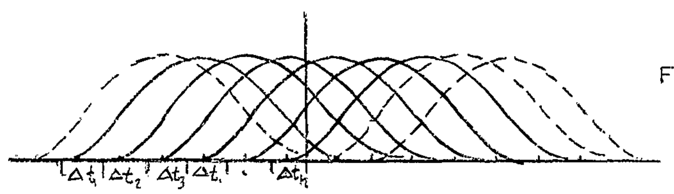

Figure 26

As shown in figure 26, only those bursts falling in time interval $\Delta t_1, \Delta t_2, \ldots \Delta t_n$ contribute to the current at t_0. All others miss the mark by arriving too early or too late. So the current is equal to the average contribution at $t = 0$ made by the bursts initiated within a given time interval multiplied by the number of bursts started in that time interval summed over all contributing time intervals.

Thus $I_a = \Delta N f(\Delta t) + \Delta N f(2\Delta t) + \cdots \Delta N f(n\Delta t)$

In compact notation: $I_a = \sum_{i=1}^{n} \Delta N f(i\Delta t)$

here f(t) is the shape function; i is the index of the summation and n) is the number of equal time intervals used to divide that portion of the time axis having curves which can be contributing to the anode current at t_0 and I_a is the anode current (not light intensity). ΔN is

the number of bursts being initiated within a time interval Δt and since each burst is initiated by a cathode electron ΔN is the cathode electron current multiplied by the time interval (or the electric current $\frac{I \text{ cathode}}{e}$ where e is the electronic charge). Thus

$$\Delta N = \frac{I_c}{e} \Delta t$$

Going to the limit $\Delta t \to 0$ the sum becomes

$$I_a = \frac{I_c}{e} \int_{t=0}^{t_b} f(t) dt$$

One can now normalize the step function and identify the normalization constant. Assume $f(t) = K \cdot F(t)$ where $F(t)$ is normalized to unity over the pulse width and K is the normalization constant.

Re-writing the previous expression and solving for K one has

$$I_a = \frac{I_c}{e} K \int_0^{t_b} F(t) dt = \frac{I_c}{e} K$$

hence $$K = \frac{I_a}{I_c} e = Me .$$

Here M is identified as the multiplication factor of the photomultiplier. The anode current takes on the new form

$$I_a = I_c M \int_0^{t_b} F(t) dt$$

Now consider figure 27 shown below

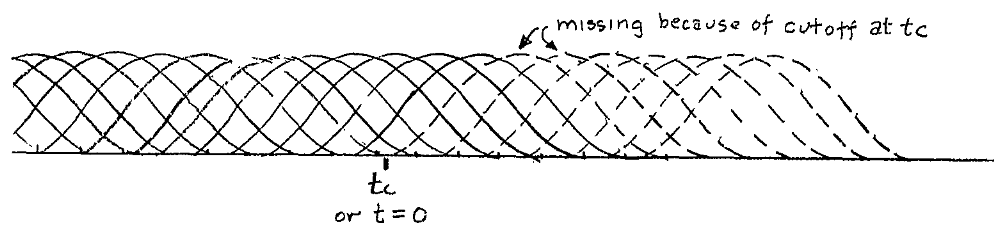

Figure 27

In figure 27 one observes that the signal is cut off such that the last bursts are just initiated at t_c. Up to this point the anode signal remains the same as derived above. As time advances however the toe of the first missing curves (dashed lines in drawing) will make no contribution; at time $(2\Delta t)$ later, more of this curve will be missing as well as the contribution from the bursts which should have started in this new interval. Expressed mathematically: At time Δt after t_c, $\Delta N f(\Delta t)$ will be missing from the total current while at $2\Delta t$, $\Delta N f(2\Delta t)$ will be missing as well as the contribution $\Delta N f(\Delta t)$ which just started in the second interval and so on. At time t seconds after t_c the missing components will add up to $\sum_{i_0}^{t/\Delta t} \Delta N f(i\Delta t)$ this is the same expression as the anode current equation except for the limits on the sum. It may be expressed by the following integral

$$I_a = \frac{I_c}{e} \int_0^t f(t)\,dt = I_c M \int_0^t F(t)\,dt$$

where the upper limit is now variable.

Thus the anode current equation is the total current minus the components which are missing.

$$I_a = I_c M \left[\int_0^{t_b} F(t)\,dt - \int_0^t F(t)\,dt \right]$$

Since the lower limits and the integrands are the same the two integrals may be combined into a single integral.

$$I_a = I_c M \int_t^{t_b} F(t)\,dt$$

Thus for a photomultiplier the anode current as function of time resulting from a step function at the cathode is the integral given above. Where $F(t)$ is the normalized burst shape function and t is understood to be zero at the instant that the cathode cutoff step function starts to alter the output current.

In order to relax some of the restrictive assumptions, assume now that the burst shape function is the same but the amplitudes of the bursts vary from burst to burst. The only change in the argument is that one must average the coefficients on the normalized shape function. Since the average value of M is the ratio of the anode current to the cathode current as determined by meter readings the identical formula applies where M must be thought of as the current ratio rather than a factor that can be associated with each burst.

If two or more distinct types of bursts should occur, one could find the time dependent current contribution for each type of curve and add them to obtain the total current at any time. This removes much of the restriction implied by assumption a).

If the cathode current is not large enough for assumption b) to hold, the shape function will give the approximate result with statistical "grass" overlaying the curve.

Under no circumstance can current arrive at the anode after the time t_b has elapsed following the cut off condition. Thus an absolute outside limit on the fall time is always equal to t_b under any circumstance.

The analysis was made for current fall time because of its importance in this research. Clearly the rise time analysis would be identical if one considered the d c current to be zero and instead of

losses one considered gains from $t = 0$ forward.

In this analysis a little reflection will show that the rise function is simply

$$I_{a\,(rise)} = I_c M \int_0^{t_b} F(t)\,dt$$

Therefore, the rise time and fall time will be equal and the only difference in shape will be the sign of the time dependant part.

The following is a table of the anode fall functions for several assumed anode electron burst shape functions.

Burst function	Fall function
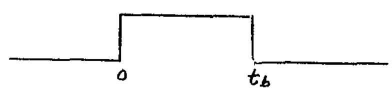	
$f = \begin{cases} 1 & 0 < t < t_b \\ 0 & t < 0,\ t > t_b \end{cases}$	$I_a(t) = K(t_t - t) \quad 0 \leq t \leq t_b$
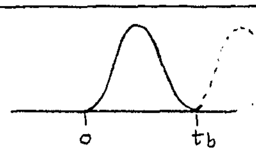	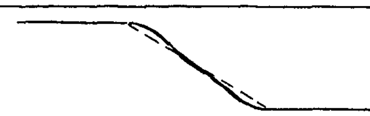
$f(t) = \begin{cases} 1 - \cos(2\pi\, t/t_b) & 0 < t < t_b \\ 0 & t < 0,\ t > t_b \end{cases}$	$I_a(t) = K'(t_b - t) + \frac{t_b}{2\pi} \sin(2\pi\, t/t_b)$
	
$f(t) = \begin{cases} t_b t - t^2 & 0 < t < t_b \\ 0 & t < 0,\ t > t_b \end{cases}$	$I_a(t) = K''(t_b^3 - 3t_b t^2 + 2t^3)$

Figure 28

APPENDIX VI

EXPERIMENTAL DETAILS AND DATA ANALYSIS

Preliminary to taking data

Just prior to taking the data the following precautions were taken:

1. The night before the data run the sweep speed and linearity of the oscillioscope were checked against a frequency standard and they proved to be as accurate as could be determined from the photograph of a sine wave.

2. Just prior to taking data the equipment had run for eleven (11) hours under no pulsing conditions with the cathode hot while sealed off from the vacuum pump. The total pressure rise was 2.5×10^{-4} mm of Hg. This is approximately 6×10^{-6} mm of Hg rise in 15 minutes.

3. All electronic timing sequence circuits had functioned for quite some time previous to the day of the experiment and seemed to be functioning mormally. They were given a 3 hour warm up period in order to be certain of their stability.

4. Many previous trial runs had been carried out prior to the day the data was taken to find the conditions that gave the most stable and consistant results. The variables being the photomultiplier voltage, the bias voltage, cathode temperature and gas pressure. These checks had been carried on for a period of several weeks with two

excitation tubes. They both seemed to function in a similar manner, although the second tube had no central electrode. It should be stated that the bias step voltage seemed a little more critical on the new tube. The new tube seemed to heat up to a higher temperature for a given induction heater voltage and produced more darkening of its window than had been the case with the previous tube. It also lacked the outgassing which the former tube had had over long periods of time. The new tube had been outgassed continuously for 5 days with the cathode at higher than operating temperature and it was this operation which contributed to the darkening of the window.

5. A great deal of time had been spent on trying to remove the lingering signal on the tail of the light relaxation curve. This included liquid nitrogen cooling of the photomultiplier within a vacuum chamber. At first the lingering signal appeared to be created within the photomultiplier. It was stronger when the excitation tube and photomultiplier were held on for longer periods of time. After adjusting the bias step delay so that the bias signal was applied before the photomultiplier could be energized the lingering signal continued to persist but at a much lower level. It was then decided that at least some of the tail signal is true light signal but whether or not there is a long delayed process within the multiplier could not be determined conclusively with the present experimental arrangement but there was fairly substantial evidence that there is photomultiplier signal too. The best check on this would be to hold the bias step and cathode excitation step constant in time and vary the trigger time on photomultiplier. If the signal tail remains unchanged independant of the time the photomultiplier is subjected to the intense light then

it would clearly indicate the tail is produced from external photons and is not a property of the photomultiplier. Unfortunately this variation in photomultiplier delay had not been built into the present electronics and only the bias step function was made variable externally.

Method of Taking Data

After the warm-up period the optical filters were laid out in order of descending wave lengths on a mat near the apparatus. On the actual data run the sequence of operation was as follows:

a) Helium was introduced (with first optical filter in place and electronics pulsing at 1 sec intervals)

b) pressure was adjusted

c) bias voltage and photomultiplier voltage readings taken

d) decay curves were photographed with an overlay of 3 to 5 traces.

e) an opaque card was slipped between filter and photomultiplier for dark current reference signal.

f) with card in place the filter was replaced with the next one in the sequence.

The sequence from d) to f) was repeated until all filters were used at the same pressure. A spot check on voltage and pressure was made at random during a single pressure run.

g) when the photograph had been completed for the last filter in the sequence the pressure and voltage were all read and the gas pumped out.

When the entire sequence was run for a new pressure the order in which the filters were used was reversed. This implies that if there were contamination problems in the 10 to 15 minutes it took to complete a run, the 5876Å and the 3889Å lines should show alternating

effects from one pressure to the next.

The entire data run including a long vacuum pumping period took approximately two hours.

There are only two other comments of interest. There was one time during the run when no signal was seen although the external electronics appeared to function properly. The fault is believed to be due to the cathode lead ribbon touching ground inside the excitation tube. This had happened previously and the cathode ground had been burned out by supplying a high current from a variac through the ribbon while the cathode was cold. During the data run this fault corrected itself within a minute each time it appeared during the data run so no special adjustments were attempted. The fault was observed three times but only persisted for a few seconds on two of the three appearances. The curve shape appeared to be identical before and after each of these interruptions.

The second observation was the fact that the .038 mm Hg pressure reading seemed to rise during that pressure run to .04 mm Hg since the pressure reading taken between these and readings had a value between these values it was believed to be a true pressure rise rather than experimental error. This rise is believed to result from the fact that in refilling the system one always fills the system to about 100 times the pressure required in this run. This results from the constant volume dosing scheme for the helium. When the pressure is high the red hot cathode absorbs helium which is again diffused out into the lower pressure zone after the pressure has been pumped down. This effect had been observed before and it is believed that it does not provide contaminants in the gas.

DISTRIBUTION LIST

Agency	No. of Copies
Commander AF Office of Scientific Research ATTN: SRY Washington 25, D.C.	3
Commander AF Research Division ATTN: RRRTL Washington 25, D.C.	2
Commander Wright Air Development Division ATTN: WWAD Wright-Patterson Air Force Base Ohio	4
Commander AF Cambridge Research Laboratories ATTN: CRREL L. G. Hanscom Field Bedford, Massachusetts	1
Commander Rome Air Development Center ATTN: RCOIL-2 Griffiss Air Force Base Rome, New York	1
Commander Detachment 1 Hq. AF Research Division The Shell Building Brussels, Belgium	2
P.O. Box AA Wright-Patterson Air Force Base Ohio	1
Aeronautical Research Laboratories ATTN: Technical Library Building 450 Wright-Patterson Air Force Base Ohio	1
Armed Services Technical Information Agency ATTN: TIPCR Arlington Hall Station Arlington 12, Virginia	10

Director of Research and Development Headquarters, USAF ATTN: AFDRD Washington 25, D.C.	1
Office of Naval Research Department of the Navy ATTN: Code 420 Washington 25, D.C.	1
Director, Naval Research Laboratory ATTN: Technical Information Officer Washington 25, D.C.	1
Director, Army Research Office ATTN: Scientific Information Branch Department of the Army Washington 25, D.C.	1
Chief, Physics Branch Division of Research U. S. Atomic Energy Commission Washington 25, D.C.	1
U. S. Atomic Energy Commission Technical Information Extension P.O. Box 62 Oak Ridge, Tennessee	1
National Bureau of Standards Library Room 203, Northwest Building Washington 25, D.C.	
Physics Program National Science Foundation Washington 25, D.C.	1
Director, Office of Ordnance Research Box CM, Duke Station Durham, North Carolina	1
Director, Department of Commerce Office of Technical Services Washington 25, D.C.	1
ARO, Inc. ATTN: AEDC Library Arnold Air Force Station Tullahoma, Tennessee	1
Commander AF Flight Test Center ATTN: FTOTL Edwards Air Force Base California	1

Commander AF Special Weapons Center ATTN: SWOI Kirtland Air Force Base New Mexico	1
Commander AF Missile Development Center ATTN: HDOI Holloman Air Force Base New Mexico	1
Commander Army Rocket & Guided Missile Agency ATTN: ORDXR-OTL Redstone Arsenal Alabama	1
Commandant Air Force Institute of Technology (AU) Library MCLI-LIB, Bldg. 125, Area B Wright-Patterson Air Force Base Ohio	1
Commander Air Research and Development Command ATTN: RDR 2cys RDRA 1 cy RDRB 1 cy RDRC 1 cy RDRS 1 cy Andrews Air Force Base Washington 25, D.C.	6
Commanding General U. S. Army Signal Corps Research and Development Laboratory ATTN: SIGFM/EL-RPO Ft. Monmouth, New Jersey	1
National Aeronautics & Space Administration Washington 25, D.C.	6
Advanced Research Projects Agency Washington 25, D.C.	1
Rand Corporation 1700 Main Street Santa Monica, California	1
Chairman, Canadian Joint Staff For DRB/DSIS 2450 Massachusetts Ave., N.W. Washington 25, D.C.	1